United Arab Emirates University

Scholarworks@UAEU

4-2021

GEO-SPATIAL MODELING OF CARBON SEQUESTRATION ASSESSMENT IN DATE PALM, ABU DHABI: AN INTEGRATED APPROACH OF FIELDWORK, REMOTE SENSING, AND GIS

Basam Saeed Dahy

United Arab Emirates University

College of Science

GEO-SPATIAL MODELING OF CARBON SEQUESTRATION
ASSESSMENT IN DATE PALM, ABU DHABI: AN INTEGRATED
APPROACH OF FIELDWORK, REMOTE SENSING, AND GIS

Basam Saeed Dahy

This dissertation is submitted in partial fulfilment of the requirements for the degree
of Doctor of Philosophy

Under the Supervision of Prof. Salem Issa

April 2021

Declaration of Original Work

I, Basam Saeed Dahy, the undersigned, a graduate student at the United Arab Emirates University (UAEU), and the author of this dissertation entitled "*Geo-Spatial Modeling of Carbon Sequestration Assessment in Date Palm, Abu Dhabi: An Integrated Approach of Fieldwork, Remote Sensing and GIS*", hereby, solemnly declare that this dissertation is my own original research work that has been done and prepared by me under the supervision of Prof. Salem Issa, in the College of Science at UAEU. This work has not previously been presented or published, or formed the basis for the award of any academic degree, diploma or a similar title at this or any other university. Any materials borrowed from other sources (whether published or unpublished) and relied upon or included in my dissertation have been properly cited and acknowledged in accordance with appropriate academic conventions. I further declare that there is no potential conflict of interest with respect to the research, data collection, authorship, presentation and/or publication of this dissertation.

Student's Signature: _____ Date: 07-03-2021

Advisory Committee

1) Advisor: Prof. Salem Issa

Title: Associate Professor

Department of Geosciences

College of Science

2) Co-advisor: Prof. Taoufik Ksiksi

Title: Professor

Department of Biology

College of Science

3) Member: Dr. Nazmi Saleous

Title: Associate Professor

Department of Geography and Urban Sustainability

College of Humanities and Social Sciences

Approval of the Doctorate Dissertation

This Doctorate Dissertation is approved by the following Examining Committee Members:

1) Advisor (Committee Chair): Dr. Salem Issa

   Title: Associate Professor

   Department of Geosciences

   College of Science

   Signature _____ Date 15-04-2021

2) Member: Dr. Mohamed Saeed Yagoub

   Title: Associate Professor

   Department of Geography and Urban Sustain.

   College of Humanities and Social Sciences

   Signature _____ Date   15-04-2021

3) Member: Dr. Youngwook Kim

   Title: Assistant Professor

   Department of Biology

   College of Science

   Signature _____ Date 15-04-2021

4) Member (External Examiner): Prof. Fares M. Howari

   Title: Dean and Professor

   College of Natural and Health Sciences

   Institution: Zayed University

   Signature _____ Date   15-04-2021

This Doctorate Dissertation is accepted by:

Dean of the College of Science: Prof. Maamar Benkraouda

Signature *Maamar Benkraouda*   Date May 19, 2021

Dean of the College of Graduate Studies: Professor Ali Al-Marzouqi

Signature   Ali Hassan   Date May 19, 2021

Copy ____ of ____

Abstract

The United Arab Emirates (UAE) has undertaken huge efforts to green the desert and afforestation projects (planted mainly with date palms) hence, reducing its carbon footprint, which have never been accounted for, because of lack of implemented mechanisms and tools to assess the amount of biomass and carbon stock (CS) sequestered by plants in the country. The purpose of this dissertation is to implement a new approach towards assessing the carbon sequestered by date palm (DP) plantations in Abu Dhabi, in both their biomass compartment as well as the soils under beneath, using geospatial technologies (RS and GIS) assessed by field measurements. The methodology proposed in this dissertation relied on both fieldwork and labwork, besides the intensive use of geospatial technology including, digital image processing of multi-scale, multi-resolution satellite imagery as well as Geographical Information Systems (GIS) modelling.

For detecting and mapping the DP, the research proposes a framework based on using multi-source/ multi-sensor data in a hierarchical integrated approach (HIA) to map DP plantations at different age stages: young, medium, and mature. The outcomes of the implemented approach were the creation of detailed and accurate maps of DP at three age stages. The overall accuracies for mixed-ages DP the value reached up to 94.5%, with an overall Kappa statistics estimated at 0.888 with total area of DP equal to 7,588.04 ha and the total number of DP planted in the study area counted an estimated number of 8,966,826 palms.

The study showed that the correlation of mature DP class alone (>10 years) with single bands was significant with shorwave infrared 1 (SWIR1) and shortwave infrared 2 (SWIR2), while the correlation was significant with all tested vegetation indices (VI) except for tasseled cap transformation index for brightness (TCB) and for greenness (TCG). By using different types of regression equations, tasseled cap transformation index for wetness (TCW) showed the strongest correlation using a second-order polynomial equation to estimate the biomass of mature DP with R^2 equal to 0.7643 and P value equal to 0.007. The exponential regression equation that uses renormalized difference vegetation index (RDVI) as RS predictor was the best single VI and had the strongest correlation among all RS variables of Landsat 8 OLI for AGB of non-mature DP, with an R^2 value of 0.4987 and P value equal 0.00002.

The findings of the dissertation work are promising and can be used to estimate the amount of biomass and carbon stock in DP plantations in the country as well as in arid land in general. Therefore, it can be applied to enhance the decision-making process on sustainable monitoring and management of carbon sequestration by date palms in other similar ecosystems. The research's approach has never been developed elsewhere for date palms in arid areas.

Keywords: Carbon Sequestration, Arid Lands, Remote Sensing, Biomass, UAE.

Title and Abstract (in Arabic)

النمذجة الجيومكانية لتقدير كمية الكربون المحتجز في نخيل التمر في أبوظبي بإستخدام القياسات الحقلية وتقانات الاستشعار عن بعد ونظم المعلومات الجغرافية

الملخص

بذلت دولة الإمارات العربية المتحدة جهوداً جبّارة لزراعة الصحراء ومشاريع التشجير (المزرعة أساساً بنخيل التمر) وبالتالي خفض بصمتها الكربونية التي لم يتم احتسابها قط بسبب الافتقار إلى الألآيات والأدوات المناسبة القابلة للتطبيق في لتقييم كمية الكتلة الحيوية والكربون المخزون والذي تحتجزه النباتات في الدولة. إن الغرض من هذه الأطروحة تطبيق مقاربة جديدة لتقدير الكربون المحتَجَز بواسطة نخيل التمر في مزارع إمارة أبوظبي سواء في كتلته الحيوية أو في التربة المزروع عليها، باستخدام التقانات الجيومكانية (الاستشعار عن بعد ونظم المعلومات الجغرافية) التي تم قياسها ميدانياً. اعتمد منهجنا المقترَح في هذه الأطروحة على كل من العمل الميداني والمخبري، وكذلك تحليل بيانات الاستشعار عن بعد ونظم المعلومات الجغرافية للنمذجة المكانية. عمدت الدراسة الى استخدام بيانات للاستشعار عن بعد متعددة المصادر/ متعددة المجسّات في نهجٍ هرمي متكامل وذلك بهدف رسم خرائط لمزارع النخيل في مختلف فئاته العمرية (صغير/ متوسط/ كبير). كانت نتائج هذه المقاربة التي تم تطبيقها هو رسم خرائط مفصلة ودقيقة لنخيل التمر في مراحله العمرية المختلفة. كانت درجات الدقة الكلية لـ نخيل التمر مختلط الأعمار هو 94.5% مع تقدير اجمالي لمعامل كابّا الإحصائي عند 0.888. تمّ تقدير إجمالي مساحة مزارع نخيل التمر في إمارة أبوظبي بـ 7588.04 هكتار كما تم تقدير أعداد نخيل التمر في إمارة أبوظبي بـ 8,966,826 نخلة. أظهرت الدراسة أن عامل الأرتباط بين الكتلة الحيوية لفئة نخيل التمر كبير العمر مع النطاقات (القنوات الفضائية) الخاصة بالقمر الصناعي لاندسات-8، كان ارتباطاً قويا مع نطاقي الطول الموجي القصير للأشعة تحت الحمراء الأولى والثانية، وكان معامل الارتباط قويا أيضاً مع كافة مؤشرات الغطاء النباتي التي تم استخدامها في هذا البحث عدا المؤشران اللذان يستخدمان تقنية تحويلات غطاء تاسلد لكشف الخضرة والسطوع (تي سي جي وأيضا تي سي بي). وعند استخدام أنواع مختلفة من معادلات الإنحدار، وجدنا أن تقنية تحويلات غطاء تاسلد لكشف الرطوبة (تي سي دبليو)، كمؤشر للغطاء النباتي قد أظهرت أقوى معامل ارتباط باستخدام معادلة متعددة الحدود من الدرجة الثانية لتقدير الكتلة الحيوية في نخيل التمر الكبير بقيمة معامل تحديد وصلت إلى 0.7643 وقيمة احتمالية تساوي 0.007 . كما وجدت الدراسة أن معادلة

الإنحدار الأسي والتي تستخدم مؤشر الفرق المُعادة معايرته للغطاء النباتي (آر دي في آي) للتنبؤ بالكتلة الحيوية لنخيل التمر غير الكبير هي الأقوى في معامل الأرتباط بين جميع متغيرات الاستشعار عن بعد المستخدمة في الدراسة، بقيمة معامل تحديد تساوي 0.4987 وقي.. ا.ت.ا.ية معنوية تساوي 0.00002. أظهرت النتائج أن مساحة تاج النخلة هي الأ فضل لتقدير كل من الكتلة الحيوية لتاجها وكذا الكربون العضوي في التربة المزروع عليها النخيل. كما أن ارتفاع جذع النخلة كان الأفضل لتقدير الكتلة الحيوية لجذعها. إن نتائج هذه الدراسة واعدة ويمكن استخدامها لتقدير الكتلة الحيوية والكربون المحتجز في مزارع نخيل التمر في عموم الدولة وكذلك في الأقاليم القاحلة بشكل عام. لذلك، يمكن تطبيقها لتعزيز عملية صنع القرار لرصدٍ وإدارةٍ مستدامين في احتجاز الكربون بواسطة نخيل التمر المزروع في أنظمة بيئية مماثلة. إن مقاربتنا المقترحة في هذه الأطروحة هي الأولى من نوعها من حيث تطبيقها على نخيل التمر في المذ اط. ا.ا.....

مفاهيم البحث الرئيسية: احتجاز الكربون، المناطق الجافة، الاستشعار عن بعد، الكتلة الحيوية، الإمارات.

Acknowledgements

Dedication

To my beloved wife and family

Table of Contents

List of Tables

List of Figures

List of Abbreviations

AGB	Aboveground Biomass
AGC	Aboveground Carbon
APAR	Absorbed Photosynthetically Active Radiation
BGB	Belowground Biomass
BGC	Belowground Carbon
CA	Crown Area
CD	Crown Diameter
CB	Crown Biomass
CS	Carbon Stock
DBH	Diameter at Breast Height
DF	Dry to Fresh Factor (biomass)
DP	Date Palm
DTM	Digital Terrain Model
DVI	Difference Vegetation Index
ETM+	Enhanced Thematic Mapper (landsat-7)
EVI	Enhanced Vegetation Index
#Fornd	Number of Palm Fronds
GEMI	Global Environmental Monitoring Index
GIS	Geographic Information Systems
H	Palm Height
Δheight	Crown Depth
Ht	Palm Trunk Height

HIA	Hierarchical Integrated Approach
HCM	Hybrid Classification Method
IR	Infrared
LAI	Leaf Area Index
LULC	Land Use/ Land Cover
OLI	Operational Land Imager (landsat-8)
OBC	Object-Based Classification
PBC	Pixel-Based Classification
MSAVI	Modified Soil-Adjusted Vegetation Index
NDFI	Normalized Difference Fraction Index
NDGI	Normalized Difference Greeness Index
NDVI	Normalized Difference Vegetation Index
NN	Nearest Neighborhood
OC	Organic Carbon
OM	Organic Matter
R	Coefficient of Correlation
R^2	Coefficient of Determination
REDD+	Reducing Emissions from Deforestation and Forest Degradation
RMSE	Root Mean Square Error
RS	Remote Sensing
RVI	Ratio Vegetation Index
SAVI	Soil Adjusted Vegetation Index
SOC	Soil Organic Carbon
SOM	Soil Organic Matter

SR	Simple Ratio
SWIR	Shortwave Infrared
TB	Trunk Biomass
TCB	Tasseled Cap Index of Brightness
TCG	Tasseled Cap Index of Greenness
TCW	Tasseled Cap Index of Wetness
TM	Thematic Mapper (landsat-5)
TSAVI	Transformed Soil-Adjusted Vegetation Index
UAE	United Arab Emirates
UTM	Universal Transverse Mercator
VIs	Vegetation Indices
WV-2	World View 2

Chapter 1: Introduction

1.1 Overview

In 1990, the United Arab Emirates (UAE) was ranked at the 3rd place as one of the top, per capita, CO_2 emitting countries (EU EDGAR, 2017). It has remained amongst the top, per capita, CO_2 emitting countries during the period 1990 – 2016 (last published statistics), when it was ranked the 5th at 23.6 tons per capita CO_2 emission in 2016 (EU EDGAR, 2017). Furthermore, the UAE became one of the first major oil-producing countries to ratify the Kyoto Protocol when it entered into force in 2005. In contrast, the country has undertaken huge efforts to green the desert hence, reducing its carbon footprint, which have never been accounted for, because of lack of implemented mechanisms and tools to assess the amount of biomass and carbon stock sequestered by plants in the country. There is a common consent that afforestation and land-use conversion to a forest (reforestation) can be used to earn carbon credits and reduce the carbon footprint. This attitude has a growing interest among policymakers and governments (Baral & Guha, 2004). Estimation of carbon stock (CS) in forests and plantations is important to assess their mitigation effects and hence balancing the carbon footprint (Ebuy et al., 2011). Many techniques exist to estimate sequestered carbon (Gibbs et al., 2007). All existing techniques ultimately rely on the ground measurement of plant biomass which is time-consuming, tedious, and destructive (Ebuy et al., 2011). Alternatively, most of the existing non-destructive methods using developed biomass estimation equations have been developed for tropical rainforests ecosystems because of their importance to the global carbon cycle (Basuki et al., 2009; Brown, 1997; Chave et al., 2005; Cole & Ewel, 2006; Makinde et al., 2017). Unfortunately, very few plant species biomass estimation equations are available for

desert ecosystems. Moreover, none of these equations were developed and used to fit one of the most important fruit crops in the arid regions, *Phoenix dactylifera*, date palm. Indeed, the only indigenous wild desert plant domesticated in its native harsh environments appears to be the date palm (Zohary & Hopf, 2000). Date palm is considered a renewable natural resource because it can be replaced in a relatively short period of time or used through conservation efforts without depletion (El-Juhany, 2010). It is estimated that the UAE has the largest number of date palms for any single country in the world with a minimum of 200 cultivars, 68 of which are commercially considered to be the most important (El-Juhany, 2010). Consequently, date palm, with its various cultivars, possesses the potential capacity to store carbon and hence be considered as a good means of carbon sequestration in such an arid ecosystem.

Nevertheless, the estimation of forest biomass raises scientific challenges to identify feasible approaches to assess carbon at the national-level (Gibbs et al., 2007). Effective management requires repetitive monitoring and accurate measuring of biomass which is a classical subject in plant population ecology (Joshi & Ghose, 2014; Avery & Burkhart, 2015; Elzinga et al., 1998; Husch et al., 1982; Schreuder et al., 1993; Shiver & Borders, 1996). Traditional biomass assessment methods (both destructive and allometric), based on field measurements are the most accurate methods; however, they are difficult to conduct over large areas besides, they are not a practical approach for broad-scale assessments (Kumar & Mutanga, 2017; Yuen et al., 2016). These difficulties make monitoring activities more costly, time-consuming, and labour-intensive (Attarchi & Gloaguen, 2014; Khalid & Hamid, 2017). Furthermore, field-based resource inventories, are carried out for economic reasons and not environmental ones. They provide good historical data on patterns and trends but are not accurate enough to estimate fluxes for the entire landscape and all carbon

pools therein (Cihlar et al., 2002). Recently, remote sensing (RS) procedures have been applied to natural resources management and biomass assessment (Kankare et al., 2013; Maynard et al., 2007; Salem Issa et al., 2019; Wannasiri et al., 2013). RS can obtain forest information over large areas with repetitive coverages, at a reasonable cost and with acceptable accuracy (Lu, 2006). Moreover, the integration of RS data into geographic information systems (GIS) models will benefit from the tools of both technologies; allowing for adding ancillary and field data to the analysis and increasing reliability in estimating the biomass, hence CS. Building GIS-based models to predict future scenarios for forest management and the implementation of afforestation plans is another more valuable product.

1.2 Statement of the Problem

The purpose of this dissertation is to implement a new approach towards assessing the carbon sequestered by date palm plantations in Abu Dhabi, in both their biomass compartment as well as the soils under beneath, using geospatial technologies (RS and GIS) assessed by field measurements. Therefore, the main questions of the dissertation are: Are geospatial technologies (RS and GIS), as an innovative method, capable of estimating biomass and CS in forests (date palm plantations in the current case) with minimum cost and time while keeping high levels of accuracies? And how? Can the geospatial technologies be considered as a reliable and feasible solution towards forest management in the UAE and hence be adopted as a long term strategy that can be integrated into the decision making process at the national level?

On the other hand, as mentioned above, the country's huge efforts undertaken to green the desert and hence, reduce its carbon footprint, have not been accounted for, because of the lack of implemented mechanisms and tools to assess the amount of biomass and CS sequestered by plants within its territories. Thus, Estimating CS in

forests and plantations by using a simple, practical, and an eco-friendly mechanism is an accompanying objective to assess decision makers and planners in their efforts for climate change mitigation and hence balancing the carbon footprint.

1.3 Aim and Objectives

Several specific objectives of the current study have been defined and specified, with the corresponding chapter in which they are treated, as follows:

1. To calculate the biomass ratios in date palm including aboveground biomass (AGB), belowground biomass (BGB), total biomass, and the carbon percentage in both biomass and soil (SOC) at three age stages (young, medium, and mature) from selected date palm plantations in Abu Dhabi. (Chapter 3).

2. To develop biomass allometric equations specifically for date palm for estimating its biomass and CS assessment. (Chapter 3).

3. To map the main LULC classes in the study area and to extract and map the date palm plantations in Abu Dhabi. (Chapter 5).

4. To build a RS-based spatial model for biomass and CS assessment of date palm. (Chapter 4 and 6).

5. To quantify and visualize the amount of biomass and CS in Abu Dhabi, using the built RS-based spatial model. (Chapter 6).

1.4 Literature Review

Note: The substantive part of this Subsection (1.4 Literature Review) has been published in peer reviewed journals during the preparation of this dissertation. These published papers are:

- Dahy, B., Issa, S., Ksiksi, T., & Saleous, N. (2020). Geospatial Technology Methods for Carbon Stock Assessment: A Comprehensive Review. IOP Conference Series: Earth and Environmental Science, Volume 540.

- Issa, S., Dahy, B., Ksiksi, T., & Saleous, N. (2020). A Review of Terrestrial Carbon Assessment Methods Using Geo-Spatial Technologies with Emphasis on Arid Lands. Remote Sensing, 12(12), 2008.

- Dahy, B., Issa, S., Ksiksi, T., & Saleous, N. (2019). Non-Conventional Methods as a New Alternative for the Estimation of Terrestrial Biomass and Carbon Sequestered: Mini Review. World Journal of Agriculture and Soil Science.

1.4.1 Phoenix dactylifera, Date Palm

Date palms (*Phoenix dactylifera L.*) are resilient, productive over long terms, and possess multipurpose economic and environmental advantages (Figure 1). Moreover, date palms have been considered an important crop and part of the farming systems in arid and semiarid regions, especially in the oases and in the forms of small farm units or as large-scale plantations (FAO, 1982). Date palms are considered precious, and have strong religious, traditional and nutritional significance (Shahin & Salem 2014). In the Arabian gulf states, date palms are heavily planted and maintained, particularly in the UAE, using abundant desalinated water and can thus be considered as a good alternative for carbon sequestration in such arid ecosystems. The UAE's economy has prospered since the discovery of oil, and the country witnessed an unprecedented pace of growth supported by revenues from oil. The government invested heavily in planting and maintaining green areas, including farms many of which are date palm plantations. During the past decades, the UAE date production

increased, as an outcome of increased demand as the population swelled (AOAD, 2008).
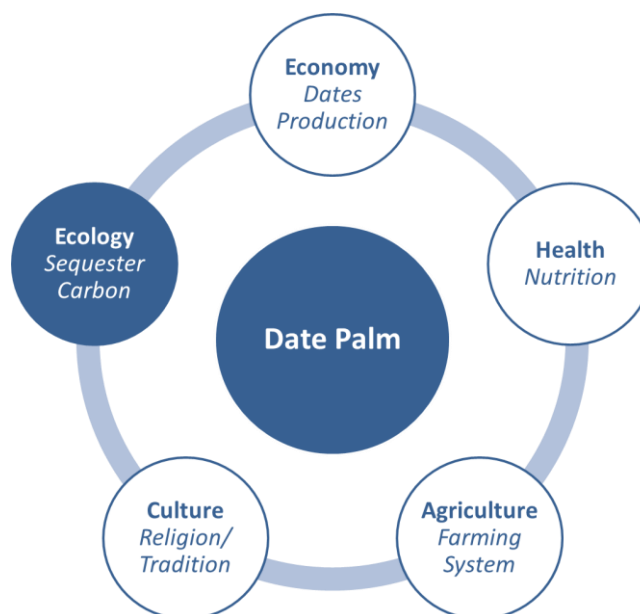
Figure 1: Multipurpose advantages of date palms. The research is focused on the ecological advantages of date palm by assessing and quantifying the CS by date palm plantations in arid lands of Abu Dhabi.

The date palm in Arab countries, in general, has been an integral part of the people's culture and tradition. However, the number of the date palm, production, and consumption vary from one country to another due to varying ecological conditions (El-Juhany, 2010). The world's highest production and consumption of dates is found in the Arabian Peninsula countries, such as UAE (Zohary & Hopf, 1993). According to Food and Agriculture Statistics Database (FAOSTAT, 2013), the total world number of date palms is about 120 million trees, distributed in 30 countries and producing nearly 7.5 million tons of fruit per year. Over two-thirds of this amount is found in the Arab countries; three of the top 10 dates producers worldwide are in the Arabian Peninsula, namely: Saudi Arabia, UAE, and Oman (Kader & Hussein, 2009; AOAD, 2008). It is estimated that the UAE has the largest number of date palms for

any single country in the world with a minimum of 200 cultivars, 68 of which are commercially considered to be the most important (El-Juhany, 2010).

Arid lands in particular, have received less attention in recent decades despite their importance to society and their exceptional vulnerability to climate change. They provide ecosystem services to more than two billion people, including significant crop production and forage for wildlife and domestic livestock (Bestelmeyer et al., 2015). While arid lands are sparsely vegetated with low annual productivity, they have been identified as an important player in the global trends and variability in atmospheric CO_2 concentrations (Ahlström et al., 2015; Biederman et al., 2017; Humphrey et al., 2018; Poulter et al., 2014). Although biomass per unit area in arid and semiarid regions is normally low, their large extent gives them a significant role as a carbon pool for the supply of essential ecosystem services (Zandler et al., 2015). Monitoring the spatiotemporal dynamics of arid lands ecosystem structure and function is, therefore, a high research priority. Satellite RS particularly, has been instrumental in exposing the role of arid lands within the context of global carbon cycling and the broader Earth system (Humphrey et al., 2018; Poulter et al., 2014). Yet, none of the plant biomass assessment measurements and its capacity of storing and sequestering carbon, were conducted for the most important fruit crops in arid regions, *Phoenix dactylifera*, date palm. In UAE, where more than two-thirds of its land area is covered by desert ecosystems, date palm species is a good alternative for CS in such ecosystems. Date palm requires minimum water supply and tolerate harsh growth conditions such as high temperatures, drought, and high levels of salinity. In fact, it is the most salt tolerant plant of all fruit crops (Alhammadi & Kurup, 2012; El-Juhany, 2010; Zohary and Hopf, 2000).

1.4.2 Quantifying Terrestrial Carbon Sequestration

Carbon sequestration is the process of capturing of CO_2 gas in the atmosphere and it's storing in liquid or solid state. This process is already occurring naturally through trees, the ocean, soil and live organic matter (Lackner, 2003). Any reservoirs or stores of carbon are called carbon pools. Specifically, storing of CO_2 occurs in three levels: in plants and soil (Terrestrial Sequestration), underground (Geological Sequestration) and deep in oceans (Ocean Sequestration) (Figure 2). Terrestrial or biologic sequestration is the process of storing atmospheric CO_2 as carbon in the stems, roots of plants and soil. The bulk of carbon sequestered terrestrially is stored in forest biomass.
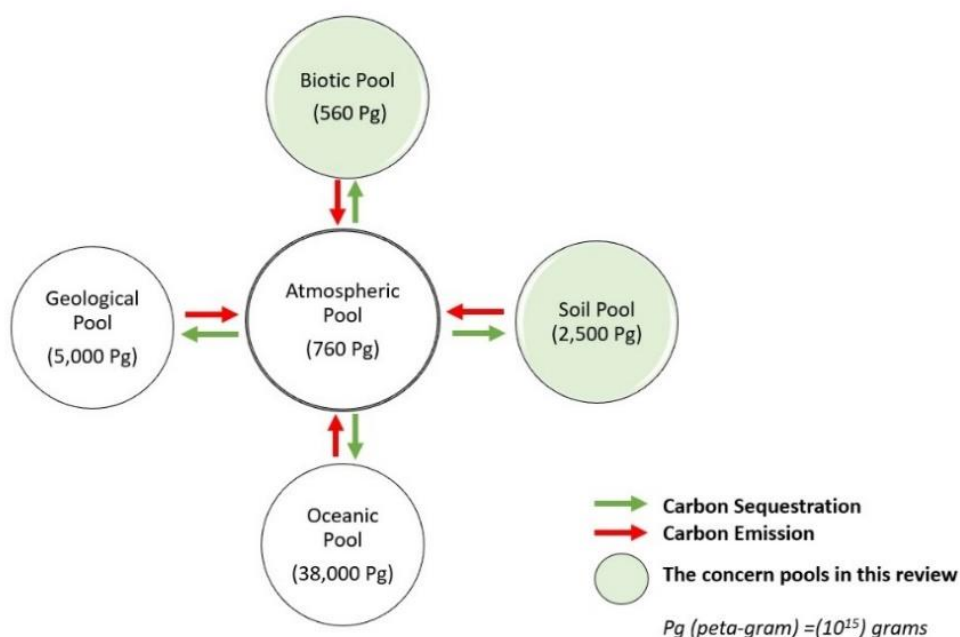
Figure 2: Carbon pools. They include: (1) Terrestrial Sequestration pool (sequestering and storing of CO2 in plants and soil); (2) Geological Sequestration (underground) pool; (3) Ocean Sequestration (deep in oceans) pool; and (4) Atmospheric pool. After (Lal, 2004; Salem Issa et al., 2020a).

Forests, as both carbon sources and sinks, can play a major role in combating global climate change (Dick OB, 2015; Ekoungoulou et al., 2014). Estimation of CS and assessing the role of forest ecosystems in regional and global carbon cycles, is

important for a better understanding of the impacts of land-cover changes on carbon fluxes, nutrient cycling and budgeting. Likewise, monitoring forest biomass, as a step in CS estimation, is not an environmental issue only; actually, more than 190 countries are committed to take action to implement and support sustainable management of forests and enhancement of forest CS according to Paris Agreement on Climate Change (United Nation, 2019).

Carbon sequestration is becoming an essential component in the fight against global warming. Afforestation projects and land use conversion to forest (reforestation) can be used to earn carbon credits and reduce the carbon footprint, hence providing a long-term reduction in greenhouse gases (GHGs) levels through carbon sequestration (Singh et al., 2018). This attitude has a growing interest among policymakers and governments (Baral & Guha, 2004). Plantation cropping as a land use system has the potential to contribute to CS, maintain soil biodiversity and improve soil fertility (Prayogo et al., 2018). It can add economic value by providing more job opportunities, better income and food security, especially the smallholder systems in developing countries, and the timber exploitation (Khalid & Hamid, 2017; Singh et al., 2018). The UN program for the reduction in emissions from deforestation and forest degradation (REDD+), is an international initiative to help nations earn financial incentives if they implement climate policies and if they demonstrate CO_2 emission reduction (Gibbs et al., 2007).

Precise CS estimation is a necessary step to define carbon emission mitigation strategies and programs at the local and regional level (Clerici et al., 2016a). This kind of studies is necessary for a better understanding of the long-term behaviour and drivers of carbon sequestration under different global climate change scenarios (Corona-Núñez et al., 2018). The total CS in any terrestrial ecosystem is the sum of

carbon in biomass and soil. A practical definition of forest biomass is the total amount of aboveground living organic matter in trees expressed as oven-dry tons per unit area (Brown, 1997). The estimation of biomass is a challenging task, especially in the areas with both complex stands and varying environmental conditions as well as in low vegetation cover density areas, such as arid lands. Both types of ecosystems require the use of accurate and consistent measurement methods.

Eggleston et al. (2006) has listed five terrestrial ecosystem carbon pools involving biomass: above-ground biomass (AGB), below-ground biomass (BGB), litter, woody debris and soil organic matter. The total CS is estimated as the sum of two quantities representing the amounts of carbon in soil and in biomass. Therefore, two routes for achieving sequestered carbon estimation: First, estimating soil organic carbon (SOC) which is part of soil organic matter (SOM). Second, estimating vegetation biomass which can be achieved by estimating the AGB and then deriving the remaining components; BGB, Litter and Debris, from the AGB as shown in (Table 1). As for SOM, it is most commonly estimated through soil sampling at various layers; SOC is then estimated using the total combustion method, as explained in (Walkley & Black, 1934). The content of SOC included in SOM may change depending on many factors (ecosystems, type of organic residues and land management, etc.). Many studies estimate SOC from SOM using the conventional factor of 1.724 (~ 58% of SOM). This figure is widely used and has appeared in many studies and published papers in the last century; while Brady and Weil (1999) concluded that this value (58% of SOM) probably applies only to highly stabilized humus. After his statistical analysis of 481 studies, Pribyl (2010) found that conventional factor varies from 1.35 to 7.50 with a mean value of 2.20, concluding that any single-number conversion factor, universally applied, has the potential for serious error when used to estimate the carbon

content of soils. However, recent studies have accepted a generic quick, simple and inexpensive coefficient of 57% for measuring SOC as a percent of SOM (Ponce-Hernandez et al., 2004).

Table 1: Calculation methods of CS components in terrestrial ecosystems.

No	Component	Calculation Method	Source
1	AGB	Destructive OR Non-destructive Methods	(Gibbs et al., 2007)
2	BGB	20% of Above-ground biomass	(Cairns et al., 1997)
3	Litters	10–20% of Above-ground biomass	(Houghton et al., 2009)
4	Debris		
5	SOC	Total combustion method	(Walkley & Black, 1934)

Of the above five pools, AGB is the most visible, dominant, dynamic and important pool of the terrestrial ecosystem, constituting around 30% of the total terrestrial ecosystem carbon pool which, in turn, represents 70–90% of the total forest biomass (Cairns et al., 1997). AGB estimation has received considerable attention over the last few decades because of increased awareness of climate warming and the role forest biomass plays in carbon sequestration and release of greenhouse gases due to deforestation (Kumar et al., 2015). While SOM holds two to three times more carbon than the total biomass carbon pool on a global scale, much of the soil carbon is more protected and not easily oxidized (Davidson & Janssen, 2006). On the other hand, AGB contributes to atmospheric carbon fluxes to a much greater extent due to fire, logging, land-use changes, etc., and so is of much greater interest. Therefore, it should be monitored and measured along the year, not only a one-time mapping; although the estimation of forest biomass is a scientific challenge as to identify efficient methods for its assessment at regional to national-levels (Gibbs et al., 2007). Moreover, estimates of AGB can also be used to predict root biomass (BGB), which is generally estimated at 20% of the AGB based on the predictive relationship applied by many

studies (Table 1) (Cairns et al., 1997; Mokany et al., 2006; Ramankutty et al., 2007). In addition, CS of dead wood or litter (e.g., felled or dead trees, dead or broken branches, leaves, etc.) in mature forests are generally assumed to be equivalent to 10 to 20% of the calculated AGB (Gibbs et al., 2007; Houghton et al., 2009).

Producing accurate maps for biomass estimation distribution is a serious challenge which has to be addressed when calculating CS. As mentioned before, plant biomass can be measured or estimated by both direct (destructive) and indirect (non-destructive) methods. The direct method which is the most precise method for determining carbon biomass by destructively harvest all plants, partition each into various constituent components (e.g. stem, branches, leaves, flowers, fruits, roots) and subsequently determine the carbon content of the various components analytically OR calculated as a fraction of measured biomass (indirect) (Yuen et al., 2016). The destructive methods of biomass estimation are limited to a small area due to the destructive nature, time, expense and labor involved and sometime illegal especially for trees. In addition, these methods ultimately rely on ground measurement and can cause severe destruction to the forests as well as a risk of environmental deterioration (Khalid & Hamid, 2017; Maulana et al., 2016). The indirect methods include the estimation based on allometric equations (Subsection 1.4.3) or through non-conventional methods using RS and GIS (Subsection 1.4.4).

1.4.3 Biomass Allometric Equations

There are many reasons that make developing biomass equations a very essential step towards guarantying an alternative to destructive methods. The main objective in developing allometric equations is to avoid destructing forests when estimating their biomass, hence its CS, and provide a cost effective and environment-friendly option since it is done without harvesting (Brown et al., 1989). In general,

allometric equation is a statistical model to estimate the biomass of the trees using their biometrical characteristics (e.g., height, diameter at breast height (DBH) or crown size), which are non-destructive and simpler to measure (Picard et al., 2012). Therefore, non-destructive methods through allometric relationships are increasingly used. Such equations have also been proven to be fast, inexpensive, and more suitable for largescale estimation of forest CS (Koala et al., 2017). Allometric models are commonly used in forest inventories and ecological studies (Brown et al., 1989). The models relate biomass of an entire tree or individual tree components (e.g., stems, branches, leaves or roots) to one or more easily tree variables and dendrometric measures (e.g. height, diameter breast height or crown size), and to estimate CS (Ebuy et al., 2011; Picard et al., 2012). The proportions between height and diameter, between crown height and diameter, and between biomass and diameter follow rules that are common to all trees which are grown under the same conditions and become more useful in uniform forests or plantations with similarly aged stands (Archibald & Bond, 2003; Bohlman & O'Brien, 2006; Dietze et al., 2008; King, 1990; Kumar & Mutanga, 2017).

The selection of appropriate and robust models, therefore, have considerable influence on the accuracy of the obtained estimates (Mahmood et al., 2019). As mentioned above the aim of using allometric equations is to estimate biomass without the need to cut trees. However, these equations are based on the destructive sampling of vegetation in a given location, before they can be applied generally. In order for those equations to be validated, cutting and weighting tree components is necessary (Vashum & Jayakumar, 2012). The number of trees destructively sampled to build allometric equations differs from one study to another. Currently, there is no consensus on that number, as this is often dependent on resource availability and permission to

harvest trees (Yuen et al., 2016). For example, Russell (1983) and Deans et al. (1996) used 15 and 14 trees, while Brown et al. (1995) and Khalid et al. (1999a) used only 8 and 10 trees, respectively to build their allometric equations. In their study of oil palm plantations of Benin forests, Aholoukpè et al. (2018) used 25 palms from several ages and different genetic origins to build a species specific allometric equation. However, a recent study showed that small sample size (≤10) results in biased allometric equations (Duncanson et al., 2015).

Generally, there is no specific procedure to build allometric equations yet there is a recommended guideline for documenting allometric equations. (Jara et al., 2015) recommended that researchers should only report all the details in methods section of how they build up their equations. Furthermore, sampled trees should be randomly selected, regardless of health condition or degree of damage, because sampling only trees with fully intact structural characteristics will likely result in an equation that overestimates biomass for the general case. In this respect, data outliers should not be removed simply to improve model fit metrics (Yuen et al., 2016).

Many allometric equations have been developed for various plant species. For example, the GlobeAllomeTree database contains over 706 equations from Europe, 2843 from North America and 1058 from Africa (Sileshi, 2014). Some of these are volume equations, and the others are biomass equations. The biomass can be calculated from volume of the biomass per hectare (VOB/ha) by using a generalized volume model, wood density and a biomass expansion factor (Brown et al., 1995; Lugo & Brown, 1992). One of the limitations of volume equations is that it can only be applied to stem while allometric equations cover a wide range of vegetation components (Cheng et al., 2014).

Allometric models can be developed for either individual or multiple species (a mixture of species) to represent a community or bioregion. They also can be developed to cover specific sites, regional or pan-tropical scales (Mahmood et al., 2019; Yuen et al., 2016). Most of biomass equations, species and multispecies, have been developed for tropical rainforests ecosystems because of their importance to the global carbon cycle (Basuki et al., 2009; Brown, 1997; Chave et al., 2005; Cole & Ewel, 2006; Makinde et al., 2017). The multispecies equations built because it is practically difficult to develop allometric equations for all species present in the ecosystem (Dick OB, 2015). Chave et al. (2005) have shown that one hectare of a tropical forest may shelter as many as 300 different tree species. Hence, the multispecies allometric models are more methodologically efficient for biomass estimation compared to those developed for individual species at specific locations. However, these models carry the potentiality to misrepresent local, species- or community-specific variations and anomalies. Therefore, they may fail to capture variations in both forest type and the full diversity of the natural vegetation communities hence leading to an increased level of uncertainty (Mahmood et al., 2019). Hence, a tailored equation for each specific species is needed for a better accuracy in estimating the biomass. Nevertheless, such an equation will still be conditioned by the ecological zone based on which it had been built. Hence weakening the estimation's accuracy of the actual forest AGB when the equation is used in another area or region. Due to the different characteristics of plant species from site to site, pre-existing equations developed at locations that are different from the one in consideration may have limited applicability, even if the equation is species-specific. In their review of allometric equations in Asia, Yuen et al. (2016) concluded that applying existing allometric equations out of convenience is potentially a key source

of uncertainty in above- and below-ground CS estimates in many Asian landscapes. The selection of allometric equations can influence local, regional and global biomass estimates, therefore, there is an importance of site-specific equations for accurate estimation of biomass as generalized equations can overestimate AGB by 50% to 65% (Maulana et al., 2016). The locally developed models are expected to provide less uncertainty than generic equations (Jara et al., 2015). Site and species specific allometric models should logically provide a greater level of accuracy at a given location to assist the assessment of biomass carbon sequestration and that make the locally built equation a better option to produce more accurate site-specific biomass estimation. Finally, since the choice of the equations is the first critical step, there has been a rapid increase in efforts to develop locally appropriate equations (Sileshi, 2014). Only a few biomass assessment equations are available for plant species in desert or arid land ecosystems. None of these measurements were used to fit one of the most important fruit crops in the arid regions, *Phoenix dactylifera*, date palm.

The mathematical model commonly used for modeling AGB is based on the power function (Yuen et al., 2016). This was founded on the basis that the growth of a plant is characterized by the relation of proportionality between its total biomass and its size (Fonton et al., 2017). Biometric variables measured in plant species were considered as independent variables (DBH, total height, crown variables, stem height, etc) and incorporated into a power function model (Da Silva et al., 2015). The allometry based on power model have good reliability as indicated by high coefficient of determination indices (R^2) (Gevana & Im, 2016). Researchers involved in the development and application of biomass allometric equations are faced with many challenges. One of them is the choice between simple bivariate power-law (typical allometric) functions and models with multiple predictors (Sileshi, 2014). Different

variables (structural and non-structural) were considered when building biomass allometric equations. Most equations for AGB, or biomass of any component (stem, branch, leaves, other) use equations with diameter and/or height as independent variables. Other variables such as girth, basal area and crown dimensions have been used even less frequently— usually in special cases (Yuen et al., 2016). Using wood density, when it is available, as a predictor is considered as significantly improving the biomass prediction equation when dealing with multispecies dataset (Chave et al., 2005). In their study to investigate the allometric equations in China, Cheng et al. (2014) found that the most frequently used predictive variable in single-variable models is DBH, and in two-variable models are DBH and tree height while wood density and crown diameter are presented in more complicated models. They found that diameter variables have a dominant proportion of 87.4% of the surveyed equations. However, DBH showed a weak correlation with biomass quantity in specific species, like palm for example (Carlos et al., 2015; Sajdak et al., 2014). Age can be used as a predictor for biomass estimation in many studies since there is a linear correlation between biomass accumulation and age (Henson & Chang, 2003; Singh et al., 2018). Many studies have highlighted the importance of tree height as a predictor variable in the AGB equation (Fonton et al., 2017; Khalid & Hamid, 2017; Picard et al., 2012; Prayogo et al., 2018). A single plant species can have more than one allometric equation, e.g., palm species (Appendix 1). Furthermore, more than one allometric equation can be developed for each plant species. The reasons behind that can be: (1) difference in ecoregion sites that these equations developed for (Tropical or Amazonian forests ..etc), (2) the decision of the developers of the allometric equations and choosing of the suitable variable/s (height, DBH, trunk height, etc.) to work as input (independent variable) to the model, (3) the use of the allometric

equations to cover either specific parts of the plant (AGB, crown biomass, trunk biomass, etc.) or specific age (young, mature, mixed, etc.), and (4) the selection of the mathematical equation form (power, linear, algorithmic, etc.).

The use of crown variables as indicators for biomass estimation became of more interest lately due to the developments in RS technologies. More recently, allometric equations have been used, coupled with RS and field-based structural variables measurements (Cihlar et al., 2002; Dahy et al., 2019; Salem Issa et al., 2018, 2019). For example, Cheng et al. (2014) recommended to develop more equations with different field structural variables that can be linked to RS predictors. Likewise, Jucker et al. (2017) suggested in their review of allometric equations to develop a new generation of allometric equations that estimate biomass based on attributes which can be remotely sensed.

1.4.4 Geospatial Technologies for Estimation of Carbon Stock

While direct field data measurements of biomass are the most accurate, they are not adequate to map AGB distribution at large scales. On the other hand, geospatial technologies proved to be practical and cost-time effective, and allows for imaging and studying inaccessible places by traditional field measurements. Geospatial technologies procedures have been applied to natural resources management and biomass assessment, hence CS (Kankare et al., 2013; Wannasiri et al., 2013). RS can obtain biomass information over large areas with repetitive coverages, at a reasonable cost and with acceptable accuracy (Lu, 2006). Various techniques and sensors have been used and tested in numerous studies. RS, both active and passive, provide some of the most time-efficient and cost-effective approaches to derive AGB estimation at the regional and national scale. Moreover, the integration of RS data into GIS models

provides advantages of both technologies, allowing for adding ancillary and field data to the analysis, besides increasing reliability in estimating AGB.

A textual search on Google Scholar was performed, in order to identify statistically relevant temporal patterns of the use of terms such as 'Carbon Sequestration', 'Carbon Sequestration + Remote Sensing' and 'Carbon Sequestration + GIS' in the literature. The search was customized to group results by ten-year intervals starting in 1951, to highlight the development of researches in the subject under review over time and the increase in the use of geospatial technologies in CS studies (Figure 3). Statistical analysis of the data revealed an exponential increase with time in the number of scientific studies on carbon sequestration considering both RS and GIS in their methodology. This can be attributed to the increase in volume of available satellite imagery and the ease of access to their archives witnessed over the last two decades to be become available to the end user either freely or commercially. Furthermore, the introduction of GIS in the late eighties contributed to this trend as well.
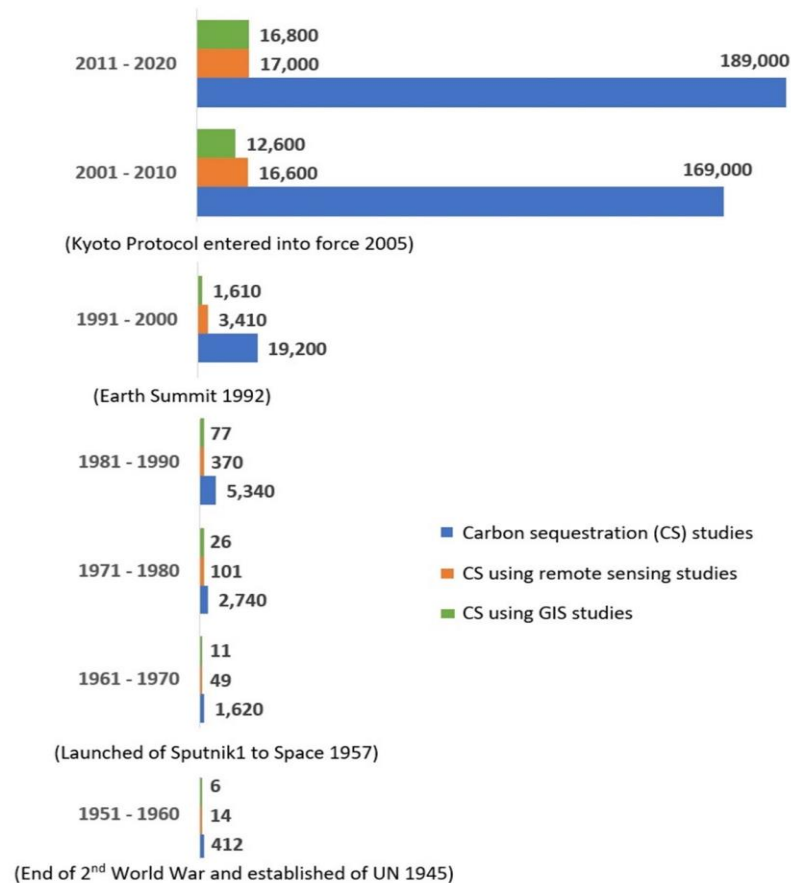
Figure 3: Textual analysis using Google Scholar. The terms used are: Carbon Sequestration, Remote Sensing and GIS. After (Dahy et al., 2019, 2020; Salem Issa et al., 2020a).

Following, a systematic review was conducted in two databases other than Google Scholar, namely, Web of Science and Science Direct. The databases were accessed using the search terms: "carbon sequestration", "above-ground biomass", "remote sensing", and "GIS". The search was applied to articles that were published in peer-reviewed journals only. These searches collectively yielded 2,771 results. The results were pared down to 647 by applying three criteria: (1) the results were NOT "review papers" OR "conference proceeding" papers and only restricted to research articles; (2) the study belonged to terrestrial ecosystems excluding the marine and coastal ecosystems; and (3) the study is not a duplicate from a previous search. All articles were downloaded and stored using the reference management software

(ZOTERO). Based on reviewing the abstracts, the list was further reduced to 171 by retaining only articles that discuss correlation between AGB and RS-based parameters, and that use GIS in the analysis (not for mapping only!). Finally, the full-text assessment of the final articles was used to review geospatial technologies for estimation of CS. The following subjects will be covered and evaluated: RS data types for estimating AGB and CS (Subsection 1.4.4.1); the RS-based methods used to attain a certain level of accuracy at the species/plant communities (multispecies) level (Subsection 1.4.4.2); surveys all biophysical predictors used in RS technology (Subsection 1.4.4.4); identifies significant RS variables (Subsection 1.4.4.5); highlights RS-GIS integrated models (Subsection 1.4.4.6); and presents arid lands case studies with challenges and opportunities (Subsection 1.4.5).

1.4.4.1 Remote Sensing Data Types

Data from RS satellites are available at various scales, from local to global, and from several different platforms. There are also different types of sensors both passive, such as optical and thermal RS sensors, and active, such as Radar and Light Detection and Ranging (LiDAR) sensors, with each having its advantages and disadvantages. Benefits and limitations of these sensors are shown in Appendix 2. The optical sensors, sometimes called passive sensors, are RS systems relying on visible and reflected infrared light (Zhao et al., 2016). Appendix 3 shows the specifications of the RS optical sensors most commonly used for AGB estimation. While active sensors are the sensors that emit and record backscatter values or interferometry technique in a portion of the electromagnetic spectrum (Ghasemi et al., 2011).

Despite the successful application of any sensors in AGB estimation, there are challenges related to acquisition costs, area coverage (swath width), and limited availability. RS data are nowadays abundant and widely available for a fraction of the

cost required only a decade ago. Furthermore, these data are captured with various, radiometric, spectral, spatial and temporal resolutions, hence meeting the needs for AGB detection, mapping and assessment. Selecting the "right" sensor is associated with the specific data availability of the area under study, project budget, technical skill requirements for data interpretation and software packages. The resolutions of the sensors used are pre-defined to meet the researcher's needs and specifications, although it happens that a specific sensor's data are the only available for a study area. Many software packages can perform digital images processing and spatial analysis like ERDAS imagine, ENVI, ArcGIS and other open source software like QGIS and Google Earth Engine. These packages are relatively easy to use and can produce exceptional results.

Statistical analysis based on the 171 papers reviewed reveals that around two thirds of these studies used passive (optical) sensors (with different spatial resolutions), while the remaining third used active sensors (almost equally split between RADAR and LiDAR) (Figure 4).
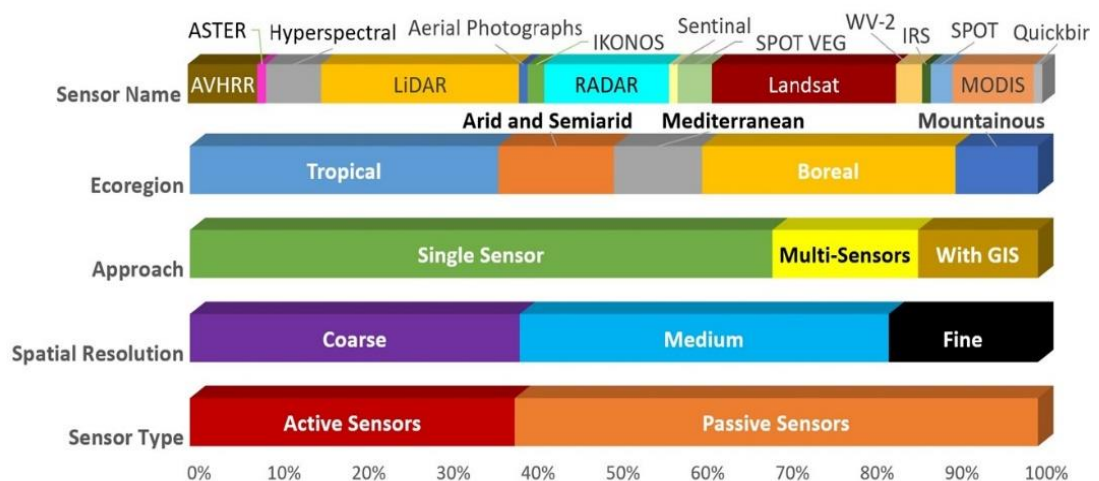
Figure 4: Geospatial input data used in reviewed papers at different forests. After (Dahy et al., 2019, 2020; Salem Issa et al., 2020a).

Around 40% of the studies using optical sensors used coarse spatial resolution (>100 meters) sensors like MODIS and SPOT VEG. Almost the same percentage of studies (40%) used moderate spatial resolution (~10- 100 meter) sensors like Landsat, IRS, and SPOT. Additionally, around 20% of these studies used fine spatial resolution sensors (sub-meter to 5 meters) like IKONOS, Quickbird and World View. To improve the accuracy of estimating AGB, integration of more than one sensor is becoming a trend (around 17% of the reviewed studies), as well as the integration with GIS-based approaches (around 14% of the reviewed studies). It was observed that more than 60 studies were conducted using these two approaches. Statistical results further showed that the number of studies that estimate AGB at plant species levels, instead of forests in general or mixed species, was increasing. Many plant species are not separable targets using RS because they are indistinguishable from other plants due to their spectral similarities (detecting, mapping, and classification of vegetation will be discussed in separate Subsection, 1.4.4.3).

Hence, resolution concerns such as high spatial resolution (e.g., IKONOS) and high spectral resolution (e.g., hyperspectral) should be taken into account as they help resolve such ambiguities and play essential roles in the quality of the resulting maps (Thenkabail et al., 2004). Nowadays, RS data are widely available for a fraction of their cost only a decade ago. Figure 4 shows the proportion of utilizing different sensors with different number of bands for the estimation of the biomass and carbon sequestered. Accurate image classification relies on the successful extraction of pure spectral signature for each species, which is often dictated by the spatial resolution of the observing sensor and the timing of observation (Xie et al., 2008). For example, archived and recent Landsat imageries are available and are freely downloadable from the USGS website, providing a globally consistent record of archived imageries since

1972; other resources are being continuously published and added to the internet. Bryceson (1991) used the habitat type, condition and soil type as the delineating parameters to locate *Chortoicetes terminifera* (Australian plague locust) by using Landsat-5 multispectral scanner data. Anderson et al. (1993) mapped *Ericameria austrotexana* infestation in a large homogenous area using Landsat Thematic Mapper (TM) imagery. The spectral radiances in the red and near-infrared regions, in addition to others, were used for vegetation mapping by RS technology. The spectral signatures of photosynthetically and nonphotosynthetically active vegetation showed noticeable differences and could be utilized to estimate forage quantity and quality of grass prairies (Xie et al., 2008). Moreover, discrimination of vegetation species from single imagery is only achievable where a combination of leaf chemistry, structure and moisture content culminates to form a unique spectral signature.

As the detection and estimation of biomass are sensed from space, the crown biomass component has gained prominence in the majority of the relevant studies (Cheng et al., 2014; Clark et al., 2005; Jucker et al., 2017; N\a esset & Økland, 2002; Ozdemir, 2008; Popescu et al., 2003). The unique pattern of crown palm plantations, for example, makes them easily distinguishable from other trees on satellite imagery (Shafri et al., 2011). It is worth mentioning that most of these studies were conducted on boreal and tropical forests with a small portion conducted on arid and semiarid regions (around 10%). This could be due to the early availability of geo-spatial technologies in the developed northern countries (boreal forests) and the relative importance of the tropical rainforests to the global carbon cycle (Figure 4).

1.4.4.2 Remote Sensing Based Methods

To explore the potential of RS-based methods for extracting biomass information in different environments, various techniques and sensors have been used

and tested in numerous studies. Optical, RADAR, and LiDAR data have been extensively used to estimate AGB with a variety of methods (Clerici et al., 2016a). AGB studies using geospatial technologies can be aggregated according to the level of the methodological complexity to several tiers including different levels of detail and accuracy. The Intergovernmental Panel on Climate Change (IPCC) proposed three tiers: Tier-1, Tier-2, and Tier-3 (Gibbs et al., 2007; Henry et al., 2011; TSITSI, 2016). Tier-1 is the basic method based on the 'biome average' approach. It is the simplest level using the globally available data, generalized equations, and provides a rough approximation of biomass, and hence CS, and could be used as a starting point for decision-makers; however, it can provide inaccurate results with a high level of uncertainty (Gibbs et al., 2007). Tier-1 considered a generalized biomass equation for the ecological zones, and is typically used when no species-specific equations exist (Henry et al., 2011). Tier-2 is an intermediate level that is based on the volume equation and wood density. It is used when species-specific volume equations exist, and woody density for the specific plant species is available. The volume is then converted to biomass using wood density and a default biomass expansion factor (BEF) (see Subsection 1.4.3) (Eggleston et al., 2006; Henry et al., 2011). Finally, Tier-3, the most demanding in terms of complexity and data requirements, is based on using a species-specific biomass equation to calculate either total or partial biomass. Partial biomass is obtained by adding up the biomass estimates obtained from the species-specific equations for the different compartments. Tier-2 and Tier-3 levels are more dependent on ground-based measurements of the tree (i.e., DBH and height) and building the predictive relationships (allometric equations) (Gibbs et al., 2007). This makes these two levels more expensive to implement than Tier-1. It is worth noting

here that the precision for a given species generally increases with the increase in the Tier number (Henry et al., 2011).

A geospatial approach is widely used to collect information regarding forest AGB and vegetation structure as well as to monitor and map vegetation biomass and productivity at large scales (Iizuka & Tateishi, 2015; Main-Knorn et al., 2011; Makinde et al., 2017; Pflugmacher, 2011). Using RS, GIS and modeling to study the current state of carbon sequestration and its future dynamics, are promising and have a potential ability as an innovative approach to tackle the ecological assessment problems (Lal, 2002). RS-based methods have seen widespread use among the research community thanks to their unique characteristics either in data collection or in results presentation. RS data can sense and record spatial variability, spatial distributions, spatial patterns of forests and assess their changes over time (Zhao et al., 2016).

For mapping vegetation using RS data, a multistep process is usually applied (detecting, mapping, and classification of vegetation will be discussed in separate Subsection, 1.4.4.3). The first step involves image preprocessing and aims at enhancing the quality of original images. For example, panchromatic band with 15 m spatial resolution, in Landsat imagery, that can be used to pan-sharpen other bands and hence increase their interpretability, has been added to Landsat's multispectral sensors (Phiri & Morgenroth, 2017). Previous studies showed that such use of the panchromatic band helped achieve dramatic improvements (15%) in classification accuracies (Gilbertson et al., 2017). The second step involves determining the level of vegetation classification (at community or species level). The third step determines the correlation between the vegetation types and spectral characteristics of RS imagery. Vegetation data is identified by interpreting satellite images based on the elements

such as image color, texture, tone, pattern and association information. Lastly, the final step includes translating the spectral classes into vegetation types by assigning each pixel of the scene to one of the vegetation groups defined in the vegetation classification system selected in the second step. Classification methods are broadly based on the pixel-based classification (PBC) approach or the object-oriented based classification (OOC) approach. Both methods have their advantages and disadvantages depending on their areas of applications, and most importantly, the RS datasets that are used for information extraction (Jawak et al., 2015). OOC methods group several pixels with homogeneous properties into an object/objects instead of pixels, which are considered as the basic unit for analysis, while PBC approaches are based on combining reflectance pixel values into separated spectral clusters (Blaschke, 2010; Myint et al., 2011a).

AGB and hence CS can be estimated from different RS data types using various approaches (Figure 5). Landsat series, for example TM, Enhanced Thematic Mapper (ETM+), and Operational Land Imager (OLI), have been historically used to map biomass and carbon in a variety of ecosystems, due to the relevance of their spectral bands, the continuity of the program, and the suitability of the 30 meter spatial resolution for regional mapping (Clerici et al., 2016a). Although biomass cannot be directly measured from space, the use of spectrally-derived parameters from sensor reflectance (bands), including vegetation indices (VIs) that were created to improve prediction accuracy, enables increased biomass prediction accuracy when combined with field-based measurements (Pandit et al., 2018).
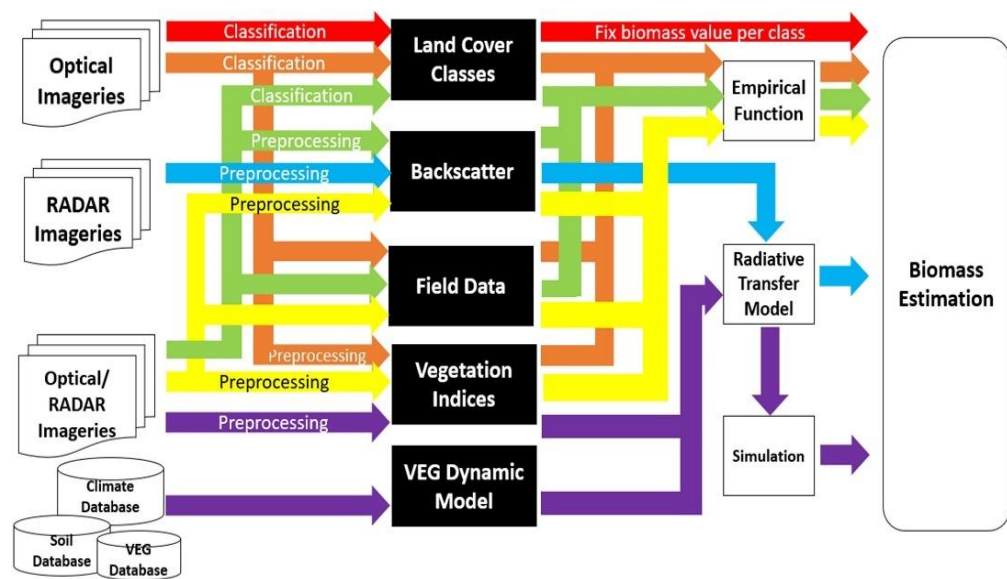
Figure 5: Different RS/GIS procedures available for estimating AGB. After (Eisfelder et al., 2012; Salem Issa et al., 2020a).
.

RS data correlates with plot-based field measurements to estimate AGB and hence CS. In general, RS data are empirically linked to AGB measurements of field plots using different regression analyses and algorithms (Wani et al., 2015). There are many methods of image analysis that can be integrated to achieve a better accuracy. Algorithm development and implementation is an important subject in studies estimating biomass (Kumar & Mutanga, 2017). The advanced machine learning algorithms methods and/or other state-of-the-art processing techniques can reveal important information about the spatial and temporal biomass patterns by determining relationships between field measurements and RS data, especially over large areas (Kumar & Mutanga, 2017). To determine the relationship between above-ground field biomass and RS data, researchers have used linear regression models with or without log transformations of field biomass data, and multiple regressions with or without stepwise selection (Clewley et al., 2012; Robinson et al., 2013). Artificial neural networks, semi-empirical models, nonlinear regression, and nonparametric estimation

techniques (e.g., k-nearest neighbor and k-means clustering) have also been used (Castel et al., 2000; Lu, 2006; Wijaya & Gloaguen, 2009). However, few studies have investigated approaches other than the empirical relationship with spectral bands or VIs (Eisfelder et al., 2012). One of these approaches is Monteith's efficiency model for obtaining indirect estimates of absorbed photosynthetically active radiation (APAR) from the red and IR reflectance characteristics of the vegetation where APAR is used as an indication of how efficiently absorbed energy is converted to dry biomass (Monteith, 1972). Rosema (1993) used a simulation of vegetation development from daily total evapotranspiration with the in/out radiation of METESTAT in order to estimate the herbaceous biomass in savannah grassland in Sahel countries. Other studies used canopy functioning process-based models coupled with physical radiative transfer models to estimate biomass production from RS data (Williams, 2010). Fourier transform textural ordination (FOTO) was used by Morel et al. (2012) with SPOT5 data for estimation AGB in Thailand with the R value equal to 0.83. Regression, ordinary kriging, co-kriging, and stepwise linear regression have been used in various studies and it was found that the combination of RS and geo-statistics can improve the accuracy of biomass estimates more than the use stepwise linear regression only (Mutanga & Rugege, 2006). Extensive field knowledge and expert knowledge may help improve classification accuracy. Studies have shown that classification accuracy can be greatly improved after applying expert knowledge (empirical rules) and ancillary data to extract thematic features (e.g., vegetation groups) (Xie et al., 2008). Fieldwork is the foundation for RS technology allowing to extend limited vegetation information to large scale predictions (Wu et al., 2016). This direct mapping approach is more accurate at depicting variations in biomass across the landscape, making it easier to update the maps as needed (Kelsey & Neff, 2014).

1.4.4.3 Detecting and Mapping Plant Species Using Satellite Imagery

Accurate mapping of vegetation is a critical and important task for many environmental-related issues such as forest management, biomass estimation, or terrestrial CS quantification. Geospatial technologies (RS & GIS) are well established for their capabilities of measuring and estimating forest AGB and for monitoring and mapping vegetation biomass at large scales (Dahy et al., 2019; Iizuka & Tateishi, 2015; Main-Knorn et al., 2011; Makinde et al., 2017; Maynard et al., 2007; Pflugmacher, 2011; Salem Issa et al., 2020a). Methods for measuring and mapping vegetation cover using RS and GIS are well developed; however, they exhibit performance issues in certain ecosystems particularly, arid land ecosystems where a high background reflectance contribution to the pixel value remains a great challenge. Besides, several plant species are hardly distinguished from other objects because of their spectral resemblances. The advent of high spectral and spatial resolutions data helped in resolving such ambiguities and played an essential role in improving the quality of land cover maps (Thenkabail et al., 2004). Furthermore, satellite imagery variables are only capable of mapping and correlating environmental variables if the vegetation spectra are detectable within the pixel, a great challenge that can only be overcome in certain arid land environment (Aly et al., 2016a; Oldeland et al., 2010; Tian et al., 2016). This last constraint presents a foremost challenge in the desert ecosystem, usually with sparse vegetation cover, producing a weak spectral object requiring a higher resolutions' imagery to be captured (Bradley et al., 2019). Hyperspectral sensors showed plausible classification accuracies in mapping major forest species and predicting the susceptible areas of fruit malformation (Nagaraja, 2009). Hebbar et al. (2014) used LISS-IV data to classify fruit trees and found that old and mature plantations were classified more accurately while young and recently planted ones (3

years or less) showed poor classification accuracy due to mixed spectral signature, wider spacing and poor stands of plantations. While high-resolution data offer more spatial detail, they present certain disadvantages including high cost especially when it applies to broad areas, the need for large data storage, complex technicalities and long processing times. Furthermore, moderate resolution satellites (e.g. Landsat, and SPOT) proved to be effective in land cover classification for different research purposes and in different regions (Aly et al., 2016a; Elhag, 2016; Rembold et al., 2000; Shaker et al., 2012). Such multispectral optical sensors have been widely utilized operationally in estimating and mapping AGB (Eisfelder et al., 2012; Kumar et al., 2015; Kumar & Mutanga, 2017; TSITSI, 2016; Vashum & Jayakumar, 2012). Indeed, moderate resolution satellite data offer plausible results after conducting specific approaches such as pan-sharpening or fusion techniques. Starting with Landsat-7 ETM+, a panchromatic band with 15 m spatial resolution, that can be used to pan-sharpen other bands and hence increase their interpretability, was added to the already existing Landsat's multispectral sensors (Phiri & Morgenroth, 2017; Shaharum et al., 2018). Previous studies showed that such use of the panchromatic band helped achieve dramatic improvements (more than 15%) in classification accuracies (Gilbertson et al., 2017). The Landsat program, MSS, TM, ETM+ and the most recent Landsat-8 OLI, present unique advantages in land cover classification applications because: (1) it is the longest running uninterrupted Earth observation program since 1972; (2) its archives are the first to offer global images free of charge (free access approach since 2008) (Phiri & Morgenroth, 2017; Turner et al., 2015); (3) the current effects of climate change make the research on land cover classification methods based on the archived Landsat images an important resource (Barbosa et al., 2014; De Sy et al., 2012); (4) it is a very good source for vegetation change detection over large areas due to its

relatively high temporal resolution (16-days revisit) and large swath (185 km); (5) another benefit of Landsat is to offer atmospherically corrected reflectances. Atmospheric correction is a critical step to minimize aerosol and cloud contamination and; (6) the suitability of the spatial resolution of Landsat series for regional mapping of biomass and carbon in a variety of ecosystems (Clerici et al., 2016b). Baumann et al. (2018) found that Landsat-8 OLI is reliable for mapping woody vegetation (tree cover and shrub cover) in their study in Gran Chaco, south America. In their study for mapping tree canopy cover and AGB in woodlands landscape of Burkina Faso using Landsat-8 OLI, Karlson et al. (2015) found that the image texture is more correlated to tree cover attributes, in particular AGB, in open canopy conditions compared to closed canopies due to its ability to capture shadow structures caused by large trees (Karlson et al., 2015).

There is no universal classification system that can be used for all types of imagery, at different scales, and for different purposes. Classification methods are broadly divided in two categories: pixel-based classification (PBC) and object-based classification (OOC). They both have advantages and disadvantages depending on their areas of applications and, most importantly, the RS datasets they use for information extraction (Jawak et al., 2015). PBC methods are based on using reflectance values to group pixels into separate spectral clusters; while OOC methods group contiguous pixels with homogeneous properties into objects, referred to as segments, that serve as the basic units for analysis (Blaschke, 2010; Myint et al., 2011b). OOC methods have gained increased interest with the advent of high and very high-resolution RS imagery (Jawak et al., 2013). Furthermore, OOC paves the way for combining spectral and spatial information, and in doing so potentially offers a more comprehensive classification approach that increases the results' accuracy (Wang et

al., 2016). However, under- and over-segmentation errors may occur in the segmentation phase and lead to a reduction of classification accuracy; especially when an image object covers multiple classes. This usually leads to classification errors as all pixels in each mixed image object are assigned to the same class (Jawak et al., 2015; Liu & Xia, 2010).

PBC, on the other hand, has proven very successful with low to moderate spatial resolution data. It uses a combined spectral response from all pixels in a training set for a target class. The resulting signature comprises spectral responses from a group of different land covers in the training samples, while the classification system merely ignores the impact of mixed pixels (Lu & Weng, 2004). PBC is commonly divided into supervised and unsupervised classification methods. Both approaches, separately or together, were used widely to run LULC classification in many regions and both have advantages and disadvantages. The use of vegetation indices (such as NDVI, EVI, SAVI) is considered as part of the unsupervised classification method. These indices use vegetation spectral characteristics to assess the status of vegetation cover (see Subsection 1.4.4.5).

The conventional PBC is quite limited because images of medium to low resolutions present a high level of heterogeneity and internal class variation within the same scene (Kux & Souza, 2012). OOC approach considers the organization of individual pixels into groups (segments) that correspond to real-world objects in the identification of classes. Object-oriented image analysis involves partitioning the image into meaningful segments that replace pixels as the basic processing units (Benz et al., 2004). In general, the OOC algorithm initially performs segmentation of the whole image, then, the user defines a set of knowledge-based classification rules (spectral, spatial, contextual and textual information) to describe each class.

Thereafter, the classifier is chosen to assign each segment to the proper class according to the user-defined rules (Jawak et al., 2015). The OOC procedure involves the selection of training samples that represent the features to be classified. These features (objects) are then defined within the software based on rules that are further used to model the individual or groups of objects based on color, size, shape, position, direction, distance, orientation, distribution throughout the image, texture, as well as other user-defined parameters.

Many algorithms were developed for tree crown detection and mapping, (Chepkochei, 2011; Hebbar et al., 2014; Lack & Bleisch, 2010; Rizvi et al., 2019; Sahay et al., 2017). Nevertheless, different methods may give different results while working in the same environment. Consequently, the results of tree detection and mapping can be affected by algorithm features. It is imperative to select the proper algorithm to get appropriate results. Likewise, for any algorithm to work properly, crowns should be detectable and segmented as an object in the image before classification. Training sets of the different classes to be identified and mapped must be selected very carefully for not to contain any contribution from the background nor any other class reflectance. This can be done by visual analysis and based on the interpreter's expertise and knowledge of the study area.

Hybrid classification approaches that combine supervised and unsupervised algorithms have gained importance. Since the early 1990s, several hybrid methods have been tried and refined in many cases to improve classification accuracy (Jawak et al., 2015; Kamusoko & Aniya, 2009; Kuemmerle et al., 2006; Lo & Choi, 2004; Pradhan et al., 2010; Rozenstein & Karnieli, 2011; Shila, 2010). Hybrid methods have demonstrated significant improvement in results' interpretation where there is complex variability in the spectral data within information classes. The algorithms of

most hybrid methods involve: 1) initial arrangement of the imagery by spectral clustering, 2) assigning clusters to user-defined classes, and 3) classification of the entire image using supervised learning (Jawak et al., 2015). Lo and Choi (2004) suggested that a hybrid approach can be economically implemented in a standard image processing software package to produce LULC maps with higher accuracy (up to 96% in urban) from moderate spatial resolution data ETM+ (Lo & Choi, 2004). In their study in eastern Europe, Kuemmerle et al. (2006) combined the advantages from supervised and unsupervised methods to derive a land cover map from Landsat data (Kuemmerle et al., 2006). They conducted unsupervised classification to minimize bias in the selection of training areas and seed signatures, then eighty class signatures were extracted to run the supervised classification using the maximum likelihood classifier. The accuracy of the approach was estimated at 84%, 87%, and 91% for agriculture area, forests, and dense forests respectively. Shila (2010), used a hybrid classification method in Isfahan, Iran from ETM+ to increase automation and improve the accuracy of image data classification by taking advantage of both supervised and unsupervised classification methods. They found that the accuracy of the produced map reached 93%. Rozenstein and Karnieli (2011) examined combining signatures from both supervised and unsupervised training data (hybrid classification) and showed that they provided significantly more accurate results in Negev desert using TM image.

The majority of the UAE's territory is formed of desert ecosystems representing the mainland cover class of the country's land area. Date palm (DP) species are known for their resilience to hard conditions requiring minimum water supply, tolerating high temperatures and drought, and sustaining high levels of salinity (see Subsection 1.4.1). Measurement and analysis of DP in the UAE, using RS and

GIS techniques, are almost absent and have seen very limited application examples in the country and the Gulf Cooperation Council region at large (Issa & Al Shuwaihi, 2012). Such investigations are vital for DP planning, management, and related resource studies. Sohl (1999) used multi-temporal TM imageries to provide locational, quantitative, and qualitative information on land cover change within the Abu Dhabi Emirate. His main concern was mapping changes in vegetation cover in Abu Dhabi emirate in general rather than DP. Goudie et al. (2000) have applied a cartographic approach to study coastal changes in Ras Al Khaimah (UAE); they reconstructed the history of coastal change in the study area. Alhameli and Alshehhi (2004) used historical aerial photographs, images and old documents to describe the rapid development of the UAE on selected sites with no measurements or analysis of DP mapping or other related parameters. Abdi and Nandipati (2010) investigated land cover changes in Abu Dhabi capital city and surrounding regions from 1972 to 2000 using Landsat images. The study conducted a simple change detection analysis of four land cover classes; none of them focused on DP plantations.

1.4.4.4 Biophysical Predictors

The biophysical predictors of vegetation growth need to be considered in RS studies due to the different rates of growth of various parts of vegetation (Chong et al., 2017). These predictors can be detected by remote sensors and are manifested through shadow, roughness, and spectral response (McMorrow, 2001). RS variables measured and correlated with biomass quantification include the spectral reflectance of vegetation as the spectral properties of AGB obtained by the sensors have unique signature correlated with chlorophyll content in the plants (Lu, 2006). The signals are sensitive to AGB structure and influenced by density, shadow, texture, soil moisture and roughness, and constitutes one of the RS variables used in estimating biomass

(Baccini et al., 2008; Eisfelder et al., 2012). The biophysical predictors used for estimating biomass include leaf area index (LAI), chlorophyll content, leaf nutrient concentration, height, DBH, stand basal area, greenness of canopy, and crown measurements like crown area (CA) and crown diameter(CD). All of these predictors are traditionally used to estimate biomass, but only some are applicable for RS based estimation (Figure 6).
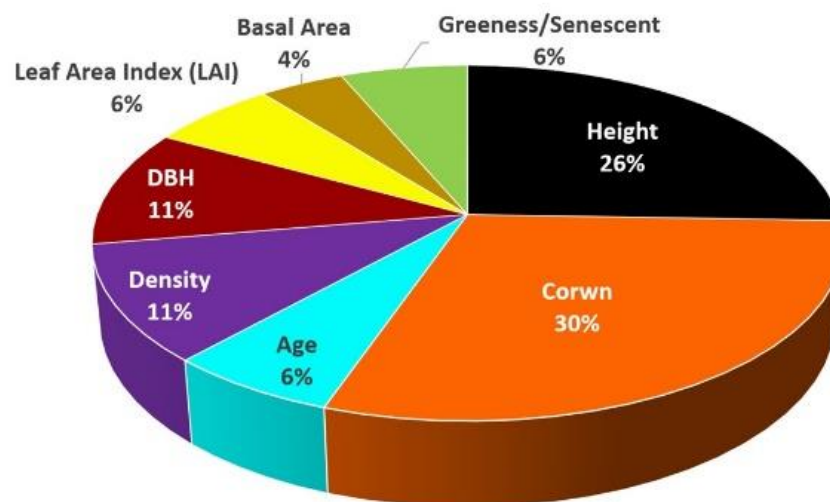
Figure 6: Different biophysical parameters used in RS based estimation of AGB. After (Dahy et al., 2020; Salem Issa et al., 2020a).

Xiaoming et al. (2005) observed a robust logarithmic correlation between LAI and AGB. LAI can be defined as the area of one-sided leaf tissue per unit ground and measures the density of the leaves surface in a canopy. Tan et al. (2013) estimated LAI of oil palm in Malaysia using UK-DMC2 and ALOS PALSAR. They concluded that an increase in the LAI shows a proportional increase in the spectral reflectivity or Normalized Difference Vegetation Index (NDVI) during the initial growth stage; however, it presents little to no increase once it attains the full canopy cover due to sensor saturation. The ability of hyperspectral RS to collect reflectance in many narrow bands makes it particularly useful for extracting vegetation parameters, such as LAI,

chlorophyll content, and leaf nutrient concentration (Im & Jensen, 2008). Large scale photographs have been used to measure various forest characteristics, such as tree height, CD, crown closure, and stand area (Clark et al., 2005). In their study on the indirect estimation of biomass, Popescu et al. (2003) used RS data to determine tree canopy parameters, such as CD, using multiple regression analysis and canopy reflectance models. The CA can be measured by satellite imageries and, thus, provide biomass estimation. Suganuma et al. (2006) found that medium-resolution or more detailed spatial resolution data could be used for the crown coverage. Crown projection area (CPA), which is the canopy area that is covered by an individual tree, can be calculated by delineating trees using object-based image analysis (Chong et al., 2017; McMorrow, 2001). Greenberg et al. (2005) have effectively used IKONOS data (spatial resolution 4 meter) for estimating crown projected area, DBH and stem density. Song et al. (2010) estimated tree crown size from IKONOS and Quickbird images and concluded that this approach could provide estimates of average tree crown size for hardwood stands.

Height information of a tree can be retrieved using various approaches of RS, e.g., LiDAR and Radar. Height has been shown to be a potentially successful indicator for age in oil palms, for example, and it is widely used in estimating forest biomass (Chong et al., 2017). Radar backscatters (P and L bands) are positively correlated not only with tree height and age but also with other major biophysical forest parameters such as DBH, basal area, and total AGB (Kumar et al., 2015). LiDAR sensor can directly measure three-dimensional (3D) components of vegetation canopy structure and is widely used in the estimation of forest biophysical parameters (Appendix 2). LiDAR data are used for biomass estimation for different forest environments; tropical forest biomass, temperate mixed deciduous forest biomass, and in measurements of

biophysical parameters such as tree height and stand volume, and CD and canopy structure in general. The two-dimensional data (2D) have limitations in estimating vertical vegetation structures such as canopy height, which is one of the critical biophysical parameters for biomass estimation (Appendix 2). Recently, optical data such as ALOS, panchromatic RS instrument for stereo mapping (PRISM), IKONOS stereo satellite images, and SPOT have been used to provide a stereo viewing capability that can be used to develop vegetation canopy height, thus improving biomass estimation performance. St-Onge et al. (2008) assessed the accuracy of the forest height and biomass estimates derived from an IKONOS stereo pair and a LiDAR digital terrain model. Reinartz et al. (2005) used SPOT 5 HRS for forest height estimations in Bavaria and Spain, while Wallerman et al. (2010) investigated 3-D information derived from SPOT 5 stereo imagery to map forest variables such as tree height, stem diameter and volume.

1.4.4.5 Remote Sensing Variables

Vegetation indices are generally used to estimate biomass in many studies (Clewley et al., 2012; Robinson et al., 2013; Schlerf et al., 2005; Salem Issa et al., 2019; Terakunpisut et al., 2007). VIs are calculated from mathematical transformations of the original spectral reflectance data and can be used to interpret land vegetation cover (Das & Singh, 2012). VIs are applied to remove the variations caused by spectral reflectance measurements while also measuring the biophysical properties that result from the soil background, sun view angles, and atmospheric conditions (Lu, 2006). The notion of VI is well adapted for quantifying vegetation over large areas, for example, over areas covering many pixels of an image (Bannari et al., 1995). VIs are quantitative measurements indicating the vigor of vegetation. They show better sensitivity for the detection of biomass than individual spectral bands

(Bannari et al., 1995). Previous studies have shown a significant positive relationship between biomass and VIs (Patel et al., 2007). In order to examine the relationship between AGB and RS variables including individual band reflectance values and VIs, Günlü et al. (2014) used Landsat TM in their study and found that VIs present better estimation of AGB in Anatolian pine forests with R^2 equal to 0.606, compared to individual band reflectance with R^2 of 0.465.

AGB models could be developed using many available predictors, grouped into two distinct categories: raw bands of the sensor as reflectance and VIs, including the simple ratio (SR), difference vegetation index (DVI), NDVI, ratio vegetation index (RVI), global environmental monitoring index (GEMI), soil adjusted vegetation index (SAVI), enhanced vegetation index (EVI), tasseled cap index of greenness (TCG), tasseled cap index of brightness (TCB), tasseled cap index of wetness (TCW), and many others. All these indices can measure the presence and density of green vegetation, overall reflectance (e.g., differentiating light from dark soils), soil moisture content, and vegetation density and structure). Most VIs rely on red and infrared (IR) bands, which are the raw bands present in earth observation satellites and often contain more than 90% of the information related to vegetation (Baret et al., 1989; Huete, 1988; Jiang et al., 2008; Pinty & Verstraete, 1992; Turner et al., 1999). Early studies have shown that both the simple ratio (Near Infrared /Red) and the NDVI were closely related to dry matter accumulation (Baret et al., 1989). The use of vegetation and other indices (e.g., NDVI, EVI, SAVI) are considered as part of the classification method. The principle of applying NDVI, for example in vegetation mapping, is that vegetation is highly reflective in the near infrared (NIR) and highly absorptive in the visible red. The contrast between these channels can be used as an indicator of the vegetation greeness (Xie et al., 2008, p. 200). Sonnenschein et al. (2011) used NDVI, SAVI and

TCG from Landsat imageries for forests mapping in Greece. In a study conducted in Saudi Arabia, Aly et al., 2016b found that NDVI images of Landsat could be classified into three classes of vegetation cover in arid regions, namely dense vegetation cover (NDVI > 0.5), moderate vegetation cover (NDVI 0.25–0.5), and sparse vegetation cover (NDVI < 0.25). The ability of VIs to separate the vegetation from its background varies from one ecoregion to another, and from one plant species to another. VIs commonly used to estimate biophysical variables such LAI, APAR and biomass include NDVI, EVI, and SAVI (Kumar et al., 2015, p. 20). NDVI is a prominent and frequently used index with different spatial resolutions of the optical sensors (Figure 7). Thenkabail et al. (2004) implemented a regression model using NDVI and optical bands reflectance number 3 and 4 of IKONOS for estimation of AGB for oil palm in Africa, with 64–72% accuracy. Morel et al. (2012) found that the Normalized Difference Fraction Index (NDFI) of Landsat ETM+ data performs better when estimating AGB for oil palm in Malaysia with kappa coefficient equal to 0.87. Srestasathiern and Rakwatin (2014) found that the best performing VI to separate oil palms from its background was the Normalized Difference Greeness Index (NDGI), which is a normalized ratio of green to the red band, and displays the highest discriminating power using a histogram dissimilarity metrics. Nevertheless, these results could not be generalized as all VIs must be tested. Zhao et al. (2016) examined specific spectral bands of Landsat and their relationships with AGB in the Zhejiang province of Eastern China. They found that, when the forest stand structure is complex, VIs including shortwave infrared spectral bands (SWIR) had a higher correlation with AGB than others. However, the VIs including NIR wavelength improved correlations with AGB in relatively simple forest stand structures. VIs can maximize the sensitivity for recording the green vegetation situation (Günlü et al., 2014). The choice of

adequately performing VIs depends on the type of ecosystem, the environmental conditions and the spectral information available. In their study on forests in Bogotá, Colombia, Clerici et al. (2016a) estimated AGB and found that the best performing AGB estimation model was based on the RVI, with R^2 equal to 0.582. They also found that atmospheric and topographic correction was vital in improving model fit, especially in high aerosol and rugged terrain.
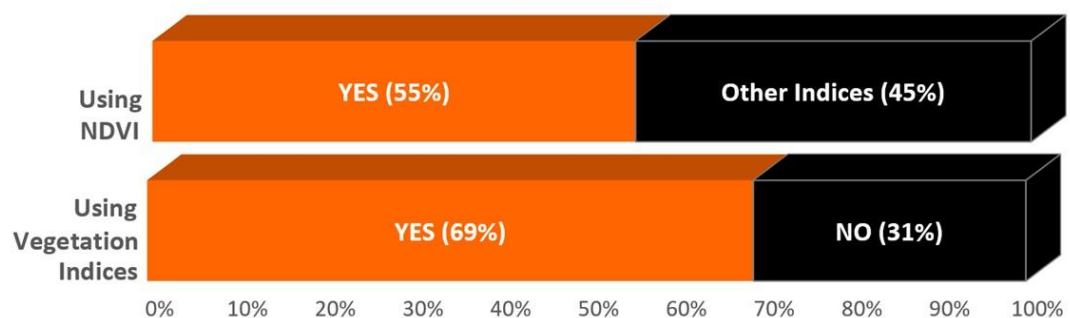
Figure 7: The use of vegetation indices and NDVI for estimating AGB. After (Dahy et al., 2020; Salem Issa et al., 2020a).

However, some studies had shown poor relationship between biomass and VIs compared with using raw bands (Onisimo, Mutanga & Skidmore, 2004). Singh et al. (2014) used two optical sensors (Landsat TM and SPOT 5) to assess their efficacy and evaluate disparities in forest composition and AGB in Sabah, Malaysia. They found that NDVI derived from SPOT 5 could distinguish between pristine forests and oil palm plantations. In fact, the reflectance values of bands 3 (red sensitive) and 4 (NIR sensitive) of Landsat TM were strongly correlated with the field-based AGB values while both VIs derived from Landsat TM and SPOT 5 (such as NDVI) were weakly correlated with the field-based AGB values. The data saturation problem in Landsat imagery is well recognized and is regarded as an important factor resulting in inaccurate forest AGB estimation, especially when AGB is high (>130 Mg.ha^{-1}) and

when the forest structure is heterogeneous (Zhao et al., 2016). In a study to estimate total living biomass of Miombo woodlands of Tanzania, Gizachew et al. (2016) found no clear evidence of data spectral saturation at higher biomass value in open canopy woodlands. They suggested that Landsat-8 OLI derived NDVI could be used as suitable auxiliary information for carbon monitoring in the context of the reducing emissions from deforestation and forest degradation program (REDD+).

1.4.4.6 Remote Sensing/GIS Integrated Models

GIS is a platform hosting spatial databases capable of assembling and integrating geographically referenced data, running spatial analysis, and integrating various types and formats of spatial data (Ardö & Olsson, 2003; Deng et al., 2011; Kamusoko & Aniya, 2009). A repository of various data sources (e.g., forest inventory, land use maps, elevation and RS data) can be used to measure vegetation parameters over large areas (Labrecque et al., 2006). GIS is usually employed to process model inputs and to visualize results (Deng et al., 2011). However, building GIS-based models to predict future scenarios for forest management and the implementation of afforestation plans is another, more valuable product. In RS-GIS integrated models, RS data are used as input to the GIS model; where GIS act as a platform for data layering and database building in order to perform spatial data analysis and map creation. This not only saves time, but also allows for faster and better communication between research centers across the globe (Deng et al., 2011). The use of geospatial modeling to study the current state of carbon sequestration and its future dynamics is a promising technique; it has the potential ability to tackle the ecological assessment problems (Rattan Lal, 2002). Furthermore, as mentioned above, the integration of RS data into GIS models enables adding ancillary and field data (soil, climate, topography, etc.), in the analysis and increasing reliability in estimating AGB. For example, there are different GIS-

based AGB estimation models that integrate other data models such as: digital terrain model (DTM), rainfall models, canopy height models, atmospheric scattering models, biomass production models, grazing models, 3D forest structure models and regression models (Aranha et al., 2008; G. Baumann, 2009; Cho et al., 2012; Deng et al., 2011; Gernhardt et al., 2010; Greenberg et al., 2005; Holm et al., 2003; Le Maire et al., 2008; Li et al., 2008; Maynard et al., 2007; Montaghi et al., 2013; Ibrahim Ozdemir & Karnieli, 2011; Ramachandran et al., 2007; Thakur & Swamy, 2012; Wang et al., 2010). An integrated classification approach, coupled with GIS analysis, has been employed successfully to improve LULC, forest, and biomass mapping for Landsat data (Kamusoko & Aniya, 2009; Labrecque et al., 2006; Ohmann & Gregory, 2002). Results show that an integration of RS and spatial analysis functions in GIS can increase the overall classification accuracy from 50.12% to 74.38% (Myint et al., 2011a). Furthermore, the integration with GIS-based models are becoming more common, used in around 14% of the reviewed studies (Figure 4).

1.4.5 Arid Lands Case Studies

Mapping vegetation for accurate measuring of biomass and assessing CS is a significant challenge, specifically for arid lands, where RS has unique challenges that are not typically encountered in other sub-humid or humid regions. Major challenges include low vegetation signal-to-noise ratios, high soil background reflectance, presence of biological soil crusts, high spatial heterogeneity from plot to regional scales, and irregular growing seasons due to unpredictable seasonal rainfall and frequent periods of drought (Bestelmeyer et al., 2015; Cheng et al., 2017; Haughton et al., 2018; Wu & Archer, 2005). Additionally, there is a relative discontinuity in the long-term measurements in arid lands, which hampers reliable calibration and

evaluation of RS data products. Consequently, RS techniques developed in other ecosystems often result in inaccurate estimates of arid lands ecosystem CS.

Arid lands, defined as regions where annual potential evapotranspiration substantially exceeds precipitation, are critically important to society, yet exceptionally vulnerable to climate change (Smith et al., 2019). Arid lands make up to 40% of the Earth's land surface and provide ecosystem services to more than two billion people, including supporting significant crop production and forage for wildlife and domestic livestock (Bestelmeyer et al., 2015). RS images can reduce the complexity of fieldwork by collecting quantitative and qualitative information at regular intervals and enabling the mapping of inaccessible places, as is the case in most arid regions (Abburu & Golla, 2015; Al-Ahmadi & Hames, 2009; Diouf & Lambin, 2001; Holm et al., 2003; Mangiarotti et al., 2008; McGwire et al., 2000; Olsen et al., 2015; Ibrahim Ozdemir & Karnieli, 2011; Qi, Huete, et al., 1994; Ren et al., 2011; Ritchie & Rango, 1996; Schucknecht et al., 2015; T. Svoray et al., 2001; Tal Svoray & Shoshany, 2003; Tucker et al., 1985; Wylie et al., 1995).

In their review, Eisfelder et al. (2012) stated that RS studies of vegetation in arid regions are scarce, and additional methodological research is needed to address the specific challenges faced by RS techniques in these environments. In this review, out of the 171 reviewed studies conducted from 1984 to 2020 to estimate AGB, only 15 studies were conducted in arid lands and another 24 studies in semiarid ecosystems (more than a third of these studies were conducted in Niger and Senegal). Figure 8 shows the proportions of RS-based AGB estimation studies in arid and semi-arid regions taking into account the proportion of reviewed studies, sensors used and their spatial resolutions, the use of GIS tools and locations of the studies.
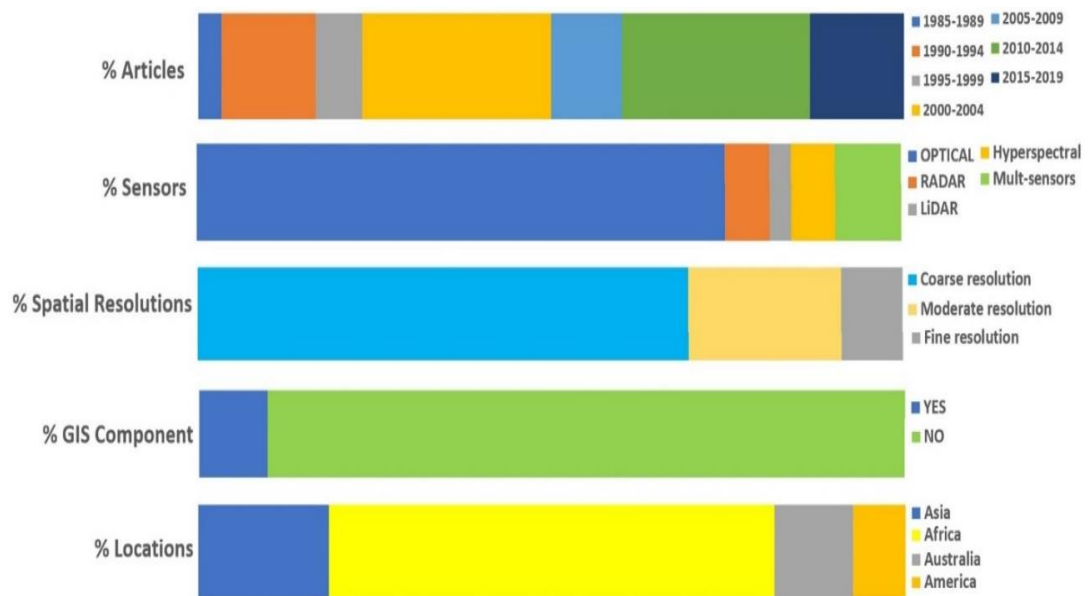
Figure 8: Studies on estimating AGB using RS in arid/semiarid ecosystems. After (Salem Issa et al., 2020a).

As mentioned above, monitoring the spatiotemporal dynamics of arid lands ecosystem structure and function is therefore a high research priority. Although the methods detailing vegetation cover mapping and estimation integrating RS and GIS are well developed, research on RS-based biomass estimation for arid lands is relatively scarce compared to other ecosystems (tropical, subtropical, temperate and boreal forests) (Eisfelder et al., 2012). Very few biomass measurements are available for plant species in desert ecosystems. Although biomass per unit area is normally low in those regions, the vast extent of the Earth's arid lands gives it a significant role as a carbon pool and for the supply of essential ecosystem services (Zandler et al., 2015). Studies showed a strong link between desertification and emission of CO_2 from soil and vegetation to the atmosphere (Lal, 2001). Desertification, and degradation of soils and vegetation in arid lands resulting from climatic and anthropogenic factors, affects more than one billion hectares of soils and more than 2.5 billion hectares of rangelands globally. Furthermore, an alarming estimate of six billion hectares of land is affected

by desertification per year (Lal, 2001). Lal (2001) concluded that the total world historic loss of carbon due to desertification in the period between 1850 and 1998 was in the order of 19–29 petagram (Pg), an amount that could have been sequestered (1 Pg = 10^{15} gram). Information on biomass helps to quantify the resilience of arid land systems and is thus essential for sustainable land-use management (G. Baumann, 2009). Hence, suitable methods to map biomass in arid land regions still need to be developed (Mangiarotti et al., 2008).

If plant species are very scattered, which is the case for most arid lands ecosystems, where vegetation is characterized by its patchiness pattern, the background reflection is mostly related to the soil. Hence, the selection of sites must be characterized by their relatively high density of plant species under study in order to reduce the background effects as much as possible. In addition, the selected sites must be relatively large in area and be homogenous, to enable the extraction of real spectral signature that represent the species to be mapped or to use a minimum number of field plots within each pixel as well as to increase the spatial/spectral resolution of the sensors used (Eisfelder et al., 2012). Moreover, using satellite images to map and correlate biomass is only possible if the target vegetation spectra are strong enough to be identified within the pixel (Aly et al., 2016b; Oldeland et al., 2010; Tian et al., 2016). This presents a major challenge in the desert where vegetation is usually sparse, offering a small spectral target that requires higher resolutions to be detected (Bradley et al., 2019). In the desert environment in China, Ren et al. (2011) estimated crop biomass of individual components (e.g., leaves, stems) for the whole season using red edge reflectance of hyperspectral data. Optical RS probably provides the best alternative to biomass estimation using RS due to its historic global coverage, repetitiveness and cost-effectiveness and thus is useful and operational in dry lands.

Such regions can be found in most of the low-income developing or least developed countries. Zandler et al. (2015) used Landsat 8 OLI in the arid regions of Tajikistan to model total biomass in extremely low vegetation cover. The coverage of the SWIR spectral region showed the importance in detecting shrubs or nonphotosynthetic vegetation. To deal with soil brightness, the study used additional soil adjusted VIs variations such as SAVI, transformed soil-adjusted vegetation index (TSAVI), and modified soil-adjusted vegetation index (MSAVI) as VIs suffer from various soil effects, especially when vegetation cover is low. The study indicated that biomass quantification in this arid setting is feasible but is subject to large uncertainties. One of the main challenges is the extreme aridity and the associated strong influence of soil background. Another challenge is the fact that large parts of arid or desert plants consist of nonphotosynthetic, woody matter and hence the photosynthetic signal, captured by most spectral bands and indices, may be low in relation to the biomass amount.

1.4.6 Learning Lessons from the Literature Review

Geospatial technologies are practical, feasible and can provide an adequate mean for AGB assessment monitoring, modeling and management of carbon sequestration. This conclusion is the main outcome of this literature review and is consistent with the consensus of numerous scientific papers on the subject published in the last five decades. The use of these technologies is an efficient tool, especially for developing countries, for measuring, mapping, monitoring, modeling and management of their CS in biomass and soil; leading to improve soil and plant productivity, to increase food security, and to control land degradation. In their turn, these countries can play a significant role in reducing the negative impact of climate change, by mitigating carbon emissions. Of course, there are many methods that can

be used for estimating CS, and all of them have their advantages and disadvantages. Traditional methods, relying on heavy fieldwork measurements, are the most accurate, however, they require significant time, expense and labor, and can be damaging for the ecosystems.

Building allometric equations can help avoid the destructive nature and other disadvantages of the fieldwork method. However, most of the allometric equations are mixed species-equations and not tailored for single one specie; most of them are also built for specific sites and ecosystems (less applicable for arid regions). Also, it is now more and more recommended to build allometric biomass equations that are correlated with and rely more on geospatial techniques to estimate biomass and CS (crown and height attributes). Building a database including the rates of carbon sequestered and stored for each plant species, especially those with high economic values, will fill the gap and increase the understanding of the atmospheric carbon sequestration potential of plant species and ecosystems.

The use of geospatial technologies should always be accompanied by ground measurements for verification and model validation of results which are required at some stages in the estimation of biomass. The best fit methodology relies on both fieldwork and the analysis of RS data and GIS techniques. The suggested process involves three steps, including: pre-field preparations to identify sample areas of interest, fieldwork that includes sample collection and measurement of plant characteristics, and post-field activity that focuses on processing RS data, classification, GIS model development and validation. Assessing CS remotely and consistently over large areas varies greatly depending on the type of instruments used, and the platforms. Nevertheless, these difficulties can be solved and tackled using different sensor options and other innovative methods, and hence avoiding the

limitations that relate to these aspects such as scale, cost, and associated errors and uncertainties.

High resolution RS data are the most accurate. However, moderate resolution satellite data, such as Landsat, have shown to be effective in estimating AGB and, consequently, CS, with good accuracy. Furthermore, these sensors provide invaluable historical data to monitor the change of CS over time. Developing algorithms that combine more than one remote sensor is highly important for tackling the challenges associated with estimating AGB and subsequently assessing carbon sequestration. Merging and fusion of more than one set of data have the potential to reduce uncertainty errors in biomass estimation. In such studies, it is important to consider the effects of bioclimatic factors depending on parameters such as plant age, species, forest type, rainfall, topography, vegetation structural variations, heterogeneity of landscapes, and seasonality. One of the common challenges in achieving this, is mapping the spatial patterns of vegetation and soil carbon and producing geo-referenced estimates of carbon. Such maps provide a better understanding of carbon dynamics and help quantify the regional and global carbon budgets. In addition, this will provide decision-makers with a strong knowledge base to be able to identify and focus on the most essential issues.

The arid lands RS-GIS research should be given a high research priority, especially given that more than 2 billion people depend on services provided by arid lands ecosystems. A combination of the field-based measurements and geo-spatial approaches reviewed have the potential to help improve carbon estimation to reduce emissions resulting from deforestation and forest degradation, and to design incentive programs in arid land regions. Therefore, it can be applied to enhance the decision-

making process on sustainable monitoring and management of carbon sequestration like afforestation, reforestation, and forest conservation projects.

1.5 Structure of the Dissertation

Chapter 2 covers the overall methodology of the dissertation. Subsections 2.1 and 2.2 specifically focus on the study area of Abu Dhabi and its geographic setting while Subsection 2.3 focuses on the RS data used during the course of this research. Subsections 2.5, 2.6, and 2.7 describe in details the proposed procedures of the developing of allometric equations for data palm (from 2.5.1 to 2.5.4), classification of LULC & accurate mapping of date palm plantations (from 2.6.1 to 2.6.4), and building RS-based models for biomass and carbon stock estimation of date palm plantations (from 2.7.1 to 2.7.6).

Chapters 3, 4, 5, and 6 display the results of applying the proposed methodology explained in the previous chapter (Chapter 2). Chapter 3 shows the results of developing date palm biomass allometric equations and calculating the carbon stock both, in date palms and their soils. Subsections 3.2.2. and 3.2.3 focus on calculating the biomass of date palm at different biomass components, while Subsection 3.2.4 focuses on estimating the carbon stock in date palm at different age-stages. Chapter 4 highlights the results of a pilot study in a date palm farm (AlFoah, north of AlAin city) to assess carbon stock in date palm plantations by using remote sensing and field measurements. Subsection 4.2.3 shows the built RS-based models to estimate biomass on different age classes (mature, non-mature, and mixed ages). Chapter 5 presents the mapping of LULC and vegetated areas of Abu Dhabi using the moderate resolution of Landsat-8 OLI images (5.2.1 and 5.2.2) and mapping of the young, medium, and mature date palms in Abu Dhabi using sub-meter world view-2 images (5.2.3). Subsections 5.2.4 and 5.2.5 focus on assessing the accuracy of the

produced maps and counting the date palms of Abu Dhabi at different age stages using a remote sensing approach. Chapter 6 displays the results of conducting a regression analysis between remote sensing variables (single bands and vegetation indices) with 54 field plots covering different age stages of date palms in the emirate of Abu Dhabi. Subsection 6.2.3 and 6.24 presents the final RS-based models and their validation to estimate biomass and carbons stock in mature (> 10 years) and non-mature date palms (≤ 10 years). The chapter ends up with an assessment map of the carbon stock by date palms of Abu Dhabi.

Chapter 7 discusses some critical issues which have emerged during the course of this study, while Chapter 8 concludes the whole learned lessons and recommendations for this dissertation.

Chapter 2: Research Methodology

2.1 Study Area

The UAE lies in the west part of the Arabian Peninsula and borders Oman to the East, Saudi Arabia to the south and west, and the Arabian Gulf to the North (Figure 9). The UAE has a coast line approaching 600 km on the Arabian Gulf and another 100 km to the east on the Indian ocean. The study area encompasses the whole emirate of Abu Dhabi, the largest of the seven emirates composing the UAE. The Emirate of Abu Dhabi is located in the West and South West part of the UAE and is bounded by 22° 55′ to 24° 48′ N, and 51° 30′ E to 56° 00′ E and extends over a land area of 67,340 km^2. It is administratively divided into 3 municipalities: Abu Dhabi, Al Ain and the Western Region. The Emirate, which hosts the capital city of Abu Dhabi, has witnessed dramatic conversions of its lands, supported by revenues from oil; from being desert / desert-like covered country to an urbanized and well-developed modern state. Furthermore, the government has heavily invested in large greening projects, to the extent that by the end of 2017, more than 540 afforested areas planted mainly with date palms (Abu Dhabi State of Environment Report, 2017; Salem Issa et al., 2019) have been added.
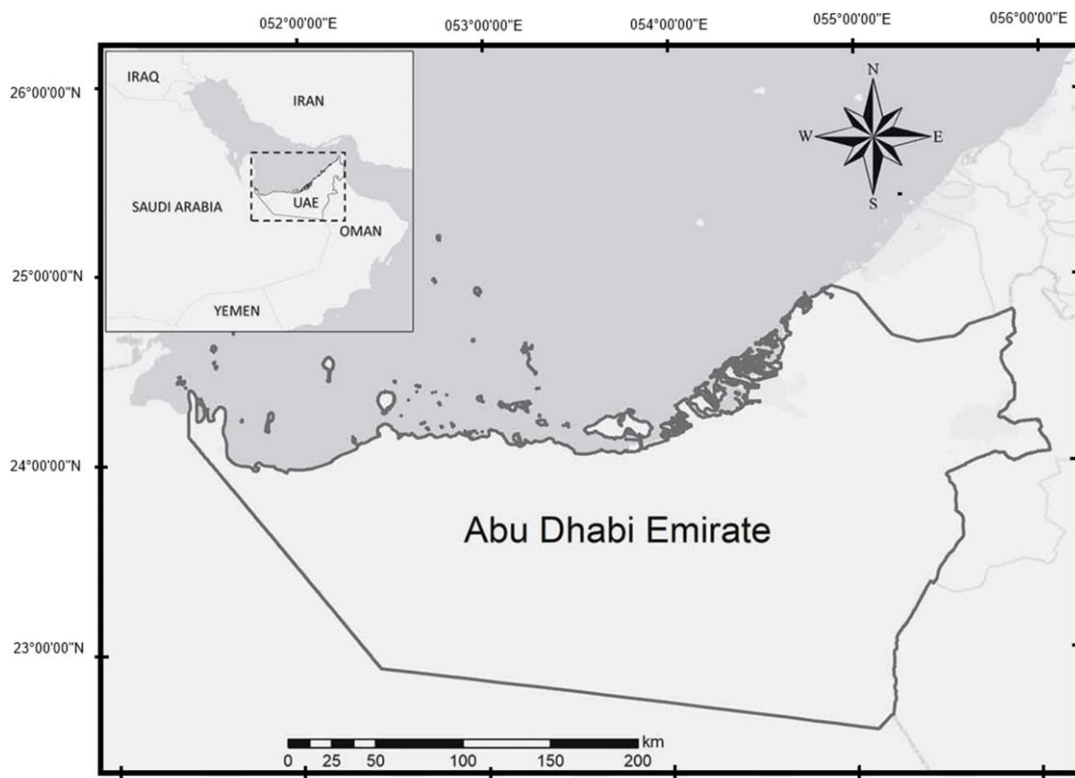
Figure 9: Study Area.

2.2 Geographic Settings

Elevations vary between zero main sea level in the coastal areas and increases smoothly in desert areas which constitute approximately 85% of the Emirate's main land, averaging an altitude of about 200 m above sea level (where most date palm plantations are found). Its geomorphology is dominated by five main landforms: sand dunes, inter-dunal sands, coastal sabkhas (flat plains with salty crust), inland sabkhas and exposed rocks. The climate of the study area is affected by its location inside the desert with proximity to the coasts of the Arabian Gulf and the sea of Oman. The Emirate's climate is manifested mainly by two seasons: summer and winter. In the summer season (April – September) temperature varies between 35° and 45°, with a climax of 48°C in July and August, accompanied with high concentration of water vapour boosting the relative humidity to reach up to 90%. On the other hand, the winter

season's (October – March) temperatures range from 10 to 24°C. The humidity throughout all seasons is relatively higher in those areas near in Arabian Gulf and lower in the south, south-west, and AlAin region. In the summer season, there is a high incidence of suspended dust throughout the country brought by the prevailing wind from the head of the Arabian Gulf (Western, 1989).

Rainfall occurs during winter season mainly between November and February with precipitation amounts barely reaching 12 cm per year (National Center of Meteorology 1995 -2018). The mean annual rainfall can be highly variable between one year to another. The western and southern deserts of Abu Dhabi are extremely dry, whereas the central desert around Al Wagan receives a relatively high amount of precipitation (Al-Rawai, 2004). The groundwater level is lowering and several wells have dried up or depleted, which increasing salinity levels, due to over-pumping, increasing in demand, and combined with scarce and sporadic rainfall (Dohai, 2007; Salem Issa & Dohai, 2008).

Abu Dhabi's soils can be categorized, broadly, into six categories: sandy, sandy calcareous, gypsiferous, saline, salinegypsiferous and hard pan soils (Shahid & Abdelfattah, 2008). Based on soil characteristics of the desert soils, "Saltation" as the dominant mechanism of soil particle movement is deduced, followed by surface creep and the suspension movement (Shahid & Abdelfattah, 2008). The only soils that tend to develop on the flat surface of a desert environment are fine-grained silts. The increase of calcium carbonate in soil, which is very high throughout the country, usually leads to many problems related to fertilization (e.g. fixing phosphorous and potassium elements), yellowness (deficiency of ferrous element), aeration of roots, and soil alkalinity. In general, biological activity in local soils is very low, and only about three percent of the whole country is naturally suitable for arable farming (Al-Rawai,

2004). About 60% of all plant species are annuals (Jongbloed, 2003). They germinate and flower soon after the first rain, generally from February to April. The perennial species generally flower from January to early May, and some in September and November (Jongbloed, 2003).

Three private farms from Al Foah farms area, north of Al Ain city, were selected to conduct the field data collection for building the allometric biomass equations specifically for DP (see Chapter 3), namely: Masakin (24° 42' N and 55° 76' E), Qattara (24° 29' N and 55° 78' E) and Salamat West (24° 15' N and 55° 42' E) (Figure 10). Al-Ain city was established around an old date palms oasis and as the city expanded, the DP plantations expanded as well. The climate of AlAin is characterized by an average minimum temperature of 14.7°C and an average maximum of 42.9°C. The annual average long-term rainfall is 59.1 mm and the humidity is 44.3% (National Center of Meteorology 1995 -2018). The geographic setting is characterized by a sand dunes barrier to the west and the mountain chains to the east, protecting Al-Ain city from the effect of wind and sea breeze coming from both east and west directions.
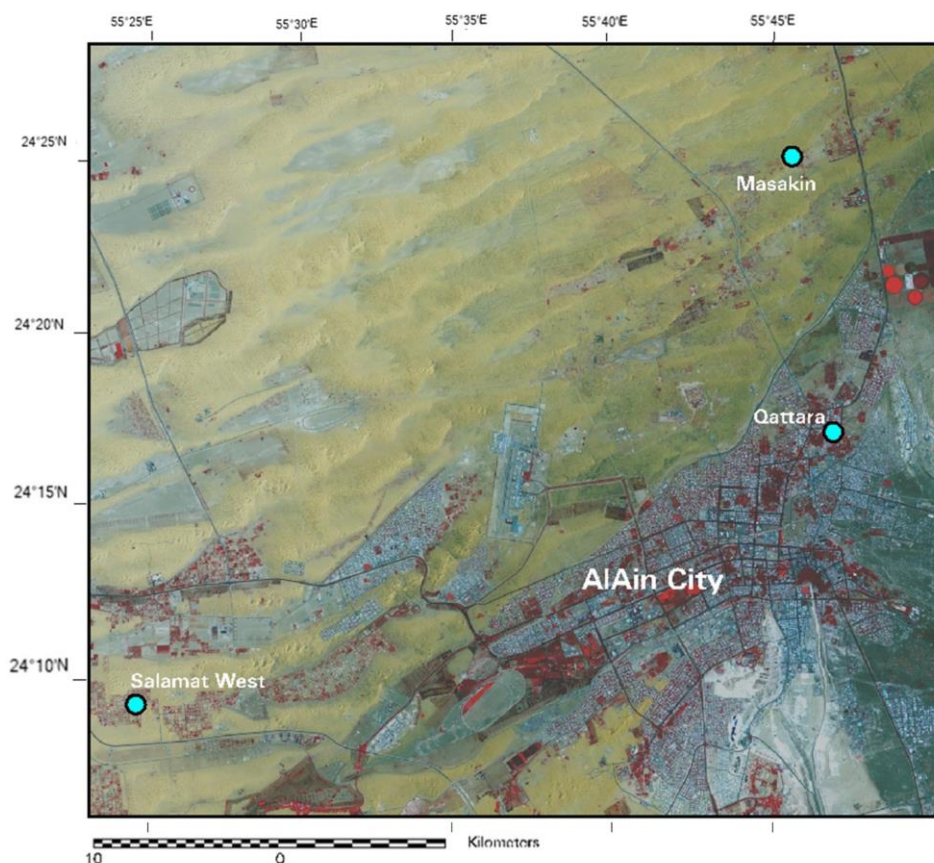
Figure 10: DP farms selected to build the biomass allometric equations. They are located on: Masakin, Qattara, and Salamat West. Date palms were uprooted, destroyed, burned and analyzed to build the biomass allometric equations. After (Salem Issa et al., 2018).

2.3 Remote Sensed Data

Six atmospherically corrected (Level-2) Landsat-8 OLI images, acquired in April and May 2017, were collected and downloaded from the U.S. Geological Survey website (https://earthexplorer.usgs.gov/) (Table 2). Additionally, six panchromatic bands (Level-1) of the same scenes were downloaded and later used for pan-sharpening of the original Level-2 scenes. All image bands were georeferenced and co-registered to the Universal Transverse Mercator (UTM) projection (Zone 40, WGS 84). Band1 (coastal/aerosol), Band2 (blue), Band3 (green), Band4 (red), Band5 (NIR), Band6 (SWIR 1), and Band7 (SWIR 2) of each image were stacked and saved using

ERDAS Imagine software. Furthermore, panchromatic band-8 (15 m resolution) and the stacked multispectral images were merged (pan-sharpened) to produce enhanced and pan-sharpened images of 15 m spatial resolution. The Nearest Neighborhood (NN) algorithm was applied during the resampling process.

Table 2: Details of the six Landsat-8 OLI Level-2 scenes used in the study.

No.	Scene (Path/Row)	Date (2017)	Bands Used (µm)	Resolution/ Swath
1	160/43	24th April	Band1 (coastal): 0.433–0.453, Band2 (blue): 0.450–0.515, Band3 (green): 0.525–0.600, Band4 (red): 0.630–0.680, Band5 (NIR): 0.845–0.885, Band6 (SWIR 1): 1.560–1.660, Band7 (SWIR 2): 2.100–2.300, and Panchromatic: 0.500–0.680	30 meters for multispectral bands and 15 meters for panchromatic. Swath area is 185 km.
2	160/44	26th May		
3	161/43	15th April		
4	161/44	15th April		
5	162/43	22nd April		
6	162/44	22nd April		

The vector boundary shapefile of the Emirate of Abu Dhabi was used to subset the study area. To achieve the goal, a single large mosaic image was created using available scenes (Table 2). Illumination equalizing as a color balancing method was used for mosaicking the scenes. Mosaic operation based on weighted seamline generation procedure was applied for scenes: 160/43, 160/44, 161/43, and 161/44 as these images involve the most significant urban centers of the study area, while for scenes: 162/43 and 162/44, the geometry-based seamline generation procedure was applied as the images contain homogenous areas such as desert and sabkhas (Figure 11), (Al Ahbabi, 2013).
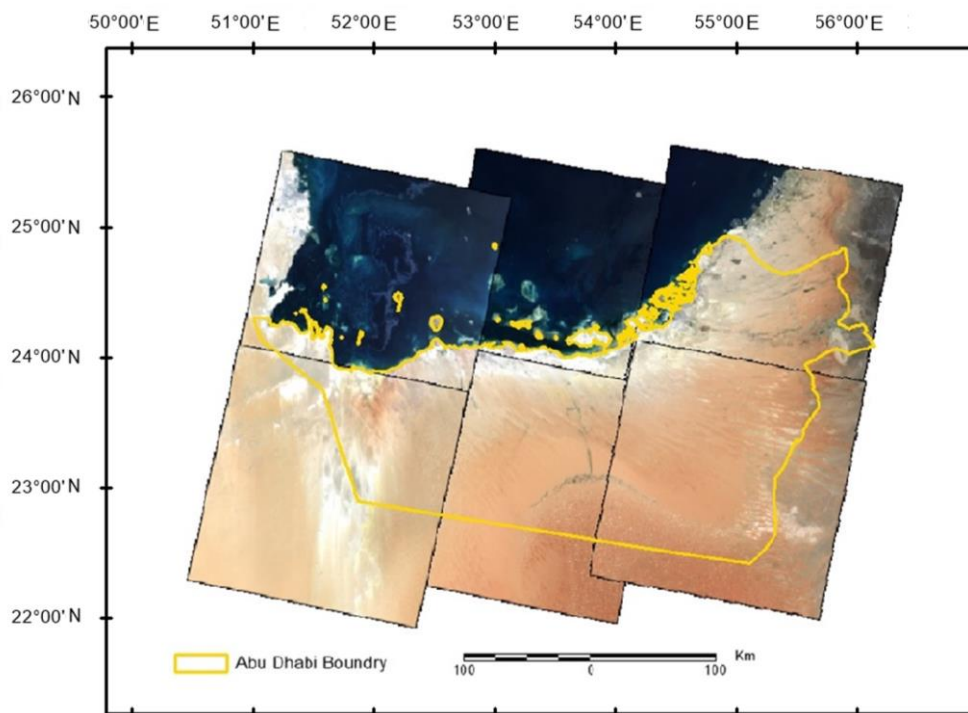
Figure 11: Mosaicking of six pan-sharpened Landsat-8 OLI scenes. The six pan-sharpened scenes were radiometrically adjusted using histogram equalization and displayed as false color; while the single large mosaic image displayed as natural color.

Mapping DP at the three age stages: young, medium, and mature (see Subsections 2.6.3 and 5.2.3), required the use of about 829 scenes of World View 2 (WV-2) acquired in 2014 (April/ May) and covering all the vegetated areas of Abu Dhabi were used. The WV-2 images have eight multispectral bands at a resolution of 1.85 m and one panchromatic band at a resolution of 0.50 m. Only the following WV-2 bands, described in Table 3, were used: Green (band 3), Red (band 5), NIR 1 (band 7), in addition to the panchromatic band. The selected WV-2 multispectral bands are equivalent to bands 3, 4, and 5 of Landsat 8 OLI which were shown to exhibit a strong correlation with significant RS variables (Salem Issa et al., 2019). The pan-sharpening of the WV-2 multispectral bands was achieved using the NN algorithm to produce images with 0.50 m pixel size (Jawak et al., 2013).

Table 3: Details of the WV-2 scenes/bands used in the study.

No.	Band	Width (μm)	Resolution/ Swath
1	Band 3 (Green)	0.510 – 0.580	1.85 meters for multispectral bands and 0.50 meters for panchromatic.
2	Band 5 (Red)	0.630 – 0.690	The swath of each scene is 16 kilometers.
3	Band 7 (NIR 1)	0.770 – 0.895	
4	Panchromatic	0.450 – 0.800	

2.4 Methodology Flowchart

Figure 12 shows the flowchart of the whole research methodology. The methodology consists of: (1) Developing allometric equations for DP to calculate biomass and sequestered carbon as function of structural palm parameters, (2) Delineating and mapping date palm plantations using multispectral classification of moderate and high-resolution RS data, (3) Developing a RS-based biomass model to calculate biomass and sequestered carbon as function of variables measured from space, and (4) Applying the RS-based biomass model to create assessment maps of sequestered carbon in date palm plantations in the study area.
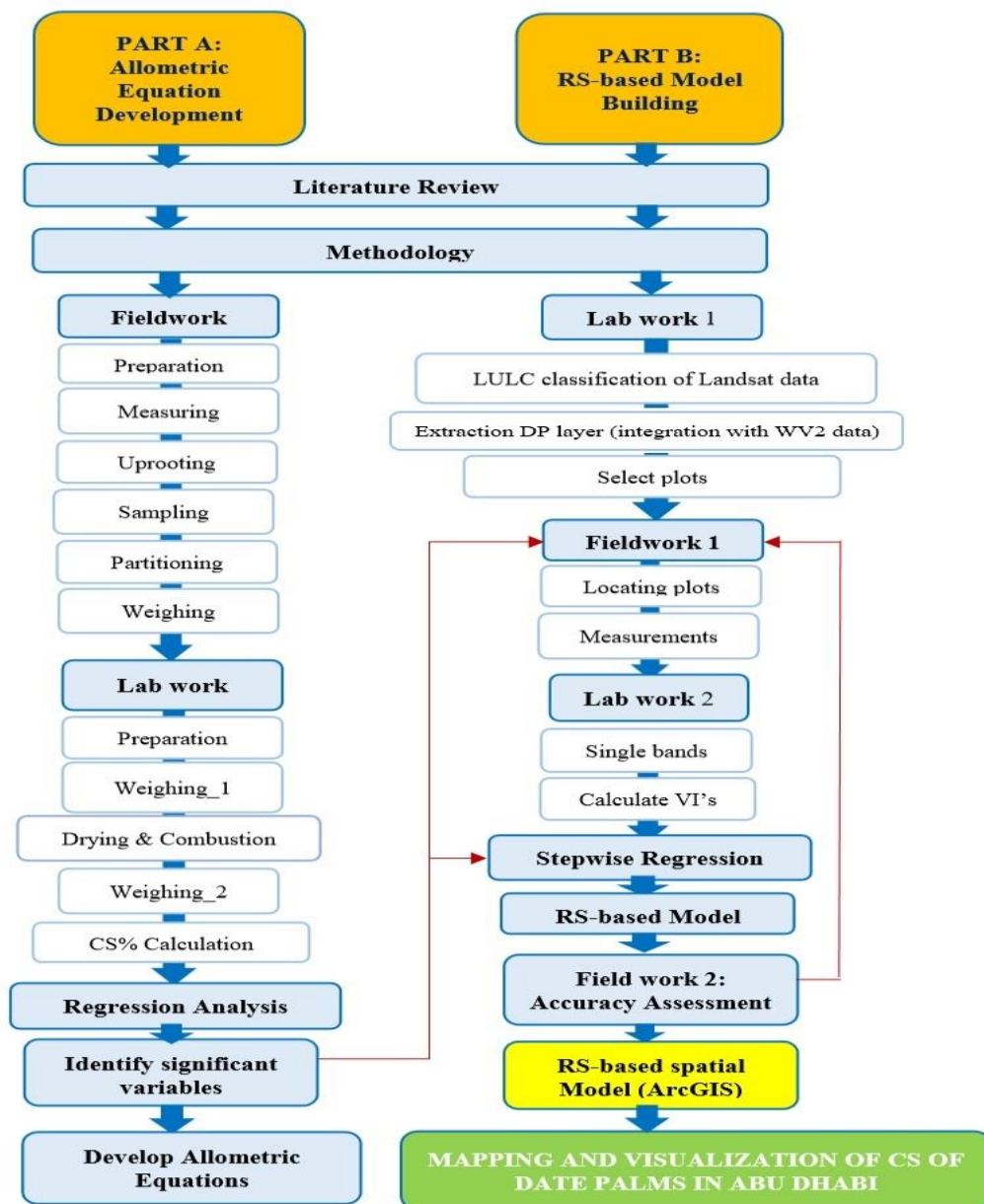
Figure 12: Methodology flowchart.

2.5 Developing Allometric Equations for Date Palm

2.5.1 Field Data Collection

A number of DP were selected to measure AGB and BGB in order to build specific allometric equations and calculate the CS in both biomass and soil for DP plantations in the study area. Age is one of the most important factors that influence

the biomass of the palm and its structural measurements (Sunaryathy et al., 2015). A substantial amount of research has been undertaken and published on the estimation of oil palm biomass at various ages (Husin et al., 1987; Kamarudzaman et al., 1995; Khalid et al., 1999a; Rees & Tinker, 1963). In the current study, a similar approach has been adopted to estimate DP' biomass at three different age stages:

- Age stage One (young) for plantations younger than 5 years;

- Age stage Two (medium) for plantations between 5 and 10 years; and

- Age stage Three (mature) for plantations exceeding 10 years of age.

Accordingly, five DP were selected, prepared and uprooted to represent each age stage. Another influencer factor in DP biomass storing is variety. Indeed, DP in the study area differ in their cultivars (varieties) with different palm growth rates as well. Therefore, field samples were selected to represent the different varieties as well as the three different age stages in the study area including Fardh, Bumaan, Khunaizi, Khlalas, Baghel, Jabri, Shahem, Jash Ramli, and Neghal (see Appendix 4).

2.5.2 Field Measurements

A fieldwork campaign was conducted during the fourth week of April 2018 where five DP were uprooted for each age stage (total of 15 palms). Each sampled palm was partitioned into three parts: crown, trunk and roots (Khalid et al., 1999a). The term biomass, in this research, refers to the value of dry weight unless indicated otherwise. Although some researchers prefer to use the fresh weight instead of dry weight for building their equations (Dewi et al., 2009; Khalid et al., 1999a) (Appendix 1). Hence, AGB is calculated as the sum of the crown and trunk weight while BGB is calculated as the weight of the root system. A large commercial scale balance was used to get the fresh weight of crown, trunk and roots in (Kg). From each part of the

uprooted palms, three samples were collected (3 crown samples, 3 trunk samples and 3 root samples), (Figure 13).

Figure 13: Uprooting, partitioning, and weighing date palms. After (Salem Issa et al., 2018, 2020b).

Structural variables of uprooted DP including total palm height, trunk height, diameter breast height (DBH), crown diameter (CD), crown area (CA) and number of fronds (#Frond), were measured and later used in the regression analysis to build specific biomass allometric equations of date palm. Before uprooting the palm, the following variables were measured: (i) DBH in cm by measuring the circumferences of the trunk at 1.3 m height and dividing by the number π. For small palms, with no developed trunk, the diameter was measured at the base of the palm, (ii) Number of palm fronds (#Frond), (iii) CD in meter, and (iv) CA in square meter was calculated using the sphere equation (CA = π CD^2/4), assuming a rounded palm crown. After uprooting the palm, the following variables were measured: (i) Palm height (H) in meter, (ii) Palm trunk height (Ht) in meter, and (iii) Crown depth (Δheight), defined as the difference between total and trunk heights in meter.

2.5.3 Biomass and Soil Samples Processing for Measuring Palm Biomass and Carbon Contents

A total of 120 biomass samples were collected during the fieldwork: (15 Crown + 10 Trunk + 15 Root) x 3 replicates. Only 10 x 3 trunk samples were collected due to the absence of developed trunk in young palms. Four soil samples were collected from underneath each palm canopy, referred to as "In". A total of 60 soil samples: 15 palms x 4 replicates were collected during the campaign. More soil samples were collected away from the palms' canopy, referred to as "Out", from two DP farms: [2 farms x 4 replicates], for comparison and quantification of the effect of DP contribution to soil carbon sequestration. Immediately after reaching the UAEU/ Biology department's Labs, the fresh weights of all samples were measured. Then, samples were air dried and transferred to paper bags to be ready for oven drying at 80℃ for 72-96 hours to measure the dry weight (Allen et al., 1974; Corley et al., 1971; Khalid et al., 1999a). Samples were prepared and grinded to calculate the biomass components' parameters using the formula listed in Table 4. Samples were weighted to get the percentage of dry weight to original fresh weight in each sample (dry to fresh factor=DF) (Figure 14). Finally, samples were combusted for 4 hours at 550℃ (Allen et al., 1974)) to calculate organic matter (OM) and organic carbon (OC) as per the formula in Table 5.

Table 4: Calculation of different date palms biomass components.

Parameter	Formula
Dry Weight of each palm part (Kg)	Crown Dry Weight = Crown Fresh Weight × Crown DF* Trunk Dry Weight = Trunk Fresh Weight × Trunk DF Root Dry Weight = Root Fresh Weight × Root DF
Percentage of BGB (Root system) from the AGB**	BGB:AGB ratio = BGB/AGB × 100
AGB weight in each palm (Kg)	AGB = Crown Dry Weight + Trunk Dry Weight
Total Biomass of each palm	Total Biomass = AGB Weight + Root biomass Weight (BGB)

*DF is dry to fresh factor
** The ratio of each biomass component (crown, trunk, and roots) to the total biomass were calculated as well.

Table 5: Calculation of OM and OC of the collected samples.

Item	Formula
The percentage of OM to dry weight in each sample	%OMD* = (1- Combustion Weight 550℃ /Dry Weight 80℃) × 100
The OM Weight for palm parts in each palm (Kg)	Crown OM Weight = Crown Dry Weight × % Crown OMD Trunk OM Weight = Trunk Dry Weight × % Trunk OMD Root OM Weight = Root Dry Weight × % Root OMD
The OC weight palm parts in each palm (Kg)**	Crown OC Weight = Crown OM Weight × 0.58 Trunk OC Weight = Trunk OM Weight × 0.58 Root OC Weight = Root OM Weight × 0.58
The OC in AGB for each palm (Kg)	OC in AGB = Crown OC Weight + Trunk OC Weight
Total OC in each palm	Total OC = OC in AGB + OC in Root biomass

* OMD is OM to dry factor
** OC is equal OM multiply by 0.58

Figure 14: Lab works, preparing samples, grinding, weighing, and drying.

Soil samples were first air dried and prepared for further processing (Allen et al., 1974). They were then placed in crucibles and oven-dried at 105℃ for 72 hours. The different soil samples' parameters were calculated using formulae listed in Table 6 following the approach described in (Ksiksi, 2012; Lemenih & Itanna, 2004).

Table 6: Formulae used to calculate the different soil parameters.

Item	Formula
% Moisture content	= (Initial Weight–Dry Weight 105℃)/Initial Weight × 100
Bulk density (g/cm^3)	= dried-oven Weight (g)/ Total volume of the sample
% SOM*	= (Dry Weight 105℃ – Loss of Combustion)/ Dry Weight 105℃ × 100
% OC**	= OM x 0.58
Soil carbon (g/m^2)***	= Z x BD × C × 10
Soil carbon in Kg/palm	= (Soil C. (g/m^2) × CA) / 1000

* Combustion was performed for 4 hours at 550℃ to estimate %SOM
**% OC is estimated as 0.58 of the calculated OM
*** Where Z = thickness of each sample depth (10 cm), BD = bulk density (1.7 g/cm^3) of each sample depth and C is the carbon concentration (g.C/Kg soil) of each sample depth. Results are reported in tons per hectare.

The total CS in and contributed by the DP is calculated as the sum of CS in the DP biomass itself plus the CS in the soil underneath the palm as explained and formulated as per equation 1 below:

Total CS = Biomass C + Soil C   Eq. (1)

2.5.4 Determination of Allometric Equations

All statistical and graphical tests for the models were performed using SPSS and Excel software packages. First, correlation coefficients between biomass in each DP part (crown, trunk and root) and all collected field variables were calculated.

Linear, logarithmic, exponential, power and polynomial expressions, were fitted in the regression analyses to identify the highest coefficient of determination (R^2). Single-variable models are most frequently used in estimating the biomass as they are easy to apply compared to those with multiple variables (Cheng et al., 2014). In the current case, the linear and non-linear regression analyses were run to develop single-variable models to predict the biomass. Individual single field measurements were considered as the independent variables (i.e. H, Ht, CD, CA, etc.), while the predicted biomass (AGB) was the dependent variable. Then, the associated R^2 values for each model were calculated at $P < 0.05$.

2.6 LULC Classification and Accurate Mapping of Date Palm Plantations

Hierarchical integrated approach (HIA) was applied to classify the LULC of Abu Dhabi and map the DP plantations at three age stages (for the RS data used, see Subsection 2.3). First, each pan-sharpened scene of Landsat-8 OLI was classified using a hybrid classification method (HCM) (supervised and unsupervised classification) to create LULC maps (Subsection 2.6.1). Next, the maps were recoded (reclassified) to create a bitmap comprising only two classes: vegetation and non-vegetation (Subsection 2.6.2). The HCM was applied to the areas covered by the vegetation class in order to delineate the date palms and create a bitmap containing date palms and non-date palms classes (DP and non-DP) (Subsection 2.6.2). However, at this stage of the classification, only mature DP plantations were depicted due to the limitations of Landsat-8 OLI to differentiate soil background from the non-mature DP plantations (less than 10 years) with average crown diameter less than 5 meters. In order to map the other two age stages (medium, and young), object-oriented classification (OOC) method was applied on the already produced vegetation bitmap.

At this level, about 829 sub-meter world view -2 (WV-2) images were used covering only the vegetated areas. The HIA classification method was able to depict the three age stages of date palms: young, medium, and mature (Subsection 2.6.3). To validate the interim and final maps, an accuracy assessment procedure was implemented at different levels for the evaluation of the LULC maps, the vegetation bit-map, and the detailed DP maps. An error matrix was produced and helped determine the overall, user's, and producer's accuracies, in addition to the kappa coefficient (Subsection 2.6.4). All processes were implemented using ERDAS Imagine 2020 and ArcGIS 10.7.1 software packages. A brief description and a detailed flowchart of the implemented methodology is presented in the following Subsections and illustrated in Figure 15.
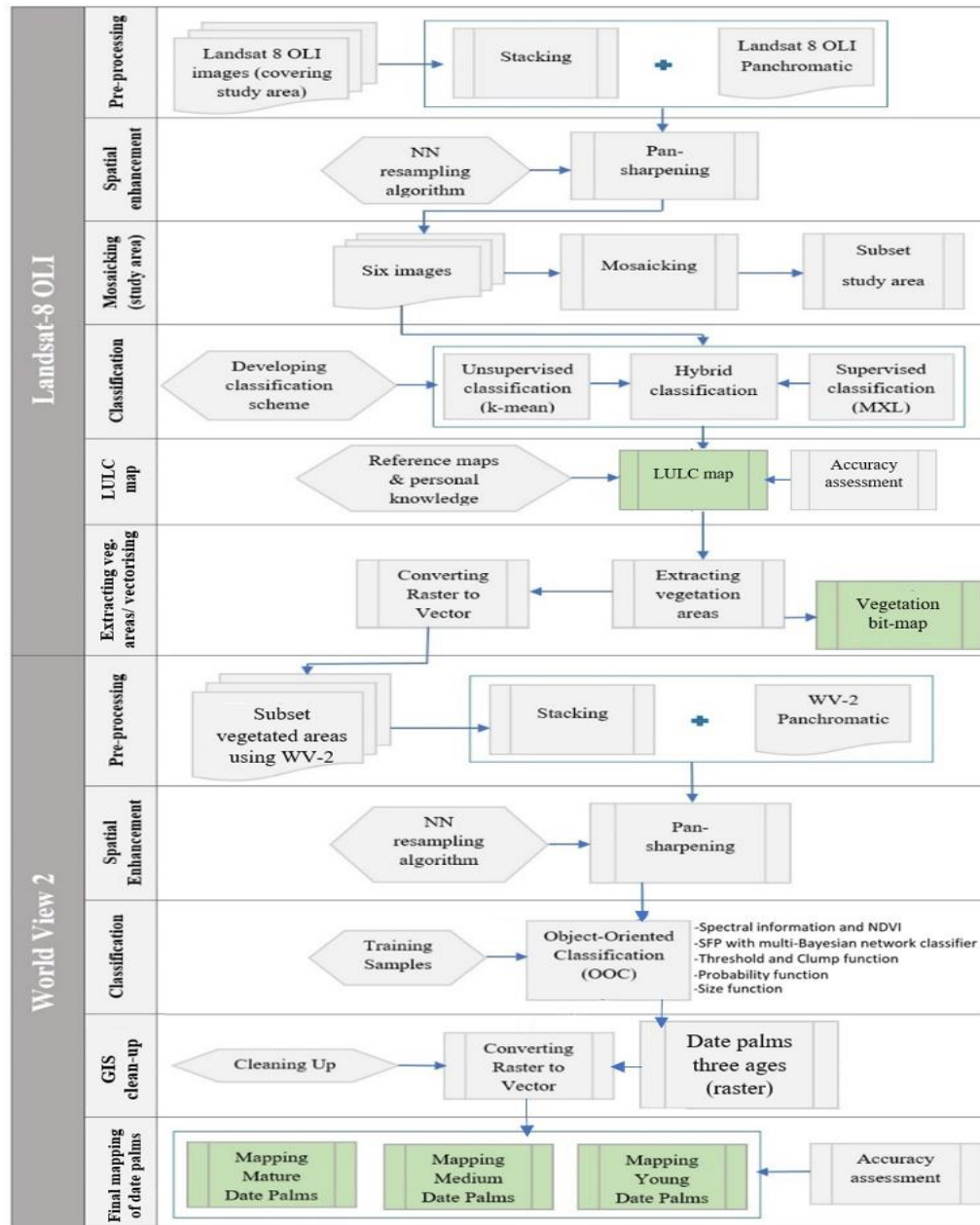
Figure 15: LULC classification and mapping the date palm plantations.

2.6.1 LULC Classification

Anderson classification scheme (Level 1) was adopted, to classify the Landsat data (Al-Ahmadi & Hames, 2009; Anderson, 1976; Rozenstein & Karnieli, 2011). Seven LULC classes were used to represent: vegetation, urban, sand sheets, sand dunes, deep water and shadows, shallow water, and sabkhas. The HCM approach was implemented: starting by performing unsupervised classification to minimize bias in

the selection of training areas and seed signatures; then, a set of spectral class signatures was created to be used as training data for the supervised classification phase (Bakr et al., 2010; Kuemmerle et al., 2006; Rozenstein & Karnieli, 2011). Each image was initially clustered into 80 classes with a maximum of 80 iterations (the optimum number of iteration for Landsat data), permitting the clustering process to stop naturally as it reaches the convergence threshold of 0.990 (Al-Shuwaihi, 2009; Kuemmerle et al., 2006; Mundia & Aniya, 2005; Yang & Lo, 2002). Next, all images were classified using the previously created signatures corresponding to the seven classes present in the study area. The signatures were collected by delineating polygons on the images to collect the training samples (total of 720 training sets). The signatures were assessed and evaluated by plotting the mean signature values of each class against the Landsat-8 OLI bands (Chapter 5, Subsection 5.2.1). The maximum likelihood classifier (MXL) was used and the resulting classes were then merged and recoded to form the final seven LULC classes. The resulting LULC map was smoothed and cleaned up using a Majority Filter with a window size of (3x3). Then, certain class boundaries were manually adjusted using the Fill Tool module in ERDAS Imagine. This is achieved by filling the misclassified pixels with the right values. Finally, the thematic LULC map was created and the area of each of the seven classes was computed in hectare (Chapter 5, Subsection 5.2.1).

2.6.2 Mapping Vegetated Area & Delineating of Date Palm Plantations

The Landsat-8 OLI images were first processed to produce a bitmap with two land cover classes: vegetated / non-vegetated (Al-Shuwaihi, 2009; Southworth et al., 2002). To that end, the LULC map of Abu Dhabi was converted to a binary map by merging all non-vegetation classes: urban, sand sheets, sand dunes, deep water, shallow water, and sabkhas, into one class named non-vegetation. A "Recode"

function was used in the process to create a vegetation bitmap having two values: 1 for vegetated area class and 0 for non-vegetated class. Vegetated areas (pixels) were extracted from the original images by masking the non-vegetated pixels using Subset/Mask functions in ERDAS Imagine. To separate the DP plantations from other vegetation types, the HCM was run within the vegetated areas following the same procedure described above. The DP plantations were mapped and their areas in hectare were computed; however, only the mature DP plantations were depicted due to the limitations of Landsat-8 OLI to differentiate soil background from the non-mature DP plantations. Consequently, the vegetation bitmap was transformed and converted to vector format and exported to a vector shapefile using ArcGIS 10.7.1. The shapefile will then be used for the selection of the corresponding WV-2 scenes that cover the vegetated areas present in the study area. The OOC classification method is applied to classify the high-resolution WV-2 images for the separation and mapping of DP age classes and calculating their statistics (Chapter 5, Subsection 5.2.3).

2.6.3 Mapping Young, Medium, and Mature Date Palm Plantations

At this level of the classification, the 829 WV-2 scenes acquired in 2014 were used (for RS data used, see Subsection 2.3). The vegetated areas, in each of the 829 scenes, were visually interpreted and subset to run the OOC. A semi-automatic object-oriented feature model has been implemented for the detection and mapping of DP using ERDAS Objective Imagine (Chepkochei, 2011; Lack and Bleisch, 2010; Rizvi et al., 2019; Issa et al., 2020b). The same Al Foah farms area, north of Al Ain city (Figure 16) was used as a pilot area to create and calibrate the Feature Model Tree (FMT). It contains more than 60,000 palms of different ages and cultivars and was subject to many visits during the study period (Issa et al., 2018; Issa et al., 2019, Issa

et al., 2020c). The FMT was then run on the entire WV-2 sharpened images (Lack & Bleisch, 2010). This model became the basis for the extraction of DP at different age stages which consisted of several sequenced "process nodes" (Figure 16). Best parameters were selected and trained following a trial-and-error approach.
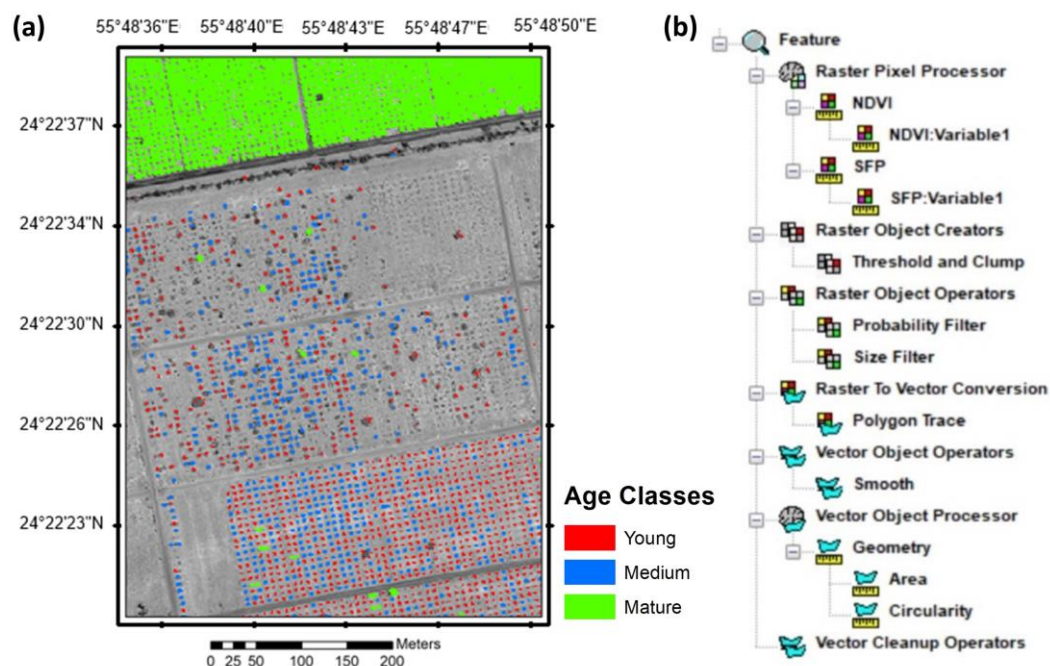
Figure 16: Object-oriented classification of DP in Abu Dhabi. (a) The three age stages of date palms produced, after applying the object-oriented approach on WV-2 images on a testing area in Al Foah DP farms area, to optimize the selected parameters. (b) FMT for the extraction of DP plantations with three age stage.

An FMT is typically used to extract one type of the desired feature, it consists of the following main components (child nodes) (see Imagine Objective tools, ERDAS Imagine User Guide): Raster Pixel Processor (RPP); Raster Object Creator (ROC); Raster Object Operator (ROO); Raster to Vector Conversion (RVC); Vector Object Operator (VOO); Vector Object Processor (VOP); and Vector Cleanup Operator (VCO). These components, usually referred to as "Process Nodes", represent the different stages of the FMT. A FMT may have all or only some of these process nodes activated. The following steps describe the application and use of the FMT in the

current case study showing the step-by-step feature extraction process for mature, medium, and young DP mapping:

i. Raster Pixel Processor (RPP): Spectral band information and NDVI were input to generate single feature probability (SFP) layer with pixels extracted from training sets. The NDVI values ranging between (0.18 to 0.45) differentiated well between DP and other vegetation types. The chosen SFP uses a multi Bayesian network classifier (statistic classification). The proper definition of training sets for both the DP crown and the background pixels is vital to the outcome. Training sets were chosen carefully to exclude any reflectance from the background. Individual palms, selected from training polygons, were used to collect pixel values for the computation of pixel cue metrics in order to train the pixel classifier. In that way, the probability layer was created.

ii. Raster Object Creator (ROC): A function that collects pixels with a probability equals or superior to a threshold value and assigns to these pixels the value of one. In the same time, other pixels will receive the value of zero. In subsequent steps, the function executes a contiguity (clump) operation on the created binary mask and convert the resulting layer into a raster probability (object) layer. In this study, the value of the threshold was set to 0.50. It should be noted here that a lower threshold would make possible the addition of non-tree pixels.

iii. Raster Object Operators (ROO): The "Probability Filter" is used to retain pixel objects with high probability while assigning to all other pixels the status of 'background'. The rule set in this study states that: all objects (raster objects) with zonal probability mean less than 0.75 should be removed. The "Size Filter" filters out raster objects that are either too small, or too large hence permitting to limit the set of raster objects to match actual date palm crown

sizes (Chepkochei, 2011; Rizvi et al., 2019). The Sub-Meter World View (WV-2) imagery was used efficiently to discriminate between three date palm age classes based on their crown size, as described below:

    a. Mature DP: with crown area $\geq$ 144 pixels (which corresponds to $\geq$ 3m of palm crown radius on the ground).

    b. Medium DP: with crown area $\geq$ 49 pixels and < 144 pixels (which corresponds to $\geq$ 1.75m and < 3m of palm crown radius on the ground)

    c. Young DP: with crown area < 49 pixels (which corresponds to < 1.75m of palm crown radius on the ground).

iv. Raster to Vector Conversion (RVC): This step converts raster object layers created in the previous step to polygon layers using a polygon trace.

v. Vector Object Operator (VOO): This step smoothens the boundaries of tree polygons created in the previous step using a "Smooth filter". A smoothening factor of 0.5 was found to be optimum.

vi. Vector Object Processor (VOP): Geometric processes run to compute the area of each polygon shape. Two object cues available were run in Imagine Objective: Area and Circularity, and finally,

vii. Vector Clean-up operators: Vector layers are cleaned using ArcGIS 10.7.1 by visual interpretation to remove erroneous vector objects if any.

The geo-processing tool (Merge) in ArcGIS was used to merge the shapefiles. Maps of mature, medium and young DP plantations were created and the area of each age stage class as well as the number of DP present in each plot were calculated.

2.6.4 Assessing Accuracy

The accuracy assessment was run for the three levels of classification: (1) the initial LULC map including the seven classes, (2) the vegetation bit-map, and (3) the DP maps at different age classes (mature, medium, and young). For the LULC map, 350 points (50 points for each class) were selected randomly using the stratified random sampling by ERDAS Imagine Accuracy Assessment Tools. For vegetation bit-map, 100 points (50 points for vegetation class and 50 points for non-vegetation class) were selected using the same procedure mentioned before. These validation points were projected on the pan-sharpened image of Abu Dhabi, visually interpreted and assessed by the use of Google Earth, reference maps, and researchers' knowledge of the area. Each point was subsequently, assigned to one of the classes defined before. For validation the classified maps of DP at different age stages (young, medium, and mature), GPS points (x,y) were collected from farms located in the study area (Wathba, Nahdha, AlAin, Swaihan, Yahar, Khatem, Salamat, Khazna, Yahar, Masakin, Hayar, and Al Foah). The collected points that represent homogeneity of one of the age stages were projected and displayed over the three age stages class (= 71 points) to assess their exact matching. A confusion matrix was produced, and accuracy metrics were computed for each class of the LULC map, as well as, the DP at different age-stages maps (Chapter 5, Subsection 5.2.4). The use of metrics such as overall accuracy, Kappa statistics, producer's accuracy, and user's accuracy, are quite common and explained in detail in numerous publications (Campbell & Wynne, 2011; Congalton, 1991; Foody, 2002; Lillesand et al., 2014; Rosenfield & Fitzpatrick-Lins, 1986; Rozenstein & Karnieli, 2011).

2.7 Building Remote Sensing based Models for Biomass and Carbon Stock Estimation of Date Palm Plantations

Note: The following method was applied at two phases. First, it was applied at a "Pilot Study" on Al Foah date palm farms area. At this level, only 19 field plots were considered applying the Subsections 2.7.1 to 2.7.4. The results of the "Pilot Study" are found in Chapter 4. Second, the following steps were applied on 54 field plots covering the whole study area (Chapter 6).

2.7.1 Field Data Collection

a. The Pilot Study

To develop the remote sensing-based biomass model, the following approach was applied to the pilot study area in Al Foah with the remote sensing data extracted from a Landsat 8 OLI scene acquired on June 17, 2017. Nineteen plots (from A to S plots), shown in Figure 17, with homogenous DP identified and where palms were counted, and their structural parameters measured (see Chapter 4 for the results). The approach can be summarized as follows:

(1) Identify a set of RS variables (predictors) used to estimate AGB.

(2) Select sample plots representing different age classes of DP in the study area.

(3) Collect necessary field data to calculate AGB. The calculated AGB serves as reference data for the RS-based model to be built.

(4) Build and validate the RS-based biomass estimation model by correlating AGB with significant RS predictors using different regression methods.

(5) Create a map visualizing CS distribution throughout the study area.
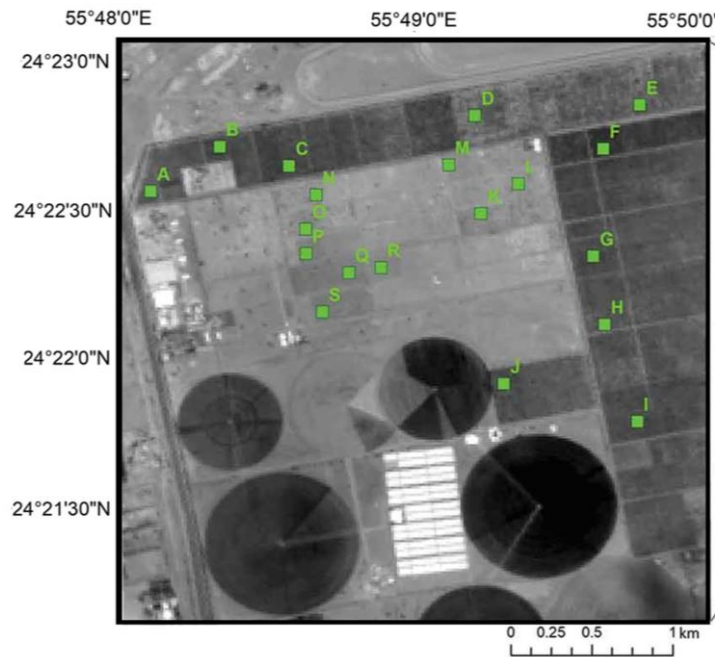
Figure 17: Pilot study area in AlFoah, AlAin. After (Salem Issa et al., 2019).

b. Emirate of Abu Dhabi

DP plantation is part of the farming systems in Abu Dhabi and is used in road landscaping as well as for economic purposes. The DP plantations existed at different age stages, therefore, they are classified according to their age into three classes: mature DP (more than 10 years), medium DP (5-10 years), and young date palm (less than 5 years). Data from a total of 54 field plots were collected within the study area, including 17, 19, and 18 field plots of mature, medium, and young DP, respectively (Figure 18). Two field visits were conducted during the winter season of 2018; the first visit was from 10th -18th September and the second one from 14th November to 6th December. Each selected plot had dimensions of 40 × 40 m to ensure that the area on the ground occupied at least one full pixel of Landsat 8 OLI image with a 30- m pixel resolution (Salem Issa et al., 2019; Vicharnakorn et al., 2014) (Figure 19). All palms in all the 54 plots were counted and the GPS coordinates of the center of each plot were identified. Trunk height (Ht) and crown diameter (CD) for each palm were

measured. Then, the crown area (CA) was calculated for each palm using the sphere equation (CA = π CD^2/4), assuming a rounded palm crown.
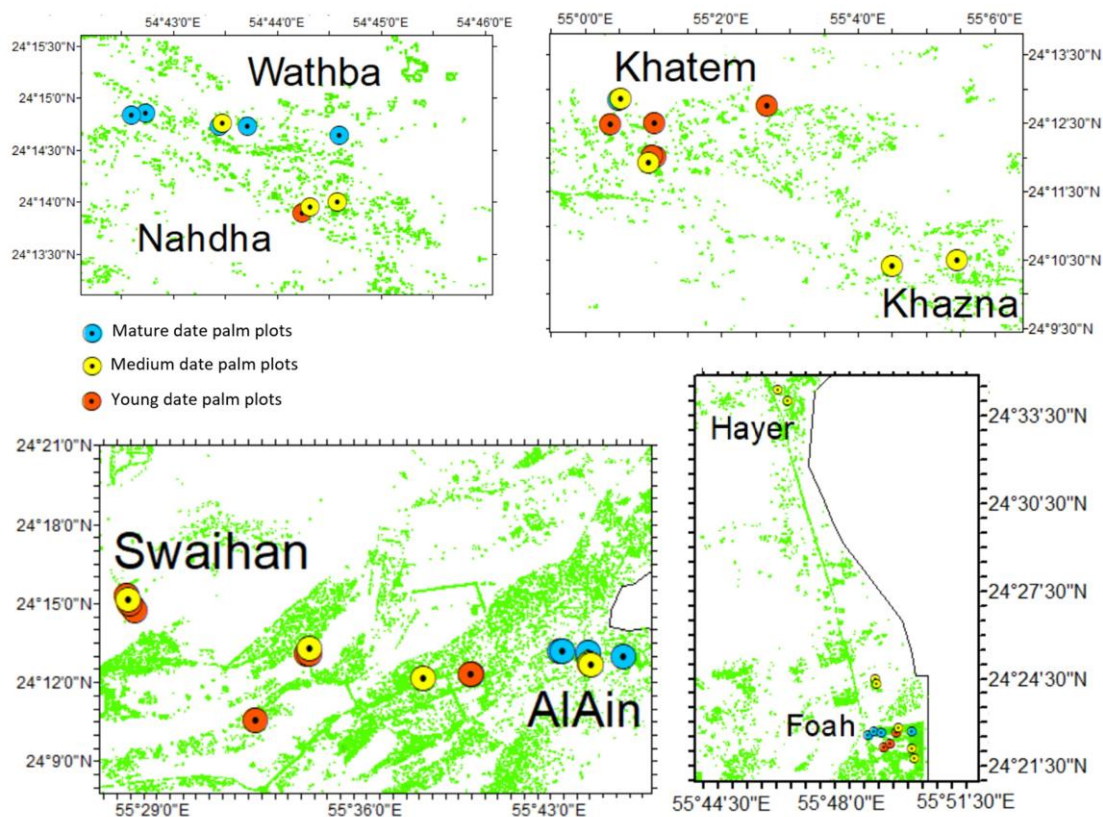
Figure 18: Location of the field observation data sites. Fifteen-meter resolution vegetation cover map for 2017 was used. The boxes present the distribution of field data (54 plots) of three age stage classes of DP (mature, medium, and young).

It is worth mentioning that collecting samples were started from 83 field plots of DP then; twenty-nine of them were excluded because of three reasons: (1) the sparse distribution of DP per plot (< 20 palm/plot), (2) the suffering of DP from abiotic stresses (e.g. drought), and (3) the high level of heterogeneity not representing, accurately, the age stage class (mature, medium, and young). Therefore, the size of sample plots was reduced from 83 to only 54 plots.
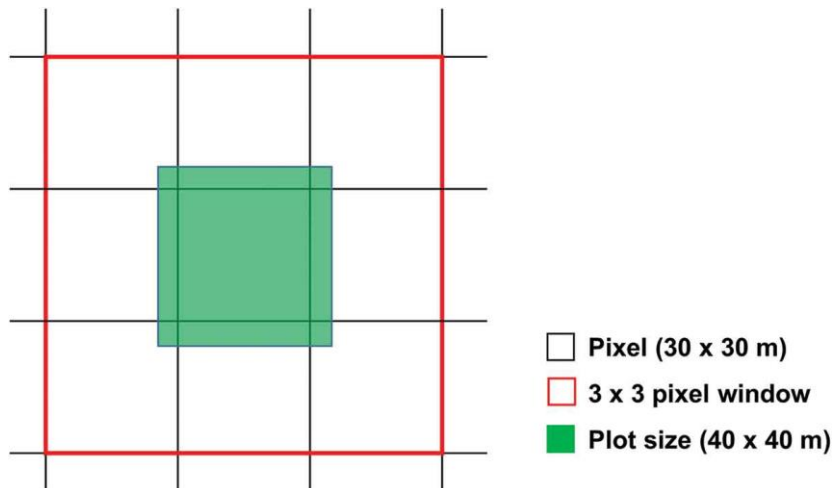
Figure 19: The 40 × 40 m plot design. The red window delimits the Landsat pixels covering the plot. After (Salem Issa et al., 2019).

The AGB at plots level was estimated by using DP biomass allometric equations which developed specifically for DP of Abu Dhabi, UAE under arid land ecosystem conditions (see Chapter 3). These equations estimate the AGB as functions of Ht and CA of DP (Table 7). AGB for each DP was calculated as the sum of crown biomass (CB) and trunk biomass (TB) in (kg. palm^{-1}). The resulting AGB of all DP in each plot was calculated and converted to tons per hectare (t. ha^{-1}).

Table 7: Equations used for AGB (kg. palm^{-1}) estimation of DP in study area.

Biomass Component	Allometric Equation	R^2	P value	Source
Crown Biomass	$= 14.034 \times 1.057^{CA}$	0.8354	0.001	see Chapter 3
Trunk Biomass	$= 40.725 \times Ht^{0.9719}$	0.8276	0.0004	
Total AGB	$= CB + TB$			

CB is crown biomass, TB is trunk biomass, AGB is aboveground biomass, CA is crown area (m^2), Ht is trunk height, R^2 is coefficient of determination.

2.7.2 Identifying Remote Sensing Variables (Predictors)

A combination of individual reflective bands and VIs were used as predictors to estimate AGB. Therefore, an approach combining multiple predictors was used in the regression analysis. RS predictors can be grouped into two distinct categories: (1)

single bands include B1, B, G, R, IR, SWIR1, and SWIR2 of Landsat 8 OLI (Table 2), and (2) traditional as well as a variety of modified VIs were tested (Table 8), this includes simple ratio (SR), ratio vegetation index (RVI), difference vegetation index (DVI), normalized difference greenness index (NDGI), normalized difference vegetation index (NDVI), transformed vegetation index (TVI), green normalized difference vegetation index (GNDVI), renormalized difference vegetation index (RDVI), soil-adjusted vegetation index (SAVI), modified soil adjusted vegetation index (MSAVI), and the three tasseled cap transformation indices for greenness (TCG), brightness (TCB) and wetness (TCW). VIs such as: NDVI, modified NDVI, GNDVI and NDGI have minimum and maximum values ranging between -1 and +1 where green surfaces occupying digital number (DN) values ranging between 0.2 and 0.9; with dense vegetation and higher biomass amount generally represented by higher DN values (more than 0.6) (Adeyeri et al., 2017). However, TVI, which is another modified NDVI, has a range of values between 0 and 1.4 with no negative values (Mróz & Sobieraj, 2004). Moreover, positive DN values of DVI and SR represents vegetation with higher values depicting higher biomass amount (Richardson & Wiegand, 1977; Rouse, 1974). Similarly, RVI shows higher values for thick vegetation than for sparse or non-vegetated surfaces (Adeyeri et al., 2017). SAVI index behaves similar to NDVI, ranging between -1 and 1 with lower values reflecting lower biomass amount/cover of green vegetation.

Table 8: The Landsat 8 OLI vegetation indices used in this study.

VI	Equation	Reference
SR	NIR/R	(Birth & McVey, 1968)
RVI	R/NIR	(Pearson & Miller, 1972)
DVI	NIR–R	(Tucker, 1979)
NDGI	(G-R)/(G+R)	(Woebbecke et al., 1993)
NDVI	(NIR-R)/(NIR+R)	(Rouse, 1974)
TVI	$\sqrt{NDVI+1}$	(Srestasathiern & Rakwatin, 2014)
GNDVI	(NIR-G)/(NIR+G)	(Gitelson et al. 1996)
RDVI	$\dfrac{(NIR-Red)}{\sqrt{(NIR+Red)}}$	(Roujean & Breon, 1995)
SAVI	$\dfrac{1.5*(NIR-Red)}{(NIR+Red+0.5)}$	(Huete, 1988)
MSAVI	$0.5 \times \left[2R_{NIR} + 1 - \sqrt{(2R_{NIR}+1)^2 - 8(R_{NIR} - R_{red})} \right]$	(Qi, Chehbouni, et al., 1994)
TCG	$-0.2941 \times$ B $- 0.2430 \times$ G $-0.5424 \times$ R $+ 0.7276 \times$ NIR $+ 0.0713 \times$ SWIR1 $- 0.1608 \times$ SWIR2	(Baig et al., 2014)
TCB	$0.3029 \times$ B $+ 0.2786 \times$ G $+ 0.4733 \times$ R $+ 0.5599 \times$ NIR $+ 0.5080 \times$ SWIR1 $+ 0.1872 \times$ SWIR2	(Baig et al., 2014)
TCW	$0.1511 \times$ B $+ 0.1973 \times$ G $+ 0.3283 \times$ R $+ 0.3407 \times$ NIR $- 0.7117 \times$ SWIR1 $-0.4559 \times$ SWIR2	(Baig et al., 2014)

The RS variables (single bands and VI's) for all plots were extracted from the mentioned Landsat 8 OLI image and saved using spectral profile tools in ERDAS Imagine software. The mean values of the spectral variables for a 3 × 3 window centered over each plot were extracted to reduce the uncertainties in RS data resulting from plot positioning errors (Salem Issa et al., 2019; Vicharnakorn et al., 2014). These errors could be created because of the mismatching of sample plots with the image

pixels introduced when the sample plots were located using GPS and UTM coordinates (Lu et al., 2002; Salem Issa et al., 2019).

2.7.3 Statistical Analysis

Different regression analysis types were conducted (linear, logarithmic, exponential, power, and polynomial) to evaluate the relationship between RS predictors and AGB which calculated on the field using ground measurements and allometric equations (Table 7). Linear regression models based on single Landsat 8 OLI bands and individual VIs (Appendix 5) were first used and their performance assessed by examining the resulting coefficients of determination (R^2) and their statistical significance. Relationships were considered significant at P-value < 0.05. Subsequently, a stepwise multiple regression analysis (backwark elimination) was used to select the best predictors from all variables correlated with AGB of DP plots with the assumption that better correlation can be achieved. Scatter plots were drawn to visualize the relationships between field estimated AGB of DP correlated with RS predictors (see Chapter 4, Subsection 4.2.3 and Chapter 6, Subsection 6.2.3).

2.7.4 Models Evaluation

The models were evaluated using cross-validation by the plot. Root mean square error (RMSE), relative RMSE (RMSE%), and bias were calculated in percentage after randomly splitting the dataset into a calibration dataset (80%), and a validation dataset (20%). The results were validated by comparing RMSE, RMSE%, and bias. The RMSE, RMSE%, and bias were calculated using equations 2, 3, and 4.

$$RMSE = \sqrt{\frac{(\hat{y}_i - y_i)^2}{n}}$$
Eq. (2)

$$RMSE\ \% = 100 \times \frac{RMSE}{\bar{y}} \qquad\qquad \text{Eq. (3)}$$

$$Bias = \hat{\bar{y}}_i - \bar{y} \qquad\qquad\qquad \text{Eq. (4)}$$

where ($\hat{y}_i$) is the predicted AGB of the ith plot, (y_i) is the observed AGB of the

ith plot, ($\hat{\bar{y}}_i$) is the mean of predicted AGB, and ($\bar{y}$) is the mean observed AGB.

2.7.5 Applying the Remote Sensing Based Models to Estimate Aboveground Biomass and Aboveground Carbon

Maps of DP of Abu Dhabi that were generated from a previous study using sub-meter WV-2 imagery were used (see Chapter 2, Subsection 2.6.3 and Chapter 5, Subsection 5.2.3). These maps were overlaid on Landsat 8 OLI images and were subset using ERDAS imagine (see Subsection 2.3 Remote Sensed Data). The spatial model that calculates and presents the amount of AGB in each pixel is built and run in the Spatial Model Editor in ERDAS Imagine. The resulting values in each pixel (digital number) are representing the AGB (t. ha^{-1}). These values were again multiplied by pixels' sizes to figure out the AGB in tons in each pixel using the Attribute Table Function in ERDAS Imagine. Finally, a map illustrating the amount of aboveground carbon (AGC) in each pixel is presented and displayed as brightness value. The percentage of carbon content in AGB was found to be 53.87% (see Chapter 3) and (Salem Issa et al., 2018, 2020b). Therefore, AGC was estimated by multiplying the resulting value by a factor of 0.5387 (equation 5).

AGC (t. ha^{-1}) = 0.5387 × AGB (t. ha^{-1})   Eq. (5)

2.7.6 Calculating the Total Carbon Stock of Date Palm Plantations of Abu Dhabi

The total CS was calculated as a sum of two quantities representing the amounts of carbon in biomass and soil respectively. The first involves estimating

vegetation biomass by calculating the AGB using it to derive the remaining components, i.e., BGB, litter, and debris. The second involves estimating SOC, which is part of SOM. The other carbon pools involving biomass of DP and SOC were presented in Chapter 6, Subsection 6.2.5, and calculated as follows:

a.*Belowground biomass (BGB)*: AGB amount can be used to predict root biomass (BGB), which is generally estimated at 20% of the AGB based on the predictive relationship applied by many studies (Cairns et al., 1997; Mokany et al., 2006; Ramankutty et al., 2007). However, the AGB: BGB ratios were found different for DP species (see Chapter 3, Subection 3.2.2) and varied among palm maturity stages with averages of 0.332, 0.925, and 0.496 for young DP, medium DP, and mature DP, respectively. Therefore, the BGB of DP was calculated in tons as per equations 6, 7, and 8.

$$BGB_{\text{Mature DP}} (t) = AGB \times 0.496 \qquad \text{Eq. (6)}$$

$$BGB_{\text{Medium DP}} (t) = AGB \times 0.925 \qquad \text{Eq. (7)}$$

$$BGB_{\text{Young DP}} (t) = AGB \times 0.332 \qquad \text{Eq. (8)}$$

The belowground carbon (BGC) was estimated in tons by multiplying the resulting value by a factor of 0.5127 (equation 9).

$$BGC (t) = 0.5127 \times BGB (t) \qquad \text{Eq. (9)}$$

b. Litters and Debris: CS of dead wood or litter and woody debris (e.g., dead or broken branches, leaves, etc.) are generally assumed to be equivalent to 10 to 20% of the calculated AGB (Gibbs et al., 2007; Houghton et al., 2009). The boundaries between dead biomass and litter, and between dead biomass and SOM, are somewhat arbitrary as stated by (Houghton et al., 2009). Therefore, an assumption was made on this study that litter and debris ratio to AGB of DP are varied and depend on the palm maturity

stages to be 0.1 in young DP, 0.15 in medium DP and 0.2 in mature DP (Chapter 6, Subsection 6.2.5).

c. Soil Organic Carbon (SOC): It was found that an estimated total of about 22.26 tons of SOC was added per hectare in the areas dominated by DP (see Chapter 3, Subsection 3.2.3.2). Therefore, the SOC in tons of DP for the three age stages were calculated as per equation 10.

$$SOC = Area \times 22.26 \text{ t. ha}^{-1} \qquad \text{Eq. (10)}$$

Chapter 3: Development of Date Palm Biomass Allometric Equations and Calculation of Carbon Stock in its Biomass Components and Soil

Note: This Chapter presents the results of developing allometric equations for date palm in the study area (see Chapter 2, Subsection 2.5 for the methodology). The substantive part of this chapter has been published in a refereed International Conference proceeding as well as in a peer-reviewed journal while working on this dissertation:

- Issa, S., Dahy, B., Ksiksi, T., & Saleous, N. (2018). Development of a new allometric equation correlated with RS variables for the assessment of date palm biomass. Proceedings of the 39th Asian Conference on Remote Sensing (ACRS 2018), Kuala Lumpur, Malaysia, 15–19 October 2018.
- Issa, S., Dahy, B., Ksiksi, T., & Saleous, N. (2020). Allometric equations coupled with remotely sensed variables to estimate carbon stocks in date palms. Journal of Arid Environments, 182, 104264.

3.1 Overview

Some palm species are considered keystone and provide multiple ecosystem services, such as CS (van der Hoek et al., 2019). The amount of carbon that can be sequestered in palms is relatively high compared to some other plant species. In their study of the relationship between land use and CS in northeastern Brazil, Carlos et al. (2015) found that land planted with palms provided 40 t. C ha^{-1} while lands used for pasture and agriculture provided only 8 t. C ha^{-1} and 5 t. C ha^{-1}, respectively. In another study in Northeast India, Singh et al. (2018) recorded considerably higher amounts of carbon in oil palm plantations than in shifting cultivation fallows. They concluded that a 10 years old oil palm plantation could sequester up to 3.7 t. C ha^{-1} year^{-1}. Hence, palms generate economic benefit and contribute to carbon storage in a more sustainable way especially when planted in areas of low productivity or on degraded lands.

Afforestation projects can be used to earn carbon credits and reduce the carbon footprint. This type of supportive efforts has a growing interest among policymakers and governments (Baral & Guha, 2004). Therefore, estimation of CS in forests and plantations is an important measure towards assessing mitigation effects on global change (Ebuy et al., 2011). Many destructive techniques (felling or harvesting) exist to directly estimate CS (Gibbs et al., 2007). Although these techniques provide the most accurate measure of biomass, they ultimately rely on ground measurements and can cause severe destruction to the forests as well as a risk of environmental deterioration (Khalid & Hamid, 2017; Maulana et al., 2016). In addition, such methods are tedious and time consuming (Ebuy et al., 2011), hence they cannot be used routinely. Therefore, developing biomass equations (allometry) that rely on non-destructive measurements, is very essential in estimating biomass. Subsequently, allometric equations have been developed and used to estimate tree biomass and CS from dendrometric measures, such as tree diameters and height (Ebuy et al., 2011; Picard et al., 2012). Notwithstanding, the number of trees destructively sampled to build allometric equations is not constant and differs from one study to another. Currently, there is no consensus on that number, as this is often dependent on resource availability and permission to harvest trees (Yuen et al., 2016). For example, Russell (1983), and Moran and Grace (1996) used 15 and 14 trees, while Brown et al. (1995) and Khalid et al. (1999a) used only 8 and 10 trees, respectively to build their allometric equations.

Different quantitative variables were considered when building oil palm biomass allometric equations (Korom & Mastuura, 2016) (Appendix 1). Henson and Chang (2003) used age as a predictor to estimate the standing biomass of oil palm in tons per hectare. Others used structural variables such as total height and trunk height

(Dewi et al., 2009; Khalid et al., 1999a; Thenkabail et al., 2004), while Corley et al. (1971) used DBH, number of fronds, leaf area, rachis and petiole length, rachis and petiole cross-sectional area at intervals, and volume of petiole sections in their pioneer study to estimate the average yield of oil palms. More recently, allometric equations have been used, coupled with RS and field-based structural variables measurements (Fonton et al., 2017; Salem Issa et al., 2019). Furthermore, Cheng et al. (2014) recommended to develop more equations with different field structural variables that can be linked to RS predictors. Likewise, Jucker et al. (2017) suggested in their review of allometric equations to develop a new generation of allometric equations that estimate biomass based on attributes which can be remotely sensed.

Most biomass equations, whether species-specific or multispecies, have been developed for tropical rainforest ecosystems because of their relevance to the global carbon cycle (Basuki et al., 2009; Brown, 1997; Chave et al., 2005; Cole & Ewel, 2006; Makinde et al., 2017). A few plant species biomass assessment equations are available for desert ecosystems. Nonetheless, none of these were used to fit one of the most important fruit crops in arid regions, *Phoenix dactylifera*, date palm (DP). Over two-third of dates production amount worldwide are produced in the Arab World (El-Juhany, 2010). Three of the top 10 date producers worldwide are located in the Arabian Peninsula, namely: Saudi Arabia, UAE, and Oman (Kader & Hussein, 2009; AOAD, 2008). On the other hand, the UAE has the largest number of DP for any single country in the world. In 2008, the UAE had more than 16 million DP producing around three quarters of a million tons of dates (El-Juhany, 2010). Furthermore, the UAE possesses at least 200 cultivars, 68 of which are the most important commercially (El-Juhany, 2010)..

DP possess multipurpose advantages, including environmental benefits, especially for the Arabian Peninsula population including the UAE, where DP have been an integral part of the farming system. More than 90% of the UAE territory is covered by desert ecosystems representing more than two-thirds of the country's land area. DP species are a good alternative for CS in such arid ecosystems. To estimate DP biomass and its carbon content, it is necessary to quantify the biomass in all palm components. Moreover, it would be more accurate to include both the AGB and BGB in estimating the CS, as both are available for recycling in the ecosystem at replanting (Khalid et al., 1999b).

The current chapter meets objectives no. 1 and 2 of the dissertation (see Chapter 1, Subsection 1.3 Aim and Objective). Specifically, this chapter aims at: (1) Identifying the most relevant structural field variables for the estimation of DP biomass; (2) Developing specific allometric biomass equations that can be correlated with RS variables; (3) Estimating CS in date palms; and (4) Assessing the potential of DP species to improve soil CS in such desert ecosystems.

3.2 Results

3.2.1 Field Variables of Date Palm at Different Age-Stages

The correlation coefficients between fresh and dry weight for the palm's crown trunk and root components were estimated at 0.99, 0.97 and 0.97, respectively; while the correlation between the total fresh weight and the total dry weight gave a value of 0.99. Furthermore, the dry to fresh ratio or factor (DF), for the BGB was estimated at 0.45, while that of the AGB was calculated at 0.40 (Table 9). As for the non-structural variables, age proved to be an important factor influencing the storing of DP biomass ($P < 0.05$). The significant correlation between age of DP and its total biomass/ AGB remains positively strong for either fresh or dry weights (Table 10).

Table 9: Average of dry to fresh weight factor for each DP component.

All Ages	Crown DF	Trunk DF	Root DF	Total DF	AGB DF
(Mean ± SE)	(0.41 ± 0.01)	(0.37 ± 0.02)	(0.45 ± 0.02)	(0.42 ± 0.01)	(0.4 ± 0.02)

*DF is dry to fresh factor calculated as a ratio between dry to fresh weights.
**AGB includes crown plus trunk only.
*** SE is the standard error.

3.2.2 Ratios of Date Palm Biomass Components

Given that the correlation between fresh and dry weights of DP (0.99 for both aboveground and total weights) was found to be very strong; dry weight was used in all subsequent calculations as well as for building the biomass allometric equations of DP. For young DP, with non-developed trunk, CB ranged between 17.2 Kg and 34.1Kg with a mean value of 22.5 Kg, contributing 75.1% of the total palm biomass. While the BGB contributed about 24.9% of that total biomass (Table 11). It is worth noting that in the case of young DP, the AGB consists of only the CB. The contribution of the crown and root to the total biomass increased with age hence, with trunk growth of the palm. The ratio of CB to total biomass decreased to 35.75% and 34.89% of the total biomass for medium and mature DP, respectively. While the root system's contribution to the total biomass increased to 35.38% as the palms grew older (Table 11).

Table 10: Field variables of DP used to assess allometric equations.

Field Variables	Young (< 5 year) (Mean ± SE)	Medium (5-10 year) (Mean ± SE)	Mature (> 10 year) (Mean ± SE)
DBH (cm)	33.87 ± 2.28	43.29 ± 7.45	51.57 ± 5.1
H (m)	4 ± 0.167	4.85 ± 0.206	8.38 ± 0.48
Ht (m)	-	0.764 ± 0.196	3.21 ± 0.52
Δ height (m)	4 ± 0.17	4.086 ± 0.22	5.17 ± 0.36
CD (m)	3.09 ± 0.46	5.66 ± 0.25	7.2 ± 0.08
CA (m^2)	8.15 ± 2.57	25.36 ± 2.28	40.73 ± 0.86
# Fronds	29.8 ± 2.27	35 ± 5.17	61.6 ± 2.32
Weight of fresh component (Kg.palm^{-1})			
Crown	50.65 ± 5.43	171.08 ± 34.47	367.24 ± 78.56
Trunk	-	74.18 ± 13.61	365.28 ± 30.65
Root	21.43 ± 6.39	187.36 ± 27.91	282.06 ± 25.25
Total weight	72.08 ± 11.19	432.62 ± 66.41	1014.58 ± 95.92
AG weight*	50.65 ± 5.43	245.26 ± 42.99	732.52 ± 91.38
Weight of dry component (Kg.palm^{-1})			
Crown	22.51 ± 3.06	65.17 ± 11.87	148.5 ± 35.85
Trunk	-	29.53 ± 8.62	135.91 ± 19.62
Root	7.46 ± 1.88	87.61 ± 14.87	141.23 ± 13.59
Total	29.97 ± 4.17	182.3 ± 32.07	425.63 ± 45.6
AG weight*	22.51 ± 3.06	94.69 ± 18.45	284.41 ± 43.15

*Aboveground weight equals crown weight plus trunk weight of the palm.
**SE is the standard error.

The trunk contained 16.20% of the total biomass in medium DP palms and 31.93% of the total biomass in mature DP. The mean % of TB in all palm age stages (with no trunk in young palm) approaches 15.98% of the total biomass (Table 11).

Table 11: DP component's biomass calculated as a ratio of total or AGB.

Component	To	Young DP%	Medium DP%	Mature DP%	Mean%
CB	Total	75.11	35.75	34.89	48.59
TB		-	16.2	31.93	15.98
BGB		24.89	48.06	33.18	35.38
AGB		75.11	51.94	66.82	64.31
CB	AGB	100	68.82	52.21	73.68
TB		-	31.18	47.79	26.32
BGB		33.15	92.52	49.66	58.44

Where CB is crown biomass, TB is trunk biomass, BGB is below ground biomass, AGB is above ground biomass, and Total is total biomass.

The AGB alone contained most of the DP biomass with an average of 75.11%, 51.94% and 66.82% for young, medium and mature DP, respectively. The crown was found to retain most of the AGB at all ages. It was noted that each component of the DP followed a different rate of biomass storing at each age stage. The BGB to AGB ratios changed considerably during growth stages of the DP with values of 33.15%, 92.52% and 49.66% for young, medium and mature DP, respectively. The average mean percentage of BGB to AGB was 58.44% when averaged over all age stages. It increased to 71.1% when including DP with developed trunks from the medium and mature stages only (Table 11).

3.2.3 Biomass Allometric Equations of Date Palm

3.2.3.1 Crown Biomass (CB)

All field variables showed significant correlation with CB except DBH and ΔHeight (Table 12). The four field variables that gave the highest correlation with CB were: Age, CA, CD and H. After applying different types of relationships (linear, polynomial, power, logarithmic, and exponential equations), it was found that the power equation (11) with 'Age' as independent variable had the highest R^2 (equal to 0.857) (see Table 12).

$$CB = 6.4575 \times Age^{1.1019} \qquad\qquad Eq. (11)$$

However, age is a non-structural variable and cannot be measured directly in the field. It has to be obtained from farmers or from the farm's records. Furthermore, it was intended to identify potential field structural variables to develop specific DP allometric equations that would be used in a RS based CS assessment model of DP in the region. Therefore, the use of other well-correlated structural variables such as CA

to estimate CB was very appropriate. Equation (12) applying an exponential expression with CA as independent variable and depicted graphically in Figure 20, was found to have the best R^2 (equal to 0.8354) (see Table 12).

$$CB = 14.034 \times e^{0.0554 \times CA} \ (CA \neq 0) \qquad \text{Eq. (12)}$$

Table 12: Best prediction equations for crwon biomass estimation of DP.

Regression Equations	Variable	R^2	*P* value
CB= 6.4575 × Age$^{1.1019}$	Age	0.857***	0.00002
CB= 0.2506 × DBH$^{1.4548}$	DBH	0.3054*	0.229
CB= 1.0874 × H$^{2.3225}$	Height	0.8114***	0.00002
CB= 2.4525 Ht^2 + 29.201 Ht + 30.12	Ht	0.7602**	0.00003
CB= 0.3013 × Δ Height$^{3.5402}$	Δ Height	0.4466*	0.02
CB= 5.8364 × e$^{0.4231 \times CD}$	CD	0.8143***	0.002
CB= 14.034 × e$^{0.0554 \times CA}$	CA	0.8354***	0.001
CB= 0.1113×#Frond^2 -6.4461×#Frond +125.63	#Fronds	0.7181**	0.0003

*weakly significant **moderately significant ***strongly significant
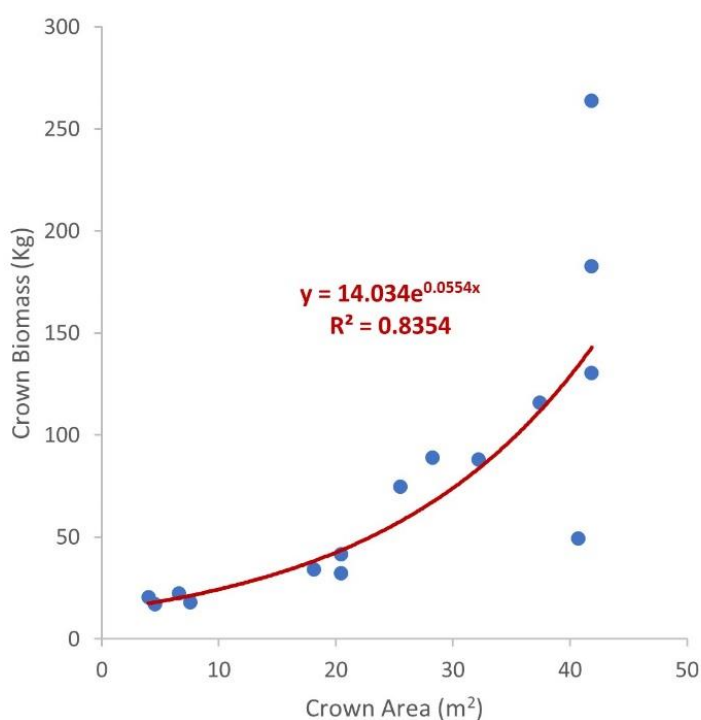
Figure 20: Allometric equation for estimating CB of DP as function of CA (Salem Issa et al., 2020b).

3.2.3.2 Trunk Biomass (TB)

All field variables were significantly correlated with TB except DBH and ΔHeight (Table 13). The three field variables that gave the highest correlation with TB were: Ht, H, and CA (Table 13). After applying same procedure as in 2.3.1, it was found that the power equation (13) using Ht as the independent variable, had the best R^2 (equal to 0.828) (see Table 13 and Figure 21).

$$TB = 40.725 \times Ht^{0.9719} \qquad\qquad \text{Eq. (13)}$$

Table 13: Best prediction equations for trunk biomass estimation of DP.

Regression Equations	Variable	R^2	P value
TB= 0.5808 × Age$^{1.9271}$	Age	0.753	0.002
TB= 0.0816 × DBH$^{1.7212}$	DBH	0.3967	0.197
TB= 0.2879 × H$^{2.8666}$	Height	0.8017	0.001
TB= 40.725 × Ht$^{0.9719}$	Ht	0.8276	0.0004
TB= 0.4644 × ΔHeight$^{3.1733}$	ΔHeight	0.3252	0.176
TB= 0.1286 × e$^{0.9487 \times CD}$	CD	0.7556	0.008
TB= 2.356 × $^{0.0966 \times CA}$	CA	0.7566	0.008
TB= 0.008 × #Frond$^{2.3274}$	#Fronds	0.7403	0.008
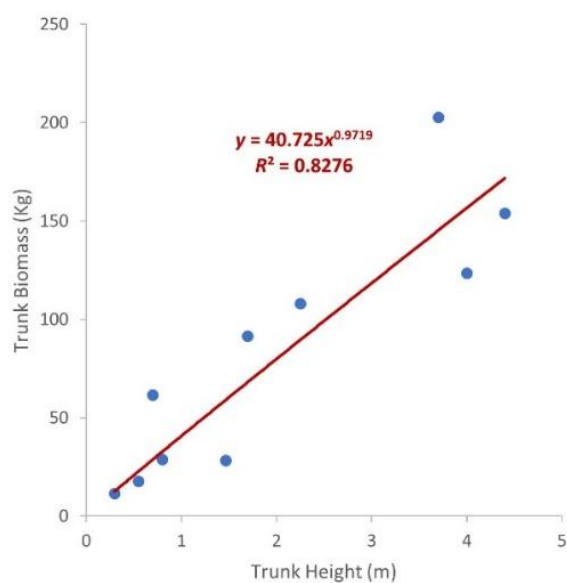
Figure 21: Allometric equation for estimating TB of DP as function of Ht (Salem Issa et al., 2020b).

3.2.3.3 Total Biomass

AGB is the resulting sum of crown biomass (CB) and trunk biomass (TB). It can be estimated from CA (Equation 12) and Ht (Equation 13) that were found to be the most significant field structural variables for predicting crown and trunk biomass, respectively. Finally, the resulting allometric equation to estimate AGB of DPs is given in equation (14) below.

$$AGB = CB + TB \qquad\qquad \text{Eq. (14)}$$

Where: $CB = 14.034e^{0.0554 \times CA}$ (with $CA \neq 0$), and $TB = 40.725 \times Ht^{0.9719}$. While BGB is estimated as a ratio of AGB as per Table 11.

3.2.4 Carbon Stock in Date Palm Plantations at Different Age-Stages

Overall trunk of DP had a higher organic matter (OM) content of its dry weight than crowns and roots with averages of 93.3%, 92.43% and 88.39%, respectively (Table 14). The average percent OM was 91.38% for the whole DP (i.e. sum of the 3 components) and 92.87% for AGB. The same was noted about the organic carbon (OC) content to dry weight of DP. The trunk had higher OC content than crown and roots (54.12%, 53.61% and 51.27%, respectively). The percentage of carbon content in the root system of DP (BGB) was found to be 51.27%, which is slightly lower than the carbon content in the AGB. The average percentage of OC for whole DP was 53% of the AGB. The total OM and OC stocks in the various DP components expressed per palm are shown in Table 14. The whole DP contains about 15.88 Kg of OC for young DP with increasing values of a maximum of 96.62 Kg and 225.58 Kg for medium and mature DP, respectively. While the AGB contained averages of 11.93 Kg, 50.19 Kg and 150.74 Kg of OC for young, medium and mature DP, respectively.

Table 14: OM and OC (Kg. palm^{-1}) in DP components at a different age stages.

DP Component	Age Stage	Dry Weight	OM		OC	
Crown	Young	22.51	92.43%	20.81	53.61%	12.07
	Medium	65.17		60.24		34.94
	Mature	148.50		137.26		79.61
Trunk	Young	-	93.31%	-	54.12%	-
	Medium	29.53		27.55		15.98
	Mature	135.91		126.82		73.55
Root	Young	7.46	88.39%	6.59	51.27%	3.82
	Medium	87.61		77.44		44.92
	Mature	141.23		124.83		72.41
Total Biomass	Young	29.97	91.38%	27.39	53.00%	15.88
	Medium	182.30		166.59		96.62
	Mature	425.63		388.94		225.58
AGB	Young	22.51	92.87%	20.91	53.87%	12.13
	Medium	94.69		87.94		51.01
	Mature	284.41		264.13		153.21

The average SOM content of samples taken from underneath the DP canopy (labeled "In") increased with age, registering 4.28%, 5.02% and 5.06% for young, medium and mature DP, respectively, with an overall mean of 4.79% (Table 15). On the other hand, the average SOM content of samples taken away from the DP canopy (labeled "Out") registered 3.0%. This percent represents only about two-third of that recorded from samples taken beneath ("In") the date palms (Table 15).

Table 15: Percent SOM and SOC for different canopy positions.

Underneath/ Far Away DP	Soil Organic Matter (%)		Soil Organic Carbon (%)	
	In	Out	In	Out
Qattara Farm	5.06	4.1	2.6	2.38
Masakin Farm	4.28	1.9	2.48	1.1
Average	4.67	3.0	2.54	1.74

Percent SOC was transformed into bulk tons of SOC per hectare (Table 16), The average bulk density ranged from 0.74 to 1.24 g/cm^3 with a mean of 0.88 g/cm^3. An estimated total of about 22.26 tons of SOC was added per hectare in the areas dominated by DP. Variations between different age stages were also detected. The average SOC at young, medium and mature DP were 20.29, 23.66 and 22.83 tons per hectare, respectively. At the individual palm level, the average SOC was 18.09 Kg.palm^{-1}, 62.59 Kg.palm^{-1} , and 92.91 Kg.palm^{-1} for young, medium and mature DP, respectively, with an overall average of 57.87 Kg.palm^{-1} (Table 16). There was a strong correlation between SOC (Kg.palm^{-1}) and palm CA (m^2) with R^2 equal 0.9523 (Figure 22). Thus, CA can be used as a suitable predictor to estimate SOC using the power regression given in Equation (15).

SOC (Kg.palm^{-1}) = 1.5474 x CA$^{1.1144}$ Eq. (15)
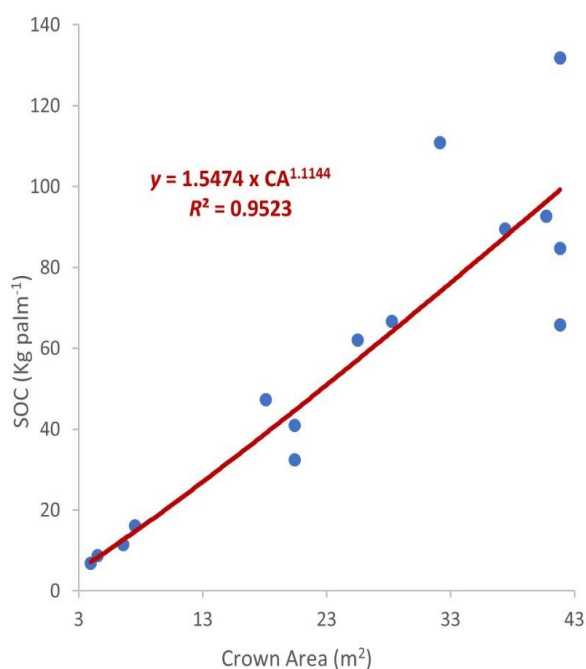
Figure 22: Prediction equation of soil organic carbon as function of CA (Salem Issa et al., 2020b).

Table 16: SOM and SOC at 10 cm depth under DP at three different age stages.

DP Age Stage	Age (year)	CA (m^2)	SOM (%)	SOC (%)	SOC (g/m^2)	SOC (Kg.palm^{-1})	SOC (ton.ha^{-1})
Young	2.5	3.98	3.08	1.79	1731.58	6.88	17.32
	2.5	4.52	4.48	2.6	1932.42	8.74	19.32
	3	7.55	3.75	2.18	2126.36	16.05	21.26
	3	6.61	3.48	2.02	1740.43	11.5	17.4
	4	18.1	6.59	3.82	2613.07	47.29	26.13
	Mean	8.152	4.276	2.482	2028.772	18.092	20.286
Medium	5	20.43	3.99	2.31	2003.73	40.93	20.04
	7	28.27	4.58	2.65	2359.16	66.7	23.59
	8	25.52	4.95	2.87	2430.97	62.03	24.31
	9	32.17	8.36	4.85	3446.96	110.89	34.47
	10	20.43	3.22	1.87	1587.22	32.42	15.87
	Mean	25.364	5.02	2.91	2365.608	62.594	23.656
Mature	11	40.72	4.06	2.35	2277.49	92.73	22.77
	14	41.85	7.27	4.22	3151.01	131.88	31.51
	16	37.39	5.74	3.33	2392.35	89.46	23.92
	18	41.85	3.79	2.2	1571.99	65.79	15.72
	20	41.85	4.46	2.59	2023.26	84.68	20.23
	Mean	40.732	5.064	2.938	2283.22	92.908	22.83
Averages			4.79	2.78	2225.87	57.87	22.26

3.3 Summary

In this chapter, specific allometric biomass equations were developed that can be integrated into a RS-based model for assessing carbon sequestered in DP. Assessing the potential of DP to improve soil carbon sequestration was another objective. The average amounts of DP biomass, organic matter, organic carbon, and soil organic carbon at different age stages were presented on Appendix 6. Here and based on field and lab work, relevant structural variables were identified and used in the development of allometric equations. Results showed that the crown area (CA) best estimated both crown biomass (CB) and soil organic carbon (SOC). Likewise, the trunk height (Ht) was the best estimator of trunk biomass (TB). Using these variables, allometric equations were developed for date palms at different age stages and were used to

estimate CB, TB and SOC with coefficients of determination (R^2) of: 0.884, 0.835 and 0.952, respectively. Furthermore, the average ratios of below ground biomass (BGB) to above ground biomass (AGB) varied with palm maturity stages averaging 0.332, 0.925 and 0.496 for young, medium and mature palms, respectively. Moreover, the results demonstrated that the amounts of organic carbon (OC) stored in date palms were considerable with values of: 15.88 Kg. palm^{-1} for young DP, 96.62 Kg. palm^{-1} for medium DP, and 225.58 Kg. palm^{-1} for mature DP. Substantially higher amounts of SOC were measured compared to other local plants with values of: 18.092 Kg. palm^{-1}, 62.594 Kg. palm^{-1}, and 92.908 Kg. palm^{-1} under young, medium and mature DP palms, respectively. The main achievement was the development of new and unprecedented allometric equations for DP species in arid land. Such equations allow the development and calibration of a RS-based model for estimating biomass and CS of date palms in the region with high accuracy.

Chapter 4: A Pilot Study to Assess Carbon Stock in Date Palm Plantations Using Remote Sensing Data and Field Measurements

Note: This Chapter presents the results of working on the "Pilot area" on Al-Foah area (north of Al-Ain city),by applying the methods detailed in sections 2.7.1 to 2.7.4 (see Chapter 2) in order to examine the approach and build the RS-based biomass model. The substantive part of this chapter has been published in a peer-reviewed journal while working on the dissertation:

- Issa, S., Dahy, B., Saleous, N., & Ksiksi, T. (2019). Carbon stock assessment of date palm using remote sensing coupled with field-based measurements in Abu Dhabi (United Arab Emirates). International Journal of Remote Sensing, 0(0), 1–20.

4.1 Overview

Forests act as large carbon pools where CO_2 from the atmosphere is converted into plant biomass by photosynthesis (Chapter 1). It is estimated that carbon sequestration in forests amounts to 2-4 gigatons annually (Qureshi et al., 2012). However, around 60% of carbon sequestered in the forest is returned to the atmosphere by deforestation (Vicharnakorn et al., 2014). Thus, forests play an important role in the carbon cycle. Understanding the long-term behavior and drivers of carbon sequestration is indispensable under the global change scenarios, land-use land-cover, and in climate change studies (Corona-Núñez et al., 2018). Afforestation, known to compensate for the increase of carbon emission resulting from deforestation and land degradation, is costly and difficult to implement especially in arid lands due to water deficiency. DP plantations have a huge capacity of storing and sequestering terrestrial carbon in both the vegetative parts (shoot and root) as well as the soil compartment is of paramount significance for this research (Chapter 3).

RS can obtain forest information (AGB and CS) over large areas with repetitive coverages, at a reasonable cost and with acceptable accuracy (Chapter 1, Subsection

1.4.4). In general, low-resolution and medium-resolution satellite images do not allow mapping land-cover change accurately. Landsat proved to be a good alternative and is frequently used for many applications as it is freely available. RS data have been correlated with plot-based field measurements to estimate AGB, hence CS. Furthermore, the integration of RS data into GIS models enables adding ancillary and field data in the analysis and increasing reliability in estimating AGB, hence CS. Building GIS-based models to predict future scenarios for forest management and the implementation of afforestation plans is another more valuable product.

This Chapter meets objective no. 3 of the dissertation by characterizing the carbon stock of date palm using a RS-based biomass model (see Chapter 1, Subsection 1.3 Aim and Objective). Specifically, this chapter aims at: (1) Identifying the most reliable RS variables to estimate AGB of DP in Abu Dhabi using Landsat 8 OLI imagery, (2) Building a RS-based biomass model to calculate CS in DP in the study area.

4.2 Results

4.2.1 Date Palm Plantations' Structure and Plot Densities

Table 17 shows the number of DP per plot, average crown area (CA), trunk height (Ht) and densities of DP plot. The number of DP in the tested plots was 401. The different numbers of DP in each plot led to different DP densities per hectare giving a range of 38 to 188 palm. ha^{-1}. Plots L, N and K had the lowest number of DP (6, 8, and 12 respectively) and densities per hectare (38, 50, and 75 respectively). While plots C and D had the highest number of DPs (30 and 27 respectively) producing the highest densities per hectare (188 and 169 respectively).

The average DP's CA values ranged between 4.85 to 43.57 m². The average DP's Ht values ranged between 0.13 to 2.79 meters. The plots that had the highest average of CA and Ht for DP (e., g., plot A, B, F) contained mature DP (22, 22, and 21 years respectively). While the plots that had the lowest average of CA and Ht for date palms (e., g., Q, R, M, and S) contained recently planted DP (less than 9 years). It was found that some young DP had CA equal 0.07 m² and Ht equal to 0 because their fronds were tied by rope with no main trunk.

Table 17: Averages of CA, Ht, and density values of DP per plot.

Plot	Cultivar	Spacing (m)	Age	No	Ave. CA (m²)	Avg. Ht (m)	Density (palm.ha^{-1})
A	Khalas	7×6	Mature	25	43.57	2.56	156
B	Khalas	8×7	Mature	25	41.85	2.72	156
C	Khalas	7×6	Mature	30	40.63	2.8	188
D	Barhi	7×6	Mature	27	20.65	1.34	169
E	Barhi	Sparse	Mature	17	29.4	2.43	106
F	Khalas	7×7	Mature	25	41.45	2.79	156
G	Khalas	7×7	Mature	22	32.07	2.02	138
H	Khalas	7×7	Mature	22	22.81	1.52	138
I	Khalas	7×7	Mature	21	29.02	1.64	131
J	Barhi	7×7	Mature	20	29.39	1.85	125
K	Majdool	Sparse	Medium	12	20.65	0.97	75
L	Majdool	Sparse	Medium	6	23.98	0.88	38
M	Majdool	8×8	Medium	25	6.42	0.48	156
N	Barhi	Sparse	Medium	8	13.79	0.38	50
O	Barhi	8×8	Medium	21	15.26	0.59	131
P	Barhi	Sparse	Medium	24	8.23	0.65	150
Q	Barhi	8×8	Young	23	4.85	0.28	144
R	Barhi	8×8	Young	23	5.86	0.19	144
S	Fahel	8×8	Young	25	7.02	0.13	156

4.2.2 The Field-Based Biomass Estimation Model

Regression analysis was performed following methodology described in Subsection 2.7.3. A summary of the AGB for the tested plots is shown in Table 18.

The highest crown biomass (CB) was found in the plot A, B, C, F while the lowest CB was found in the plot N, L, Q, and R. These results were largely influenced by the average of CA of these plots. Same can be said about trunk biomass (TB) which was largely influenced by the average of Ht. The average number of DP per plot was 23.4 which, given a plot area of 1600 m^2, corresponds to around 146 palm ha^{-1}. The average AGB in ton.ha^{-1} was then calculated by multiplying the average AGB per palm by 146. For mature, medium and young DP, the average AGB was estimated at: 29.35, 9.59, and 4.11 ton.ha-^{1} respectively. For mixed ages class, the average was estimated at 19.13 ton.ha^{-1} respectively. The total CS was estimated by multiplying the AGB (ton.ha^{-1}) by 0.5387 according to Equation (5) (see Chapter 2, Subsection 2.7.5). Therefore, the CS for mature, medium and young DP were estimated at: 15.81, 5.17, and 2.22 ton.ha^{-1} respectively. For mixed ages class, the average CS was estimated at 10.3 ton.ha^{-1}.

Table 18: The AGB of each date palm component per palm, and per hectare.

Plot	Age	No.	Per Palm (Kg)			Per Hectare (Ton)		
			CB	TB	AGB	CB	TB	AGB
A	Mature	25	180.42	112.99	293.41	26.34	16.50	42.84
B	Mature	25	151.86	117.92	269.77	22.17	17.22	39.39
C	Mature	30	141.41	120.43	261.84	20.65	17.58	38.23
D	Mature	27	52.58	58.59	111.17	7.68	8.55	16.23
E	Mature	17	81.43	103.76	185.19	11.89	15.15	27.04
F	Mature	25	143.79	120.66	264.44	20.99	17.62	38.61
G	Mature	22	90.46	92.11	182.56	13.21	13.45	26.65
H	Mature	22	53.32	71.41	124.73	7.78	10.43	18.21
I	Mature	21	73.38	77.43	150.81	10.71	11.30	22.02
J	Mature	20	73.83	85.93	159.76	10.78	12.55	23.32
K	Medium	12	45.05	47.77	92.82	6.58	6.97	13.55
L	Medium	6	54.37	43.48	97.85	7.94	6.35	14.29
M	Medium	25	22.18	14.6	36.78	3.24	2.13	5.37
N	Medium	8	30.98	18.07	49.05	4.52	2.64	7.16
O	Medium	21	33.26	28.78	62.04	4.86	4.20	9.06
P	Medium	24	22.24	32.18	54.42	3.25	4.70	7.95
Q	Young	23	18.49	12.91	31.4	2.70	1.88	4.58
R	Young	23	19.53	7.95	27.48	2.85	1.16	4.01
S	Young	25	21.3	3.9	25.2	3.11	0.57	3.68

4.2.3 The RS-Based Biomass Estimation Model

4.2.3.1 Mature Date palms

Mindful of the effect of DP age on their biomass, the regression of RS variables with the field estimated biomass of DP was run for each one of the DP age classes defined earlier. For mature DP (10 plots), the correlation with single bands: SWIR1 and SWIR2 was found significant; while the correlation was significant with all tested VI's except for TCB vegetation index (Appendix 5). SWIR2 was the best single band for AGB DP with R^2 values equal to 0.570. While TCG, GNDVI, and DVI were among the best single VI's for AGB of mature DP with R^2 values equal to 0.797, 0.790, and 0.789 respectively. The results of the stepwise regression analysis on AGB of only the

mature DP showed that a combination of single bands (Red, SWIR1, and SWIR2) highly improved R^2 from 0.398 for Red band, 0.445 for SWIR1 band, and 0.553 for SWIR2 band to a higher value of 0.961 and P-value equal 0.0001 (Equation 16).

$$\text{AGB}_{\text{Mature DP}}(\text{ton.ha}^{-1}) = -25.953 + 0.004(\text{Red}) + 0.008(\text{SWIR1}) - 0.011(\text{SWIR2}) \quad \text{Eq. (16)}$$

4.2.3.2 Non Mature Date palms

For medium and young DP, none of the RS variables of Landsat showed any significant correlation with AGB (except with the single band, SWIR1, and TCB index for medium DP only) (Appendix 5). This could be attributed to the small sample size of medium and young DP (only three plots for each), but also may be due to the less developed crown (for young DP) to be able to compensate for the effect of the soil background reflectance values. Therefore, increasing the number of sample size and using higher spatial resolution data should improve largely the results of the regression analysis to predict the AGB and CS of non-mature DP (see Chapter 6, Subsection 6.2.3).

4.2.3.3 Mixed Ages Date Palms

Considering all DP as one age class (mixed class) resulted in a stronger relationship between AGB (the dependant variable) and RS variables (the independent variables) in the regression analysis. All RS variables of Landsat 8 OLI, single bands and tested VI's, were significantly correlated with AGB of DP (except NIR band, see Table 19). SWIR2 was found to be the best single band and had the strongest regression coefficient among other bands of Landsat 8 OLI for AGB of DP, with R^2 value of 0.754 and *P*-value equal 0.00001. The VIs increasingly improved the relationship between the AGB and the spectral signature for the AGB of DP (Figure

23). SR was the best single VI and had the strongest correlation among all RS variables

of Landsat 8 OLI for AGB of DP, with R^2 value of 0.871 and P-value equal 0.0000001.

Table 19: Linear correlation between RS variables and AGB of DP.

Independent Variable	Constant	Coefficient	R²	P value
Single Band				
B1	58.246	-0.004	0.635	0.0002
B	43.039	-0.003	0.660	0.0001
G	29.439	-0.002	0.670	0.0001
R	19.964	-0.001	0.699	0.00005
NIR	14.765	-0.001	0.036	0.482
SWIR1	18.066	-0.001	0.725	0.00003
SWIR2	15.398	-0.001	0.754	0.00001
Vegetation Index				
DVI	-7.247	0.002	0.859	0.0000003
GNDVI	-13.795	76.126	0.815	0.000002
NDGI	6.287	0.768	0.731	0.00002
NDVI	-5.187	44.843	0.848	0.0000004
RVI	25.284	-32.191	0.833	0.0000008
SAVI	-5.381	30.642	0.851	0.0000004
SR	-18.802	14.956	0.871	0.0000001
TCB	24.918	-0.001	0.638	0.0002
TCG	4.552	0.002	0.851	0.0000004
TCW	7.939	0.001	0.816	0.000006
TVI	-110.982	104.816	0.864	0.0000002
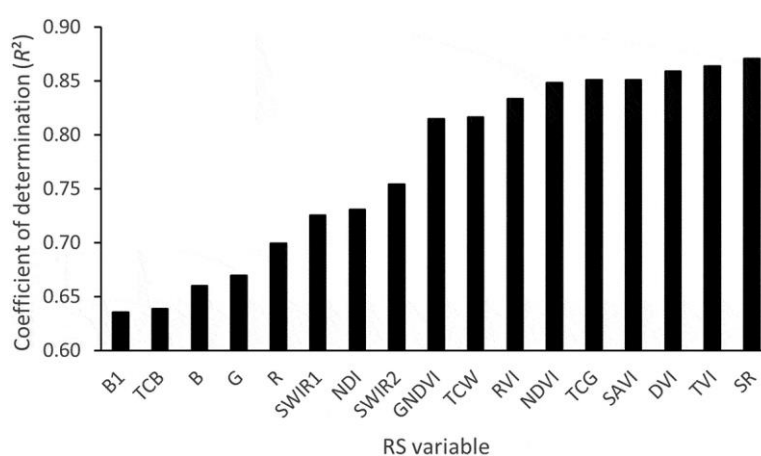
Figure 23: Coefficient of determinations versus RS variables.

By using different types of regression equations, SWIR2 showed the strongest

Figure 24); while SR showed the strongest correlation using a second order polynomial

equation with R^2 equal 0.8947 (Equation 18 and Figure 25).

$$\text{AGB}_{\text{Mixed DP}} \ (\text{ton. ha}^{-1}) = 4 \times 10^{21} \times (\text{SWIR2})^{-4.907} \qquad \text{Eq. (17)}$$

$$\text{AGB}_{\text{Mixed DP}} \ (\text{ton. ha}^{-1}) = 53.261(\text{SR})^2 - 68.472(\text{SR}) + 4.4894 \qquad \text{Eq. (18)}$$
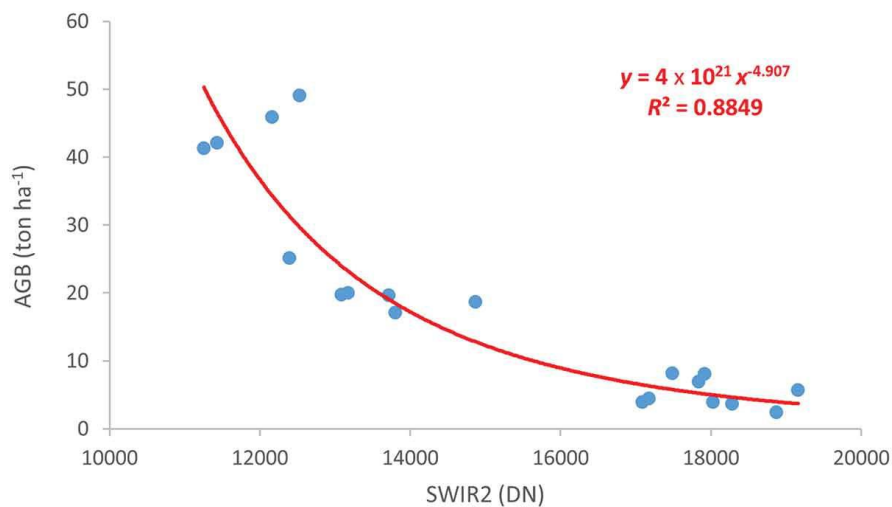
Figure 24: AGB of date palm as a function of SWIR2 of Landsat 8 OLI (Salem Issa et al., 2019).
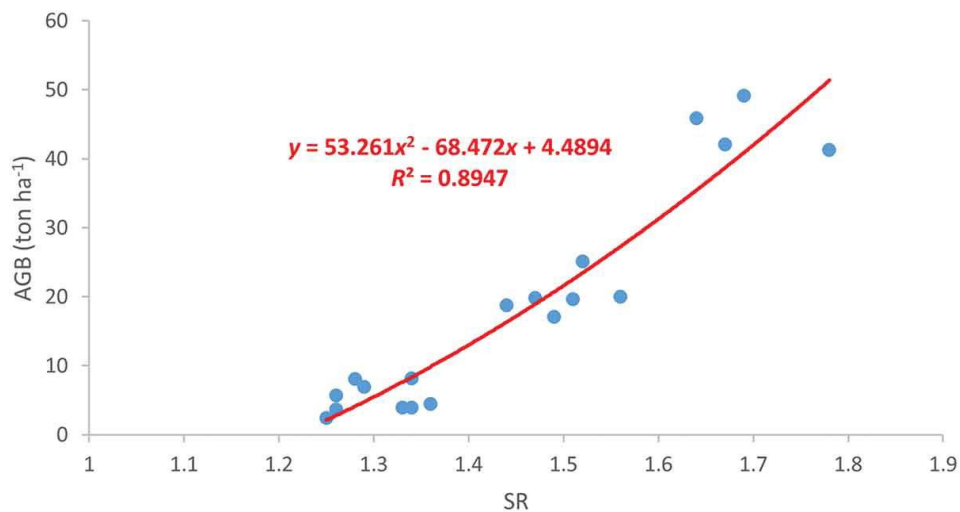
Figure 25: AGB of date palm as a function of SR of Landsat 8 OLI (Salem Issa et al., 2019).

Although the analysis showed that a single band (e.g. SWIR2) or a single VI (e.g. SR) had a correlation that was sufficiently strong to allow the use of the model coefficient in developing biomass estimation model, a stepwise regression analysis indicated that the R^2 is significantly improved if two or more independent variables (bands or VIs) were used in multiple regression models. Furthermore, Bands B1 and B were excluded from the stepwise regression analysis because they contained erroneous values. The results of the stepwise regression showed that a linear regression model combining single bands of Landsat 8 OLI (G, NIR and SWIR2) and VIs (DVI, NDGI, and RVI) improved the R^2 value for the prediction of AGB for DP and therefore giving more accurate results of biomass prediction and CS (Equations 19 and 20). The combination of VIs (DVI, NDGI, and RVI) showed and higher with R^2 equal to 0.952 compared with R^2 values when using the same VIs separately (0.859 for DVI, 0.731 for NDGI, and 0.833 for RVI).

AGB $_{Mixed\ DP}$ (ton. ha^{-1}) = -29.129+0.004(G)+ 0.001(NIR) - 0.002(SWIR2)

Eq. (19)

With (R^2 = 0.927, P-value = 0.0000004)

AGB $_{Mixed\ DP}$ (ton. ha^{-1}) = -189.101+0.009(DVI) + 2.123(NDGI) + 213.612(RVI)

Eq. (20)

With (R^2 = 0.952, P-value = 0.00000004)

4.2.3.4 Models Validation

The model was established based on field measurement and on the statistical accuracy assessment. The accuracy statistics covered the RMSE and RMSE% as explained previously in Chapter 2, Subsection 2.7.4. Table 20 summarized the best regression models for estimation the AGB based on bands values and VIs obtained from the Landsat 8 OLI. The best models to estimate AGB for both, mixed age class

and mature age class, were determined as the model with highest R^2 and lowest RSME, RSME%, and P-values.

Table 20: Results of model performance evaluation (RMSE and RMSE%).

Regression Models	Class	R^2	P value	RMSE	RMSE%
AGB=-89.101+0.009(DVI)+ 2.123(NDGI)+213.612(RVI)	Mixed	0.95	4E-08	6.05	35.73
AGB=-25.953+0.004(R)+ 0.008(SWIR1)-.011(SWIR2)	Mature	0.96	0.0001	9.18	50.77

4.2.3.5 Map Creation

The CS map was constructed using the best performing AGB model constructed from three RS predictors variables as a combination the VI's which are DVI, NDGI, and RVI. The AGB map multiplied by the conversion factor, 0.5387 as per the Equation 5 (see Chapter 2, Subsection 2.7.5) in order to visualize the CS map on part of the study area (Figure 26). The map of CS for the best model of the study area produced by using the spatial modelling tool in ERDAS software.
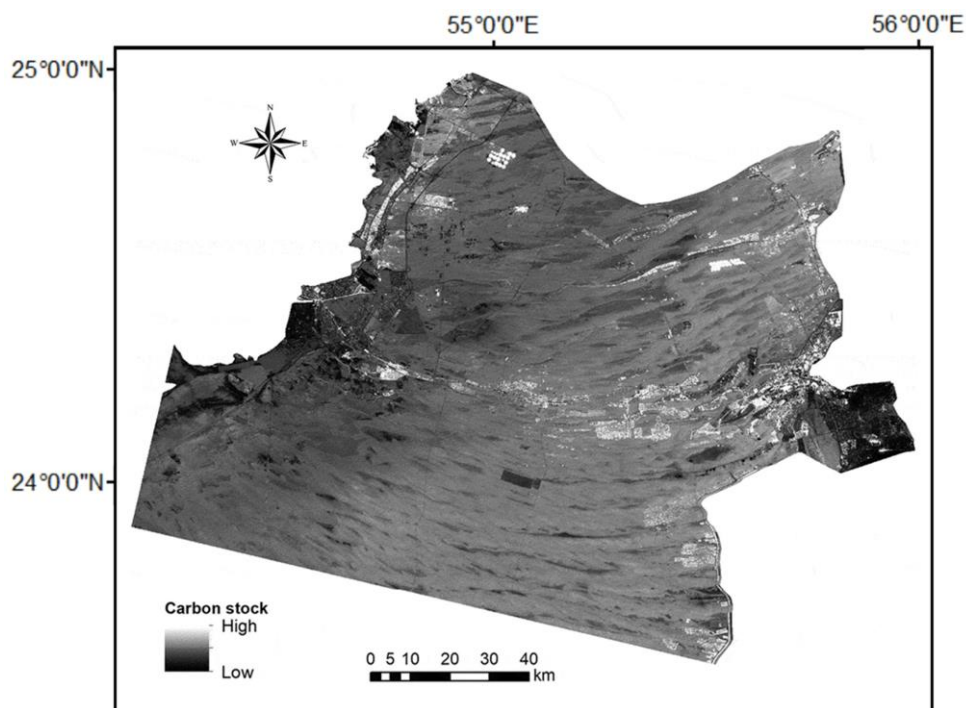
Figure 26: The carbon stock map of the northern east part of study area (Salem Issa et al., 2019).

4.3 Summary

A RS-based biomass model was developed to estimate CS in DP in the study area. Data from Landsat 8 OLI were used to assess the correlation between spectral reflectance of single bands and different VIs on one side, and AGB derived from ground measurements on the other. AGB and CS (ton. ha^{-1}) were estimated using allometric equations developed in a previous study for DP in the area (see Chapter 3). The relationships between the estimated AGB and parameters derived from RS data were tested using single and multiple linear regression analysis. The results indicated a significant correlation with certain RS parameters. For mature DP class alone (>10 years), the correlation with single bands was only significant with SWIR1 and SWIR2 while the correlation was significant with all tested VI's except for TCB vegetation index. A combination of bands R, SWIR1, and SWIR2 improved the determination of

this class to an R^2 value of 0.961. However, for the medium and young DP (10–5 and less than 5 years), the correlation was not significant (with the exception of SWIR1 and TCB index for medium DP), where the use of higher spatial resolution should be a good alternative (see Chapter 5); in addition to expanding the actual field plots to include more plots representing all three age stages of DP (see Chapter 6). On the other hand, for mixed ages (young, medium and mature DP), the strongest correlations were found using SWIR2 single band and the SR vegetation index; having R^2 values of 0.753 and 0.871, respectively. A stepwise multiple regression analysis combining DVI, NDGI, and RVI vegetation indices improved the value the R^2 to a value of 0.952. Finally, results obtained showed that CS represented 53.87% of the total AGB in DP. Subsequently, the average amount of CS for both mature and mixed DP was calculated at 15.81 and 10.3 ton. ha^{-1} respectively. To visualize the results on maps of DP's CS accurately, an accurate mapping of DP plantations (at different age stages) is achieved in subsequent Chapter 5.

Chapter 5: LULC Classification of Abu Dhabi and Accurate Mapping of Date Palm Plantations at Different Age-Stages

Note: This Chapter presents the results of applying the methods which discussed in Chapter 2, Subsection 2.6 in order to classify the main LULC classes of Abu Dhabi and map its date palm plantations. The substantive part of this Chapter has been published and submitted to peer-reviewed journals during the working on the dissertation as follows:

- Dahy, B., Issa, S., & Saleous, N. (2021). Detecting and mapping of mature, medium, and young age date palms in the arid lands of Abu Dhabi, using multi-source / multi-resolution satellite data. Journal of Remote Sensing Applications: Society and Environment (Submitted).

- Issa, S. M., Dahy, B. S., & Saleous, N. (2020). Accurate mapping of date palms at different age-stages for the purpose of estimating their biomass. ISPRS Annals of Photogrammetry, Remote Sensing and Spatial Information Sciences, V-3–2020, 461–467.

5.1 Overview

In this Chapter, a hybrid classification method (HCM) was developed to produce a classified map of the study area comprising seven LULC classes. A GIS-based semi-automatic approach, benefiting from the researcher's prior knowledge of the study area, was then implemented to group the classes and to produce a bitmap (binary mask) of only two types: vegetation and non-vegetation (the vegetation bitmap) (see Chapter 2, Subsections 2.6.1 and 2.6.2). Finally, a set of high-resolution WV-2 imagery was used to classify and map DP plantations at different age stages, within the vegetation bitmap, to create an accurate and reliable DP map (see Chapter

2, Subsections 2.6.3). The output product will be used as an input to the built RS-based biomass model to assess CS in DP plantations in the study area (see Chapter 6). This Chapter meets the objective no. 4 (see Chapter 1, Subsection 1.3 Aim and Objective).

For the purpose of tree crown detection and delineation, many algorithms were developed (Chepkochei, 2011; Hebbar et al., 2014; Lack & Bleisch, 2010; Rizvi et al., 2019; Sahay et al., 2017). However, results of tree detection and delineation can be affected by algorithm characteristics. Indeed, different approaches may give different results despite working in the same environment. Thus, it is important to select the appropriate algorithm to get the suitable results. Moreover, for any algorithm to work properly, crowns should be, at least, detectable and segmented as an object in the image before classification. Training areas of the classes that are to be extracted must be chosen very carefully for not to include any background pixels and non-targeted classes based on visual analysis and on previous knowledge of the area by the interpreter. By using the pan-sharpened WV-2 images (spatial resolution 0.5 meter) (see Chapter 2, Subsection 2.3), DP crowns can be differentiated from the background (soils, grasses, and weeds) and other shrubs and trees using colour, tone, texture, size and planting arrangement (Figure 27). In general, the steps followed could be divided to multi-levels (see Chapter 2 for more details): (1) raster data analysis which includes identifying DP from other vegetation and classifying their age stages (mature, medium, and young) according to their crowns, and (2) vectorising, cleaning up the vector layers and creating the maps. Furthermore, a pixel-based classifier relying on spectral, textural and site information, is used in the raster analysis part (Figure 28b, and 28c). The second level of analysis was done on the vector data model by first vectorising the three raster outputs (mature, medium, and young), smoothing the polygons, calculating the areas, and cleaning up the maps manually (Figures 29d, 29e, and 29f).
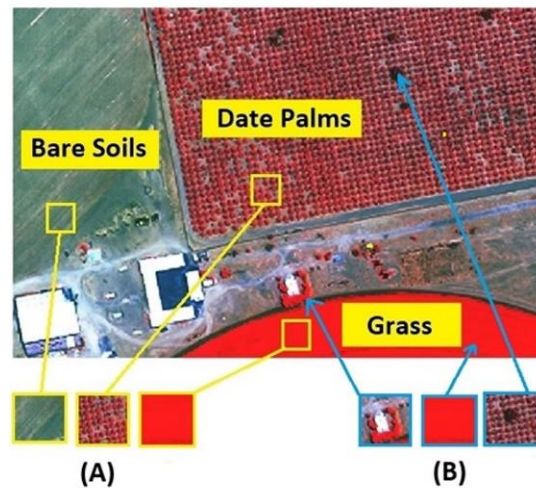
Figure 27: A subset of pan-sharpened WV-2 image. Green, red, and NIR1 bands were used with a spatial resolution of 0.5 meters. The image is displayed in false color. (A) The DP can be differentiated from bare soils and grass visually by using color, tone, and texture; and (B) The DP can be differentiated from other vegetation (grasses, trees, and shrubs) visually using the mentioned tools plus the planting arrangements and spacing.
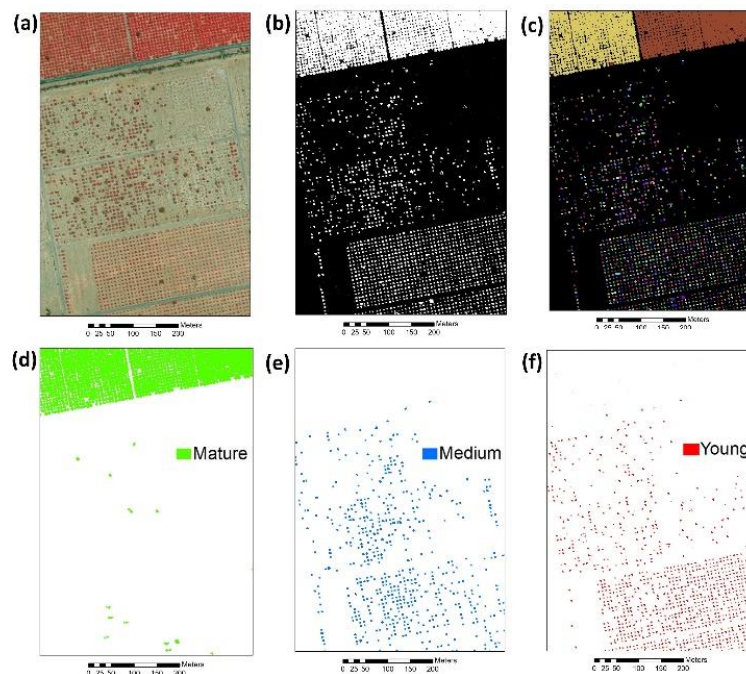
Figure 28: Separating age classes of date palm plantations. The example is from Al Foah DP farm: (a) Original WV-2 image (RGB:7,5,4); (b) SFP using Bayesian network; (c) Threshold and clump applied; (d) Mature palms layer; (e) Medium palms layer; and (f) Young palms layer (Salem Issa et al., 2020).

5.2 Results

5.2.1 LULC Map Creation Using Hybrid Classification

The evaluation of spectral signatures separability (total of 740 training sets) is displayed in Figure 29 where the Y-axis represents the mean signature value of each class (pixel or DN value) and the X-axis represents the Landsat-8 OLI bands. Shortwave infrared bands (SWIR1& SWIR2) had the best separability power of all Landsat 8 OLI bands.
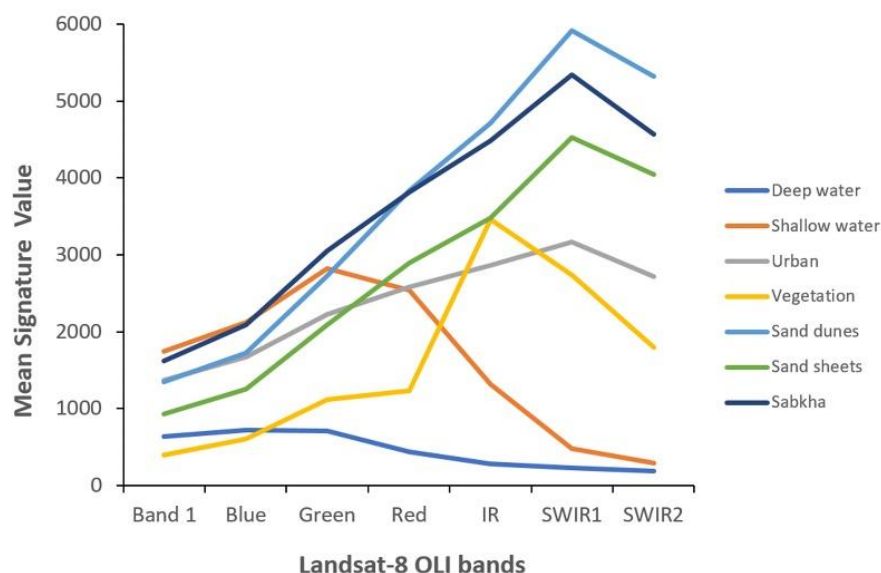
Figure 29: Mean signature value of LULC classes vs. Landsat-8 bands.

Figure 30 displays the class distribution and Table 21 shows their respective areas and percentages in the study area. Sand dunes formed about 70% of the study area with nearly 5 million hectares. Sabkhas occupied 15.51%, while sand sheets, including gravel, made up 8.6% of the study area. Finally, Urban and Vegetation classes constituted only 0.49% with 32,333 hectares and 0.6% with 40,102.6 hectares of the study area, respectively.
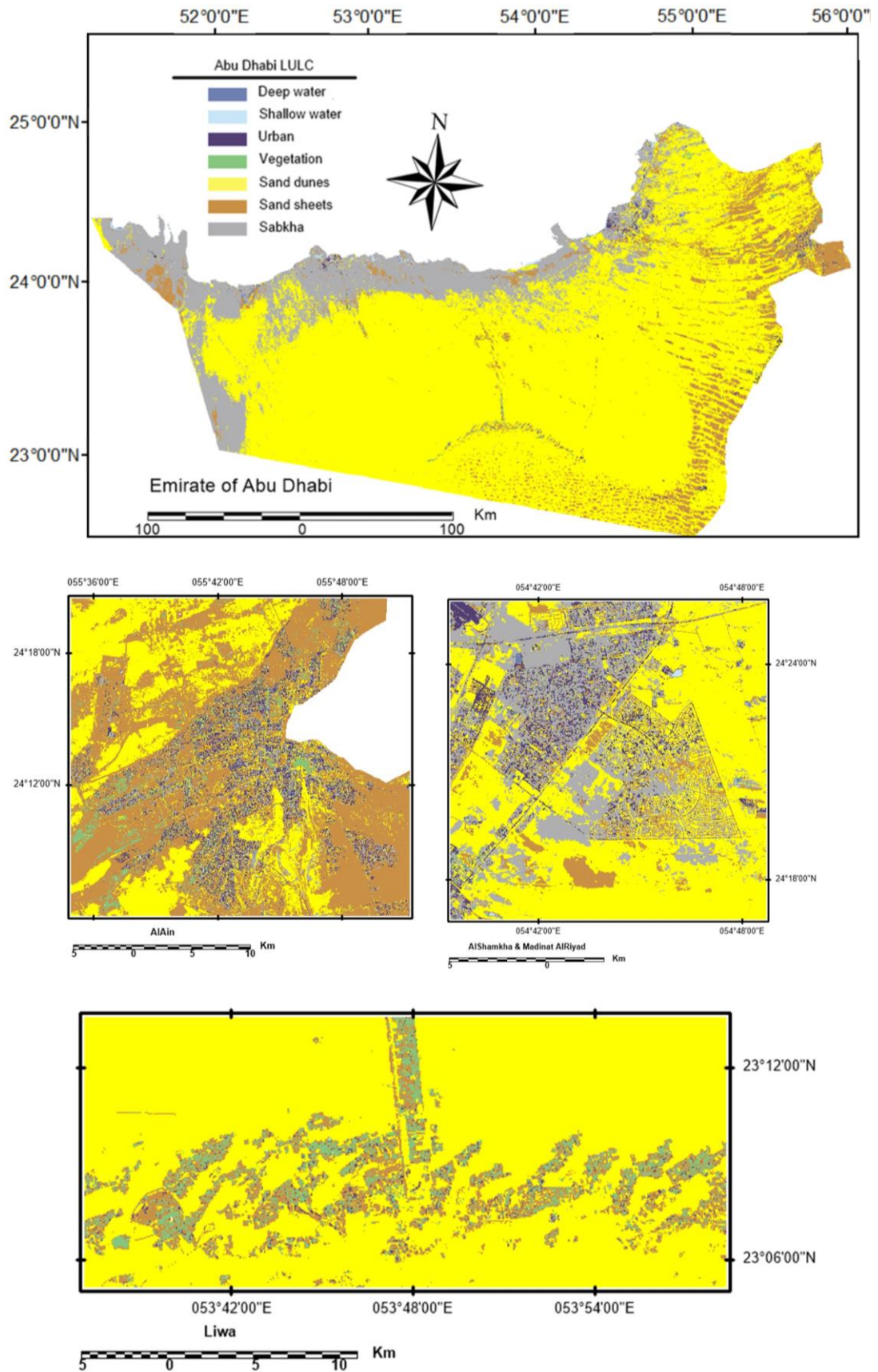
Figure 30: LULC map of the study area.

Table 21: The area and percentage of each class LULC of Abu Dhabi.

LULC Class	Deep Water	Shallow Water	Urban	Vegetation	Sand Dunes	Sand Sheets	Sabkha
Area (ha)	9,677.7	11,847.2	40,102.6	32,333.3	4,957,180	572,665	1,032,170
(%)	0.15	0.18	0.6	0.49	74.48%	8.6	15.15

5.2.2 Mapping Vegetation and Date Palm Using Landsat-8 OLI Images

5.2.2.1 Creating Vegetation Bitmap

All non-vegetated classes of the LULC map were merged to produce one Non-vegetated class (see Chapter 2, Subsection 2.6.2); where the vegetated class was given the value of One, while the Non-Vegetated class was set to Zero (Figure 31).
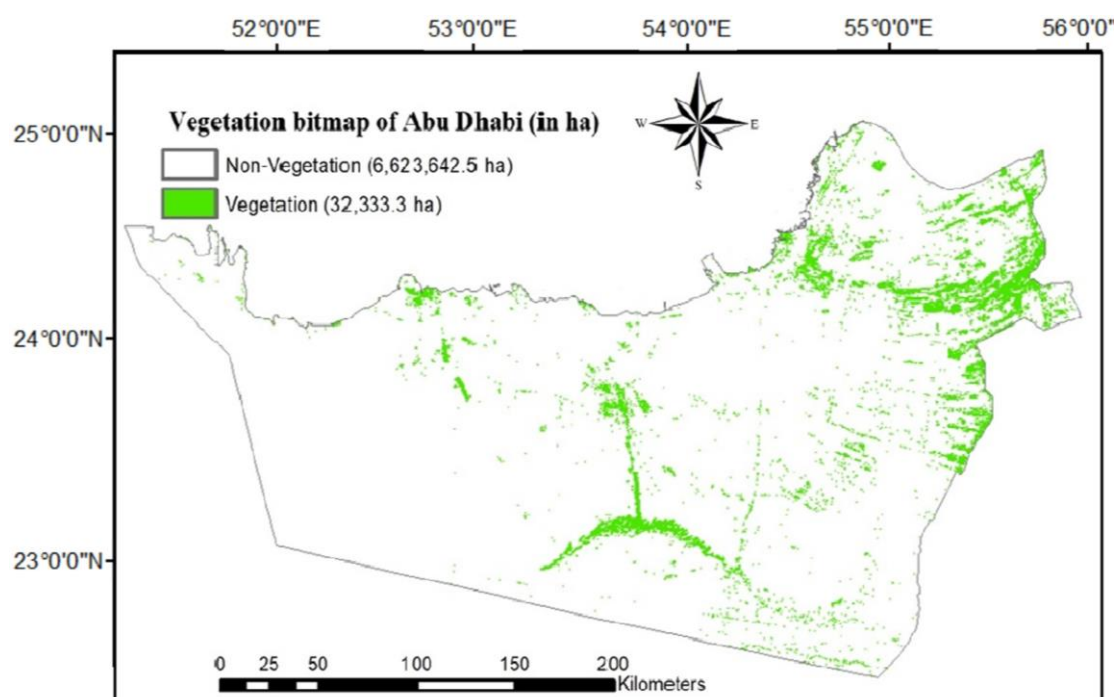
Figure 31: Vegetation bitmap of Abu Dhabi.

5.2.2.2 Mapping Date Palm Plantations

Pure spectral signatures of DP were selected from pixels representing DP planted in Abu Dhabi. They all were collected during intensive field visits to different

locations of DP farms in the study area. These DP farms are different in their phenological cycle (mature, medium, and young). Besides, they have different farming systems, management practices (irrigation and fertilizing) and healthy conditions (stressed/ not stressed). In order to separate and map DP from other vegetation types, the spectral signature values (minimum, maximum, and mean) of DP plantations were analyzed. It was revealed that only mature DP had good separability and hence could be detected at this stage, using Landsat-8 OLI. This is due to the limitations of Landsat-8 OLI to differentiate soil background from the non-mature DP plantations. The results are displayed in Figure 32; where the Y-axis represents the signature values (pixel or DN value) of DP (mature DP) while the X-axis represents the Landsat-8 OLI bands. It was noticed that the best discriminatory bands of the Landsat-8 OLI for mature DP spectral separation are found in the Red-Red edge-IR boundaries.
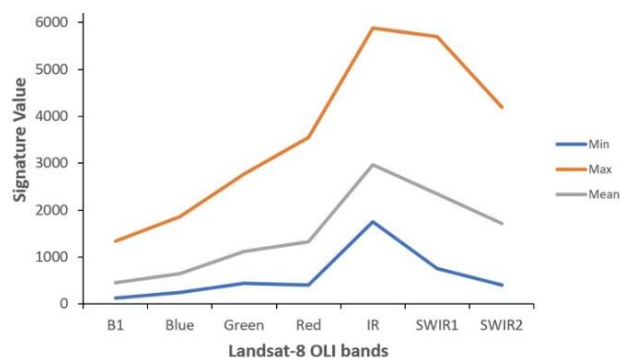
Figure 32: Min., max., and mean signature value of DP versus Landsat bands.

Therefore, non-mature DP (medium and young) were not mapped, and only mapping of mature DP was performed using the Landsat-8 OLI imagery at this stage. The HCM was applied to the vegetation bitmap produced previously and, the same procedure described above was implemented. Maps were created and their areas in hectare were computed (Figure 33).
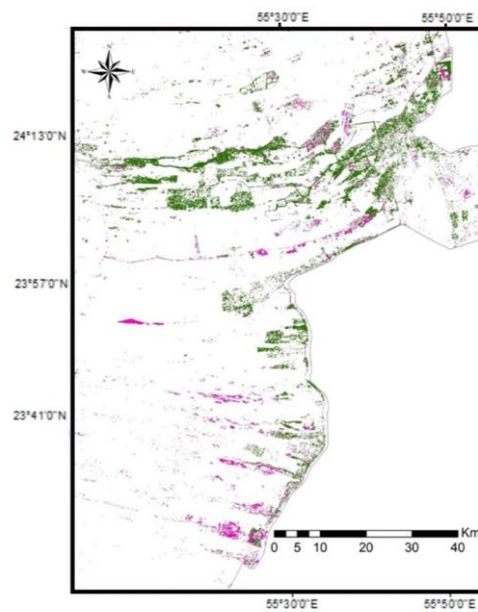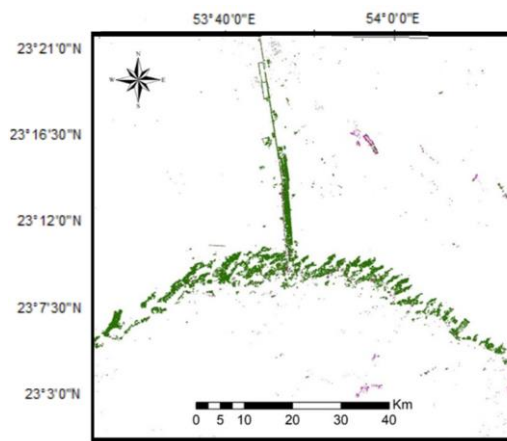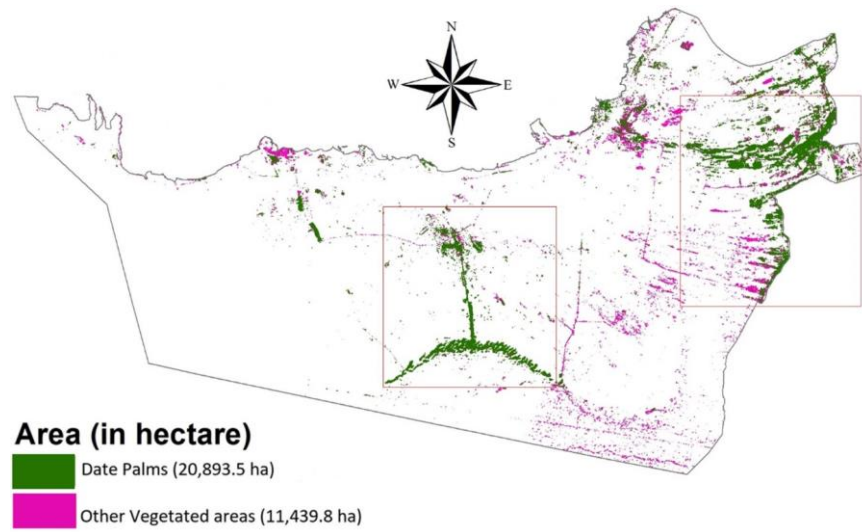
Figure 33: Abu Dhabi DP plantations map (mature DP) using Landsat-8 OLI. It is shown that most of the DP plantations are found in AlAin (right box) and Liwa (left box).

The area (in hectare) of the DP plantations was estimated at 20,893.5 ha, hence contributing to more than 64% of the vegetated areas in the emirate. Most of DP plantations were found in AlAin (east of the emirate) and Liwa (south of the emirate). Note that these figures represent only the mature DP plantations (> 10 years) of Abu Dhabi as Landsat-8 OLI couldn't depict the non-mature DP (medium and young) of an average crown diameter less than 5 meters due to mixed spectral signature with soil background and wider spacing.

5.2.3 Mapping Young, Medium, and Mature Date Palm Plantations Using Sub-Meter WorldView-2 Images

Maps of DP at three age stages: young, medium, and mature were created using the sub-meter WV-2 imagery. GIS tools for cleaning up the vector shapefile resulting from the OOC method were used successfully to enhance and improve highly the accuracy of the final maps. Figure 34 shows the final DP map at three different age stages in AD emirate (mature, medium, and young); while Table 22 displays areas (in hectare) of each category with a total area equal to 7,588.04 ha. It can be noted that more than half of the Abu Dhabi DP plantations areas were mature DP (> 10 years).

Table 22: Mature, medium, and young DP total areas and percentages in AD.

Class	Mature DP	Medium DP	Young DP	Total
Area (ha)	4,193.86	1,672.14	1,722.05	7,588.05
Percentage (%)	55.27	22.04	22.69	100
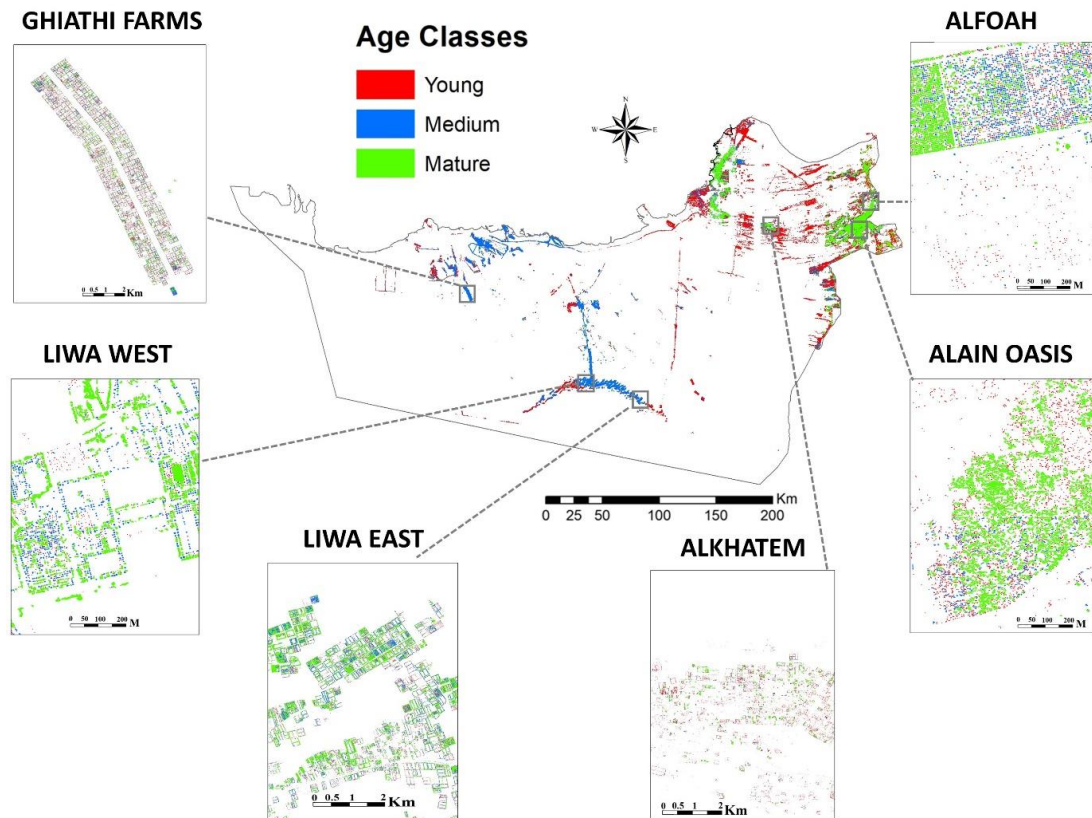
Figure 34: Map of DP plantations showing three age stages using WV-2. The boxes represent the DP maps at different scales and different locations (Alfoah, Alain Oasis, Alkhatem, Liwa west, Liwa east, and Ghiathi).

5.2.4 Maps Validation

The accuracy of the classified maps was assessed using standard statistical tools. The results are summarized and shown in (Table 23), they show a good overall performance of the classification process with an overall accuracy of about 81.7% for LULC map and 87% for the vegetation bit-map using Landsat-8 OLI. Furthermore, the overall accuracies of the DP maps, produced using the sub-meter WV-2, at different age stages, were determined to be 86.8%, 88% to 90.7%, for young, medium, and mature DP plantations respectively. Also, the accuracy of the DP map derived from WV-2 was assessed for all three age stages combined (considered as one DP class only). The resulting map had an overall accuracy of 94.5% and a kappa coefficient of

88% (Table 23). These figures are considered a great achievement considering the efforts exerted by the government to inventory DP in the emirate.

Table 23: Accuracy assessment of the classified maps.

Data Source	Classified map	Producer's Accuracy %	User's Accuracy %	Overall Accuracy %	Overall Kappa
Landsat-8	LULC (7 classes)				
	Deep Water	92.68	76.00		
	Shallow Water	95.65	88.00		
	Urban	85.71	72.00	81.71	0.8094
	Vegetation	74.07	80.00		
	Sand Dunes	81.81	90.00		
	Sand Sheets	74.07	80.00		
	Sabkha	74.14	86.00		
Landsat-8	Vegetation bitmap				
	Vegetation	97.44	76.00	87.00	0.7400
	Non-vegetation	80.33	98.00		
Landsat-8	DP bitmap				
	DP	92.24	61.67	77.5	0.5500
	Non-DP	70.89	93.33		
WV-2	Mature	100.0	81.48	90.74	0.8148
	Medium	95.34	80.00	88.00	0.7600
	Young	93.75	78.95	86.82	0.7368
	All Ages				
	DP	94.59	95.45	94.5	0.888
	Non-DP	94.38	93.33		

5.2.5 Date Palm Counting

Mapping DP using the sub-meter WV-2 instrument allowed not only to delineate the edges of DP crowns but also provide with the ability to count their numbers in Abu Dhabi. The counting of DP was simpler for non-mature DP (medium and young), where there is no overlapping between DP crowns, hence each palm was delineated by only one polygon "one entity". However, the counting became more complicated for mature DP (i.e., full canopy producing non-district objects representing each mature DP) or, in dense planting farming systems (small spacing among palms is the common practice), where the straight forward method of counting polygons become difficult. Each category (age stage) was processed separately;

therefore, the count of DP in each planted area (young, medium, and mature) was determined by dividing the area (in meter) by the mean crown area (CA) of each DP age stage which were: 2.41 m^2, 17.72 m^2, and 47.78 m^2, for young, medium, and mature respectively. The total number of DP planted in the study area counted an estimated number of: 8,966,826 palms (Table 24).

Table 24: The preliminary results of the total numbers of the DP in AD.

Age stage (year)	Number (palm)
Young (< 5)	7,145,436
Medium (5 – 10)	943,646
Mature (> 10)	877,744
Total	8,966,826

5.3 Summary

A framework for mapping DP in the study area with varying age stags and based on integrating multi-source/multi-sensor data in a hierarchical integrated approach (HIA) was proposed. Landsat-8 OLI scenes succeeded in delineating and mapping mature DP plantations with acceptable accuracy. However, it failed to depict young and medium DP, because of inadequate sensor resolutions at such level of detail. Consequently, an object-oriented classification (OOC) approach was applied using sub-meter WorldView-2 (WV-2) imagery, at the DP plantation level, to depict and map medium and young aged DP. GIS helped in converting from raster to vector formats, allowing for manual editing of certain polygons hence, increasing the accuracy of the produced maps, more specifically for young DP. The outcomes of the implemented approach were the creation of detailed and accurate maps of DP at three age stages. This step is essential in the building process of the RS-based biomass estimation model, for the assessment of the CS of DP (see Chapter 6). The produced

maps were validated using existing ancillary data and field checks. The overall accuracies for young, medium, and mature DP plantations were 86.8%, 88% to 90.7%, respectively; while for mixed-ages DP the value reached up to 94.5%, with an overall Kappa statistics estimated at 0.888.

Chapter 6: Remote Sensing Based Models for Assessing Date Palm Biomass and Carbon Stock in Abu Dhabi

Note: This Chapter presents the results of applying the methods discussed in Chapter 2, Subsection 2.7 to build the RS-based spatial model for biomass and CS assessment of DP, quantify and visualize the amount of biomass and CS at the Emirate of Abu Dhabi level. It presents the results of extending the models derived from the pilot study area discussed in Chapter 4 to the entire emirate. The RS-based model development methods were applied using 54 field plots covering the whole study area as opposed to the 19 field plots used in the pilot study (see Chapter 4). A substantive part of this Chapter has been prepared to be published and submitted to a peer-reviewed journal as follows:

- Dahy, B., Issa, S., Saleous, N., & Ksiksi, T., (2021). Modeling Above-ground Biomass (AGB) and Carbon Stock (CS) Assessment of Date Palm Plantations in Abu Dhabi (UAE) Using Landsat-8 (OLI). Remote Sensing (Under preparation).

6.1 Overview

The number of field plots was increased to 54 collected across the study area (see Chapter 4, Subsection 4.3). They included 17 plots representing mature DP, 19 plots representing medium DP, and 18 plots representing young DP (see Chapter 2, Subsection 2.7.1 b). A regression analysis using RS predictors derived from Landsat OLI and the AGB predicted using field measurements and the allometric equations developed earlier in the study allowed the identification of the most significant RS predictors and the development of AGB estimation RS-based models for the different age stages of DP. These models were then applied to Landsat OLI data to DP

plantations at different age stages as identified in the DP maps created previously from sub-meter WV-2 imageries (see Chapter 5, Subsection 5.2.3). The areas of DP were estimated at 7,588.04 hectares (1,722.05 ha for young DP, 1,672.14 ha for medium DP, and 4,193.86 ha for mature DP) with overall accuracy reached up to 94.5%, with an overall kappa statistics estimated at 0.888 (see Chapter 5, Tables 22 and 23). This Chapter meets objectives 5 and 6 of the dissertation (see Chapter 1, Subsection 1.3 Aim and Objective). Specifically, this chapter presents (1) building a RS-based spatial model for biomass and CS assessment of DP, and (2) quantifying and visualizing the amount of biomass and CS in Abu Dhabi, using the built RS-based spatial models.

6.2 Results

6.2.1 Descriptive Statistics of the Field Variables Assessed

Structural variables of 2063 palms included in the 54 plots were measured in the field. Statistics about these measurements including the number of DP for each age stage class, average CA, Ht, and densities of DP per hectare, are summarized in Table 25. The average palm CA's of the mature DP, medium DP, and young DP plots were 36.00, 22.51, and 6.65 m^2, respectively. The average palm Ht's of the mature DP, medium DP, and young DP plots were 2.89, 1.07, and 0.15 meters, respectively. It is obvious that CA and Ht increase as DP age. It is noticeable that there is a significant overlap between the range of CA in the mature and medium DP because palms, in general, are subject to regular pruning of their fronds by the farmers. The pruning process aims to keep a specific number of fronds in the palm allowing more carbohydrates to go to the fruits (dates) than the fronds. It is rare to find Ht of DP taller than 5 meters in modern DP farms as the farmers tend to remove tall palms as they are more difficult to maintain and manage. However, during field measurements, the researcher observed some DP that exceed 5 meters. Some were extremely tall with Ht

reaching 15.2 m, especially in the oases and old farms. In contrast, it was found that most young DP had Ht equal to zero and some of them has CA equal to 0.07 m^2 because their fronds were tied by rope with no main trunk. The average number of DP per plot for mature, medium, and young DP were 41, 38, and 35, respectively. Given a plot area of 1600 m^2, this corresponds to densities of around 258, 238, and 221 palm. ha^{-1}, respectively. The highest average of DP density was found on mature DP plots. In two cases, the number of mature DP reached 88 and 96 palms per plot corresponding to around 550 and 600 palm. ha^{-1}, respectively. This could be due to an old farming systems used when the mature DP were planted where the palms were distributed randomly in the farm and the spacing among them was small to get the benefits from the traditional irrigation practices (e.g. Aflaj irrigation systems). Nowadays, the DP inside the farms are distributed in more organized ways with wider spacing among palms (7m×7m, 8m×8m, and 9m×9m) which led to lower densities in modern DP farms allowing agricultural tractors and machinery to navigate more easily.

Table 25: Average CA, Ht, and density values of DP at 54 field plots.

DP Age Stage	No. Palms	Average CA (m^2)	Average Ht (m)	Avg. Density (palm. ha^{-1})
Mature	701	36.00 (19.54 – 44.15)	2.89 (1.90 – 5.07)	258 (131 – 600)
Medium	725	22.51 (11.85 – 32.45)	1.07 (0.39 – 1.64)	238 (131 – 450)
Young	637	6.65 (2.52 – 13.94)	0.15 (0 – 0.37)	221 (144 – 306)

6.2.2 The Aboveground Biomass Analysis and Estimating its Carbon Content

A summary of the AGB for the tested plots is shown in Table 26. The highest CB was found in mature DP plots while the lowest CB was found in young DP plots. These results were largely influenced by the average CA of these plots (Table 26). The same can be said about TB which was largely influenced by the average of Ht (Table

26). The averages of AGB in tons per hectare of mature, medium, and young DP were estimated at 59.39, 23.33, and 6.15 t. ha^{-1}, respectively. The aboveground carbon (AGC) in (t. ha^{-1}) was estimated by multiplying the average AGB in tons per hectare by 0.5387 (Salem Issa et al., 2018, 2020b). Therefore, the averages AGC for mature, medium, and young DP plots were estimated at 31.99, 12.57, and 3.31 t. ha^{-1}, respectively.

Table 26: The AGB of DP components by age stages at all 54 field plots.

DP Age Stages	No. Plots	Biomass (ton. ha^{-1})		
		Crown Biomass	Trunk Biomass	AGB
Mature	17	29.02 (12.45 – 49.49)	30.37 (11.95 – 106.76)	59.39 (24.41 – 149.35)
Medium	19	13.34 (5.62 – 27.21)	9.98 (4.18 – 20.63)	23.33 (11.11 – 44.60)
Young	18	4.85 (2.72 – 8.16)	1.30 (0 – 4.08)	6.15 (2.72 – 9.90)

6.2.3 Models Development and RS Variables Importance

As the age of DP has an important role in their biomass and CS (see Table 26), the regression of RS variables with the estimated biomass of DP in the field plots was calculated according to the DP age stages defined earlier.

6.2.3.1 Mature Date Palms

In mature DP plots (17 plots), the linear correlation between AGB and single bands was significant for SWIR1 and SWIR2, while that correlation was significant for all tested VI's except TCB and TCG (see Appendix 7). SWIR1 and SWIR2 were among the most highly correlated single band to AGB of mature DP with R^2 values equal to 0.302 and 0.290, respectively. While NDGI and SR were among the best single VIs for estimation of AGB of mature DP with R^2 values equal to 0.609 and 0.545, respectively. The use of a stepwise multiple regression analysis revealed that

TCW showed the strongest correlation to AGB using a second-order polynomial equation. Results of that regression analysis are summarized in Table 27 for all predictors.

Table 27: The prediction equations for AGB estimation of the mature DP.

Regression Equations	Predictor	R^2	*P* value	RMSE	RMSE%	Bias
AGB= $0.00003x^2$ - $0.1908x$ + 330.1	SWIR1*	0.7019	0.022	15.3528	36.2101	-2.9669
AGB= $0.00004x^2$ - $0.1723x$ + 235.59	SWIR2	0.6834	0.026	64.3271	151.7179	19.5399
AGB= $34.878x^2$ - $146.61x$ + 196.93	SR*	0.7357	0.0007	10.3136	24.3250	2.9513
AGB= $1494.8x^2$ - $1511.1x$ + 417.6	RVI	0.6400	0.019	10.5130	24.7954	2.7318
AGB= $0.0002x^2$ - $0.7534x$ + 687.29	DVI	0.6244	0.006	175.0286	412.8114	-57.9171
AGB= $9820.7x^2$ + $1589.1x$ + 106.87	NDGI*	0.7581	0.0002	13.4727	31.7758	3.0822
AGB= $1540x^2$ - $1043.4x$ + 215.2	NDVI*	0.7012	0.007	9.2559	21.8303	2.5235
AGB= $8584.3x^2$ – $19786x$ + 11438	TVI	0.6836	0.009	7.6617	18.0704	1.7423
AGB= $3565x^2$ - $2922.1x$ + 634.81	GNDVI	0.6301	0.020	12.396	29.2364	3.2638
AGB= $0.5244x^2$ - $24.955x$ + 336.14	RDVI	0.6918	0.005	13.3152	31.4044	3.2562
AGB= $664.06x^2$ - $667.46x$ + 206.36	SAVI*	0.7156	0.005	8.0556	18.9993	2.0658
AGB= $1527.9x^2$ - $1501.9x$ + 404.79	MSAVI	0.6967	0.013	10.4487	24.6437	3.0979
AGB= $0.00006x^2$ + $0.1212x$ + 96.708	TCW*	0.7643	0.007	6.3224	14.9118	1.4248

*The strongest RS predictors for AGB estimation of mature DP.

Additionally, the results of the stepwise multiple regression analysis on AGB of the mature DP showed that a combination of single bands or of VIs does not improve the *R²*. Therefore, the second-order polynomial equation that uses only TCW as RS predictor is the strongest model to estimate the biomass of mature DP with *R²* equal 0.7643 and *P*-value equal of 0.007 (Equation 21 and Figure 35).

$$\text{AGB}_{\text{Mature DP}}\ (\text{ton.ha}^{-1}) = 0.00006\ (\text{TCW})^2 + 0.1212\ (\text{TCW}) + 96.708 \qquad \text{Eq. (21)}$$

6.2.3.2 Non-Mature Date Palms

a. Medium DP

For medium DP (19 plots), the correlation was not significant with all single bands and all tested VI's except DVI and RDVI with R^2 values equal to 0.208 and 0.205, respectively (see Appendix 7). The R^2 was slightly improved by using a second-order polynomial equation with DVI as RS predictor, increasing from 0.208 to 0.229. The results of the stepwise regression analysis on AGB of medium DP showed that a combination of single bands or a combination of VIs does not improve the R^2. Therefore, the second-order polynomial equation that uses only DVI as RS predictor is the strongest model to estimate the biomass of medium DP with R^2 equal to 0.2286 and P value equal to 0.049 (Equation 22).

$$\text{AGB}_{\text{Medium DP}}\ (\text{ton.ha}^{-1}) = 0.00002(\text{DVI})^2 + 0.0819(\text{DVI}) - 49.454 \qquad \text{Eq. (22)}$$

b. Young DP

For young DP (18 plots), the correlation was found to be significant with only NIR with R^2 value equal to 0.283 (see Appendix 7). No improvement in R^2 was achieved when using various type equations (logarithmic, exponential, power, and polynomial regression). Besides, the results of the stepwise regression analysis on AGB of the young DP showed that a combination of single bands does not improve the R^2. Therefore, the linear regression equation that uses only NIR as RS predictor is the strongest model to estimate the biomass of young DP with R^2 equal 0.2828 and P value equal 0.023 (Equation 23).

$$\text{AGB}_{\text{Young DP}}\ (\text{ton.ha}^{-1}) = 0.0034(\text{NIR}) - 7.1855 \qquad \text{Eq. (23)}$$

c. Non-Mature DP

Although Equation 22 and Equation 23 for estimating AGB of medium DP and young DP using the RS predictors DVI and NIR, respectively, were significant (P value < 0.05), it was found that R^2 could be improved by considering medium and young DP as one age class, the non-mature class (non-mature DP). Running the regression analysis for non-mature DP (37 plots = the combine of medium and young DP) resulted in a stronger relationship between AGB and RS variables. Except for B, G, and NIR bands and NDGI, all RS variables of Landsat 8 OLI, single bands, and tested VIs, were significantly correlated with AGB of the non-mature DP (Table 28). The exponential regression equation that uses RDVI as RS predictor was the best single VI and yielded the strongest correlation with AGB of non-mature DP, resulting in an R^2 value of 0.4987 and P value equal 0.00002 (Equation 24 and Figure 35). Table 28 summarizes the prediction equations for estimating AGB in the non-mature DP.

Table 28: The prediction equations for AGB estimation of the non-mature DP.

Regression Equations	Predictor	R^2	P value	RMSE	RMSE%	Bias
AGB= 24002x - 1.156	B1	0.1722	0.044	10.4856	67.0020	-6.6021
AGB= 0.0000002x -1.858	R	0.2454	0.018	18.5347	118.4350	-15.650
AGB= 121.96 $e^{-0.0006\,x}$	SWIR1	0.2502	0.019	7.2303	46.2007	-4.5065
AGB= 99.508 $e^{-0.0007\,x}$	SWIR2	0.2943	0.012	8.0543	51.4664	-5.7480
AGB= 0.1533 $e^{2.6274\,x}$	SR*	0.4852	0.0003	20.0397	128.0516	0.7865
AGB= 1.4914 $x^{-4.25}$	RVI*	0.4623	0.0005	9.4645	60.4776	-3.8157
AGB= 0.00000001 $x^{2.8765}$	DVI*	0.4718	0.0003	9.4193	60.1885	-7.6892
AGB= 1.3797 $e^{8.987x}$	NDVI*	0.4658	0.0004	8.8506	56.5545	-4.3188
AGB=0.000000003 $e^{19.759x}$	TVI*	0.4556	0.0007	10.3655	66.2349	-7.2824
AGB= 0.5001 $e^{8.7867x}$	GNDVI	0.3104	0.005	8.9697	57.3157	-6.8684
AGB= 0.8257 $e^{0.1469x}$	RDVI*	0.4987	0.00002	8.0402	51.3762	-5.0426
AGB= 1.3436 $e^{6.0627x}$	SAVI*	0.4698	0.0004	8.9735	57.3400	-4.2404
AGB= 0.9026 $e^{6.7631x}$	MSAVI*	0.4578	0.0005	7.9429	50.7547	-5.2735
AGB= 94.527 $e^{-0.0003x}$	TCB	0.1841	0.044	7.9370	50.7170	-4.1559
AGB= 5.0314 $e^{0.0019x}$	TCG	0.4177	0.0006	8.1560	52.1164	-6.4067
AGB= 75.625 $e^{0.0012x}$	TCW	0.3505	0.006	7.6676	48.9952	-4.1108

*The strongest RS predictors for AGB estimation of non-mature DP.

The results of the stepwise regression analysis on AGB of the non-mature DP showed that a combination of single bands or a combination of VIs does not improve the R^2. Therefore, the exponential equation that uses only RDVI as RS predictor is the strongest model to estimate the biomass of non-mature DP with R^2 equal to 0.4987 and P value = 0.00002 (Equation 24, Figure 35).

$$\text{AGB}_{\text{Non-Mature DP}} \ (\text{ton.ha}^{-1}) \ = 0.8257 \ \text{x} \ e^{0.1469(\text{RDVI})} \qquad \text{Eq. (24)}$$

6.2.4 Models Validation

The models were established based on field measurement and the statistical accuracy assessment. The accuracy statistics covered the RMSE, RMSE%, and bias as explained previously in the methods chapter (Chapter 2, Subsection 2.6.4). Table 29 summarizes the best regression models for the estimation of AGB based on band values and VIs obtained from Landsat 8 OLI. The best models to estimate AGB for both, mature DP and non-mature DP classes, were determined as the model with the highest R^2 and lowest RSME, RSME%, bias, and P values.

(a)

(b)
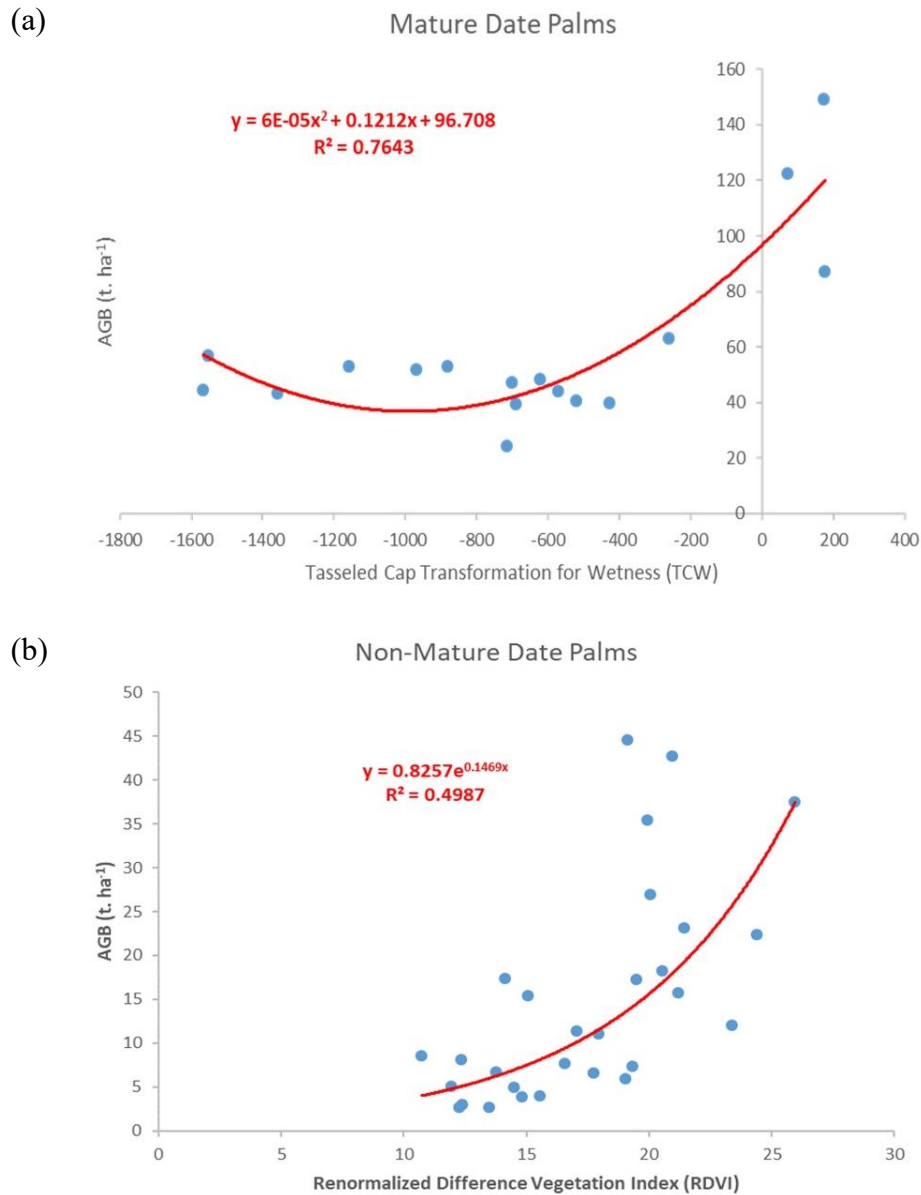
Figure 35: AGB for DP in function of TCW and RDVI. TCW for mature DP (a), and RDVI for non-mature DP (b).

Table 29: Models used for AGB estimation for mature and non-mature DP.

Regression Model	DP Class	R^2	P value	RMSE	RMSE%	Bias
AGB= $0.00006(TCW)^2$ + $0.1212(TCW)$ + 96.708	Mature	0.764	0.007	6.322	14.912	1.43
AGB= $0.8257 \times 1.1582^{(RDVI)}$	Non-mature	0.4987	0.00002	8.040	51.376	-5.04

6.2.5 Creation of the AGB Map of DP and Estimating Total CS in the Study Area

The final AGB map was created using the best performing models constructed from two RS VI predictors: TWC for mature DP and RDVI for non-mature DP (medium plus young DP). The aboveground carbon (AGC), shown in Figure 36, was then created by multiplying the estimated AGB by a conversion factor of 0.5387 as explained in the methods chapter (Chapter 2, Subsection 2.7.5).
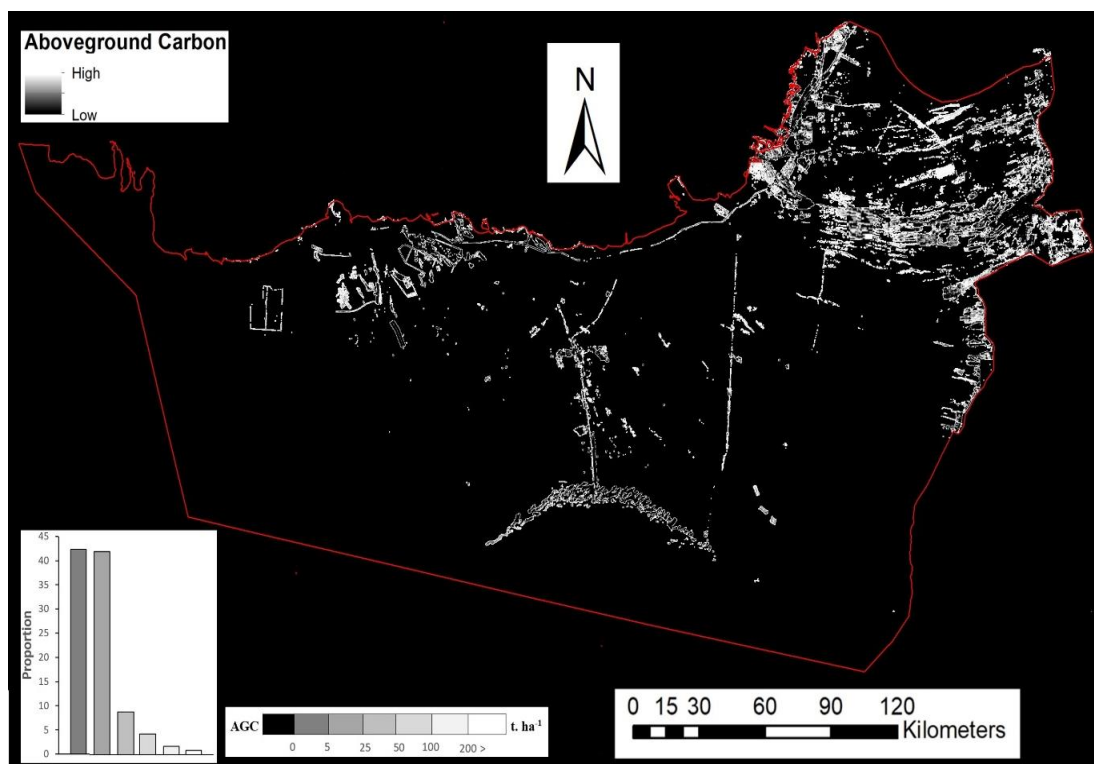
Figure 36: The aboveground carbon (AGC) map of DP in the study area. The lighter pixels, the more amount of AGC (t. ha^{-1}). The black area represents area without DP. The histogram in lower left represents the proportion of each AGC class.

The results of the CS analysis are presented in Table 30. This analysis found that the overall CS by DP plantations in Abu Dhabi is 2,447,856.87 tons with an average of 322.6 ton.ha^{-1}.

Table 30: The total CS by DP plantations in megaton (Mt) in Abu Dhabi.

DP Class	Above Ground		Below Ground		Litter & Debris		SOC	Total
	AGB	BGC	BGB	BGC	Biomass	C		
Mature	1.210	0.652	0.600	0.308	0.242	0.130	0.093	1,183
Medium	0.384	0.207	0.356	0.182	0.058	0.031	0.037	0.458
Young	1.008	0.543	0.335	0.172	0.101	0.054	0.038	0.807
Total	2.602	1.402	1.290	0.662	0.400	0.216	0.169	2.448

1 Mt = million tons.

6.3 Summary

This chapter presented the expansion of the RS-based models to estimate CS in DP in the pilot study area presented in chapter 4, to cover the whole Emirate of Abu Dhabi by using additional field plots and rerunning the statistical analysis. Data from Landsat 8 OLI were used to assess the correlation between spectral reflectance and different VIs on one side, and AGB derived from ground measurements on the other. RS data of moderate resolution such as the freely available long record of Landsat satellite imagery were used successfully to build a RS-based biomass estimation models at different age stages of DP (mature DP and non-mature DP). The allometric equations developed previously (see Chapter 3) provided an important element in the design, calibration, and implementation of a novel approach to assess AGB (ton. ha^{-1}) and to estimate CS stored (ton. ha^{-1}) in DP plantations. The relationships between the estimated AGB and parameters derived from RS data were tested using single and multiple linear regression analysis. The results helped identify the RS predictors that exhibited the highest and most significant correlation with AGB calculated from field measurements and the allometric equations developed in this study. Models using theses predictors were adopted to estimate AGB from RS data for the different age classes of DP consequently map and estimate CS for the whole study area (see Table 31). For mature DP class alone (>10 years), the strongest correlation between AGB and RS predictors was found for the VI TCW using a second-order polynomial

equation with R^2 equal to 0.7643 and P value equal to 0.007. For medium DP, the second-order polynomial equation that uses only DVI as RS predictor is the strongest model to estimate the biomass of medium DP with R^2 equal to 0.2286 and P value equal to 0.049. While for young DP, the linear regression equation that uses only NIR as RS predictor is the strongest model to estimate the biomass of young DP with R^2 equal to 0.2828 and P value equal to 0.023. However, combining these two classes into one non-mature class yielded a stronger and more significant correlation. An exponential regression equation that uses RDVI as RS predictor was the best single VI and had the strongest correlation among all RS variables of Landsat 8 OLI for AGB of non-mature DP, with an R^2 value of 0.4987 and P value equal 0.00002. Finally, the models applied on the DP maps of Abu Dhabi that were produced previously (Chapter 5) to map and quantify the CS of DP of Abu Dhabi. The overall CS by DP plantations in Abu Dhabi (including the five components: AGB, BGB, litter, debris, and SOC) is 2,447,856.87 tons with an average of 322.6 ton.ha^{-1} (see Table 30).

Table 31: RS predictive variables used in the RS based biomass models

RS Model	Vegetation Indices	Significant Variables
Model 1 (Mature): AGB= $0.00006(TCW)^2 + 0.1212(TCW) + 96.708$	TCW: $(= 0.1511 \times B + 0.1973 \times G + 0.3283 \times R + 0.3407 \times NIR - 0.7117 \times SWIR1 - 0.4559 \times SWIR2)$	B (0.450–0.515 μm) G (0.525–0.600 μm) R (0.630–0.680 μm) NIR (0.845–0.885 μm) SWIR1(1.560–1.660 μm) SWIR2 (2.100–2.300 μm)
Model 2 (Non-Mature): AGB= $0.8257 \times 1.1582^{(RDVI)}$	RDVI: $(NIR - R)/\sqrt{(NIR+R)}$	R (0.630–0.680 μm) NIR (0.845–0.885 μm)

Where B is blue band, G is green band, R is red band, NIR is near infrared band, and SWIRs are shortwave infrared bands.

Chapter 7: Discussion

One of the first steps in the development of models for estimation CS was the development of allometric equations that relate AGB to palm structural variables. In previous studies, some authors used fresh weight to build allometric equations, as it was the case in some southern Asia oil palms studies (Dewi et al., 2009; Khalid et al., 1999a). Others used dry weight as in some tropical and west African regions (Corley et al., 1971; Thenkabail et al., 2004) (see Appendix 1). For DP, it was found that the correlation coefficient between the total fresh and dry weights of DP to be 0.99, in agreement with values usually recorded in palm experiments (Corley et al., 1971). Consequently, dry weight was adopted as a surrogate to develop specific allometric equations for the calculation of AGB of DP in the UAE. Results showed that the dry weight of DP averaged 42% of their fresh weight (Chapter 3, Table 9). When considering the trunk alone, that ratio averaged around 37%. This is higher than trunk dry/wet ratios of 20% reported in other studies (Khalid et al., 1999a) and can be attributed to the conditions of desert ecosystems where plants adapt to water stress due to the limited availability of water intake (Aronson et al., 1992; Felker, 2009; Figueiredo et al., 1999; Kappen et al., 1972; Mwanamwenge et al., 1999; Ramos et al., 2003).

The total palm biomass was calculated as the sum of AGB and BGB, where BGB was derived from AGB using different ratios according to age stage. The ratio of BGB to AGB in DP was estimated at 0.33 for young DP. Such ratio increased to 0.92 for medium DP and decreased to about 0.5 for mature DP. The increase observed in medium age may be attributed to the substantial growth of the palm's root system at this age stage to support the emergence of the trunk and help the palm keep balance.

Resource allocation within plants generally is affected by biotic and abiotic stresses (Ketterings et al. 2001; Koala et al. 2017; Litton and Boone Kauffman 2008; Adam and Jusoh 2018; Diédhiou et al. 2017). Still, in the current case the BGB to AGB ratios in DP, at all age stages, were found to be consistently higher than the ratio of 0.2, commonly used by many researchers for other forest species biomass estimation (Achard et al., 2002; Cairns et al., 1997; Gibbs et al., 2007; Houghton et al., 2009; Mokany et al., 2006; Ramankutty et al., 2007). It is important to note that these published ratios were derived from regular tree species, other than palms, in tropical, boreal and temperate ecosystems which are completely different from those growing in desert ecosystems (Mokany et al., 2006). DP species in particular, show unique plant architecture and anatomical characteristic (Da Silva et al., 2015).

Age stages have substantially affected biomass accumulating in DP. In young DP, with no developed trunk, the AGB averaged 22.5 Kg.palm^{-1}. Progressively, AGB increased with age where medium palms AGB increased to an average of 94.7 Kg.palm^{-1} due to the trunk development and the increase in number and diameter of crown fronds (Figure 37). The increase in AGB continued in mature palms to exceed 284 Kg. palm^{-1}. The percentage of AGB to total biomass also varied during growth with averages of 75.1%, 51.9% and 66.8% for young, medium and mature palms, respectively. The average AGB to total biomass ratio was found to be 64.3%.
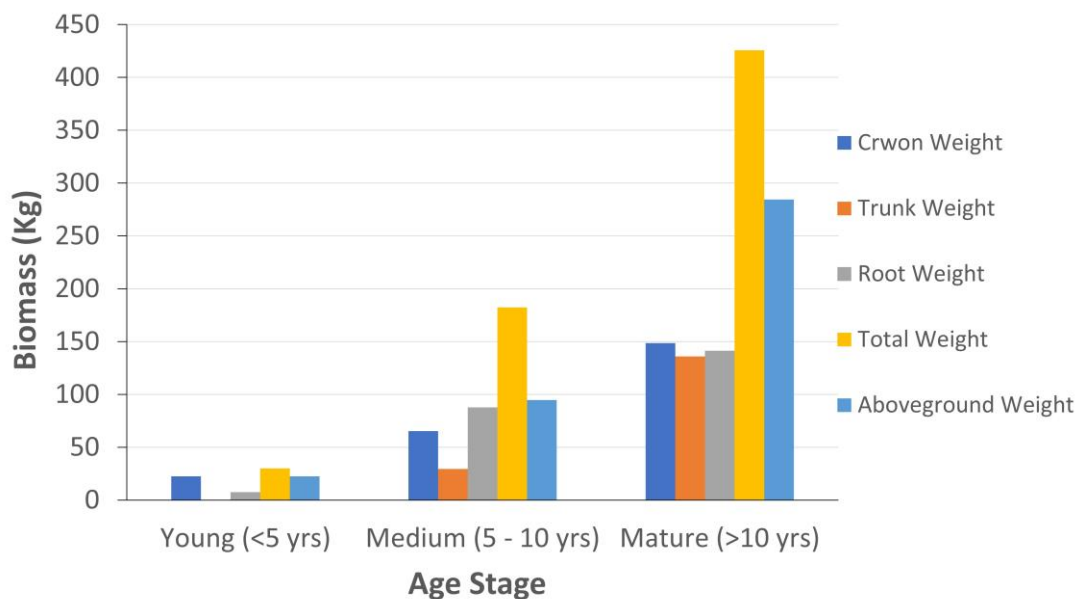
Figure 37: The biomass (dry weight) of DP versus age stages.

The high correlation between age and biomass indicated that age was the best parameter to estimate AGB of DP with three distinguished stages of storing biomass. Firstly, young DP stage, where most of the biomass was stored in its crown representing about 75.11% of the total biomass. Secondly, medium aged DP where trunk started developing and taking a portion from the total biomass (around 16.2%). This portion was offset by doubling that of the root biomass from 24.89% to 48.06% of the total biomass. Thirdly, mature DP where the dry biomass was distributed equally among the three palm components (crown, trunk and root). Similarly, Henson and Chang (2003) used age to calculate the standing biomass of oil palm while Corley and Tinker (2008) found that the density of dry trunk increased with palm age. The regression analysis of age with AGB of the DP showed that CB increased at about 14% per year and that TB increased 18% yearly.

Nonetheless, age is a non-structural variable that cannot account for biomass variations within the same stage in a plantation and measured directly in the field

(Korom et al., 2016). In addition, it does not satisfy the aim of identifying variables that can be directly measured by RS and hence provide an alternative approach to estimating the biomass and CS in DP plantations (Salem Issa et al., 2019). Therefore, using structural variables such as H, Ht and DBH, to build AGB regression equations are preferred (Corley & Tinker, 2008; Dewi et al., 2009; Khalid et al., 1999a; Thenkabail et al., 2004). Generally, DBH is widely used in biomass equations in tropical regions because of the high correlation between DBH and AGB (Brown, 1997). However, in the current study, a weak to intermediate correlation between DBH and biomass was found. The correlation was insignificant with both CB (*P* value = 0.229) and TB (*P* value = 0.197) (see Chapter 3, Tables 13 and 14). This may be due to the growing effects of the palm trunk where the DBH becomes more stable and there is no significant increase in DBH from medium to mature DP. In addition, palms being monocots, have a different anatomy and form than other trees. The DBH does not increase with age, which may explain the weak relationship observed with biomass (Sajdak et al., 2014).

As the AGB is the resulting sum of crown and trunk biomasses, it could be estimated from CA and Ht, which were found to be the most significant field predictors (see Chapter 3, Tables 13 and 14). CB was highly correlated with CA with the highest R^2 of 0.8354 obtained using an exponential regression equation. While the TB was highly correlated with the Ht with the highest R^2 of 0.828 reached using a power regression equation. Correlations between CB and CA in one hand, and TB and Ht in the other, were also observed by others. Carlos et al. (2015), for instance, found that foliage (crown) biomass was strongly correlated with palm crown variables in Brazil. Similarly, Korom and Matsuura (2016) studied the AGB of oil palms in Malaysia and analyzed different allometric equations. They reported that AGB could be estimated

using CD of oil palms consistently at all ages with R^2 ranging between 0.95 and 0.97. The same can be said about CA as it could be calculated from CD using sphere equation (CA $= \pi \, CD^2/4$), assuming a rounded palm crown. Palm species height was reported to be more useful as an independent variable than DBH in AGB estimations (Yuen et al., 2016). Likewise, in a study conducted in Malaysia, Asari et al. (2013) concluded that palm height was more strongly associated with age. Carlos et al. (2015) found that the biomass was strongly correlated with age and very strongly with Ht. Recently, Singh et al. (2018) found that AGB was highly correlated with the Ht in their study on oil palm plantations in India. This could be explained by the fact that palm species growth pattern were nonlinear and each biomass component had its unique characteristics which would be reflected in the allometric model for estimating biomass (Korom et al., 2016; Da Silva et al., 2015). Crown dimensions have been used less frequently in equations for AGB or biomass of any component (Yuen et al., 2016). However, as the detection of biomass and its estimation by RS techniques greatly increase the efficiency in forest monitoring and measurement (Holmgren et al., 1994), CB component has gained prominence in most research (Kumar & Mutanga, 2017).

The novelty introduced in the current study highlighted the value of integrating allometric equations with RS. The predictive power of such variables derived from moderate resolution satellite data, such as Landsat TM and ETM+ imagery, were valid to estimate palm biomass. The results of the regression analysis for the estimation of AGB and CS from the allometric equations on one hand, and the RS indicators on the other (Issa et al., 2019), showed high correlation (see Chapter 4, Table 19 and Chapter 6, Table 31). The significant correlations reported here supported the aim of the study

to ultimately use RS data for estimating CS (see Chapter 1, Subsection 1.3 Aim and Objectives). The approach provided a significant advantage by enabling the calculation of AGB and CS for large areas based on field measurements at a limited number of representative sites used to derive the allometric equations.

The regression analysis yielded positive correlation between CA and SOC with a coefficient of 0.903 (P<0.0001), concluding that for DP's CA could be used as a good predictor of SOC in DP. The average SOC added to the area dominated by DP ranged from 15.7 ton. ha^{-1} to 34.5 ton. ha^{-1} with a mean of 22.26 ton. ha^{-1}(see Chapter 3, Table 16). These figures were determined from the fifteen DP destructively sampled measurements belonging to age stages ranging from 2.5 to 20 years. Comparatively, in Southern Ethiopia, Lemenih & Itanna (2004) found that semiarid acacia woodland added 14.7 ton. ha^{-1} of SOC in the top 10 cm of the soil, while Nyssen et al. (2008) found that grazing lands of Ethiopia could add 26 ton. ha^{-1} of SOC. In the UAE, *Acacia tortilis* added around 14.7 tons of SOC per hectare while *Colotropis procera* added only 6.6 tons of SOC per hectare (Ksiksi, 2012). It is worth noting that different land management practices can lead to differences in the accumulation of SOC in different date palms plantations (El Tahir et al., 2009). Likewise, plant species differ markedly in their impact on soil carbon concentration and distribution, mainly because of differences in their root systems (Ksiksi, 2012; Lal, 2002). LULC change leads to change in SOC stock (Guo & Gifford, 2002). Afforestation, for instance, results in sequestration of new C and stabilization of old C in physically protected SOM fractions, associated with micro-aggregates and silt and clay (Nyssen et al., 2008).

Objective number 3 of this dissertation is to map DP plantations in the study area with high accuracy, regardless of their age stages, using different types of

available RS data (see Chapter 1, Subsection 1.3 Aim and Objectives). The accuracy of capturing all DPs is crucial to the current research, as these layers are used as an input to a RS-based biomass and CS estimation model (see Chapter 6, Subsection 6.1). Because of the reasons explained in Chapter 1 (Subsections 1.4.4.3), the moderate resolution Landsat-8 OLI imagery was chosen. However, this choice raised many challenges, particularly when mapping the non-mature DP (< 10 years), with an average CD of fewer than 5 meters. The low canopy cover combined with the high contribution of desert background reflectance limited the efficiency of capturing the less developed and sparse DP plantations at moderate resolution. Therefore, an integrated approach was proposed in this research, the HIA, applied to the multi-source / multi-resolution data from moderate Landsat-8 OLI and high-resolution WV-2 integrated with GIS. The HIA was able to depict the three age stages of DPs: mature, medium, and young with high accuracy.

First, a LULC map of the major seven classes in the study area was created, namely: urban, vegetation (including DP), sand sheets, sand dunes, deep water and shadows, shallow water, and sabkhas. The PBC method was applied to the Landsat-8 OLI scenes to perform this task, which was achieved successfully. The seven LULC classes were mapped and their spectral reflectance separability was achieved effectively. Although the overall accuracy of the LULC map was below the 85% level set as satisfactory for planning and management purposes (Anderson, 1976). However, there is a debate about the usefulness to take this level as standard; many publications reported accuracies mostly below the usually advised 85% target (Foody, 2002; Rozenstein & Karnieli, 2011). Further light was shed by examining the user's and the producer's accuracies, which measure the commission and omission errors, respectively. The analysis of misclassified pixels in the LULC map indicates that most

of the errors are mainly of omission (see the accuracies of vegetation, sand dunes, sand sheets, and sabkhas layers at the LULC map in Chapter 5, Table 24). The HCM, which combines both supervised and unsupervised classification, seems to provide an acceptable accuracy especially in the case of arid lands. This fact has also been reported by other researchers (Rozenstein & Karnieli, 2011) as well as in other ecoregions (Kamusoko & Aniya, 2009; Lo & Choi, 2004). The created LULC map showed that vegetated and urban areas constituted only 0.6% with 40,102.6 hectares, and 0.49% with 32,333 hectares of the total area of the emirate respectively. It is worth noting that sand dunes, sabkhas, and sand sheets areas were the dominant LULC classes in the whole emirate, making up more than 98% of the total area (see Chapter 5, Figure 31). Finally, the overall classification accuracy of the LULC maps was 81.71% with an overall Kappa Statistics equal to 0.81.

Second, a vegetation bitmap of Abu Dhabi was created by merging all non-vegetation classes into one class. The "recode" function in ERDAS Imagine was used to produce the binary mask with only two values: the value of "1" for the vegetation class, and the value of "0" for the non-vegetation class. Vegetation in the study area were sparse and small in size (=32,333.3 ha, representing only 0.49% of the total study area). The overall classification accuracy of the created vegetation bitmap was 87%, with a Kappa coefficient equal to 0.74 (see Chapter 5, Table 24). The second phase of the classification approach of DP was run on the vegetation bitmap using the same HCM to isolate the DP plantation pixels. However, at this stage of the classification, only the mature DP plantations were depicted due to the limitations of Landsat-8 OLI to differentiate soil background from the non-mature DP plantations ($\leq$ 10 years and have an average CD of fewer than 5 meters). Therefore, a different approach using

different sensor characteristics was needed to map the other DP categories (medium and young) with accuracy.

Third, mapping of DP at all age stages was achieved using the OOC method applied to the sub-meter WV-2 imagery. Using high-resolution sensors such as WV-2, to detect low-density DP and map of the spatial distribution of DP in AD at different age stages: young (< 5 years), medium (5-10 years), and mature (> 10 years), proved very successful and added innovation to the actual research. Indeed, many studies upraised the use of high spatial-resolution for depicting and revealing information about the distribution and type of vegetation, especially in arid lands, and hence increase their distinguishability (Bradley et al., 2019; Immitzer et al., 2012; Li et al., 2015; Mugiraneza et al., 2019; Xie et al., 2008). Several software packages supporting OOC and feature extraction are available. ERDAS Imagine 2020 Objective tool was used, it employs "feature model tree" which applies to objects created by image segmentation and other pixel-based algorithms which, after being vectorized, can be processed using geometric and textural parameters (Lack & Bleisch, 2010). The "cue metrics" are the result of many trials and errors (see Chapter 2, Subsection 2.5.3). There were two-level steps of analysis: (1) raster data analysis and, (2) vectorizing (the three raster outputs: mature, medium, and young) and cleaning up the vector layers by visual interpretation to remove erroneous vector if any.

The OOC comprised many steps summarized as follows: i) starting with 0.5 m pan-sharpened WV-2 images covering a test site (AlFoah farm, east of study area), optimum RS parameters were initially selected, analyzed and defined, for discriminating DP plantations at three different age stages; ii) applying the produced parameters to the whole WV-2 dataset; iii) differentiating DP crowns visually from the

background; iv) training areas were carefully selected to exclude any background pixel and; v) pixels of individual palms were submitted to compute pixel cue metrics to train the classifier. However, it should be noted here that, one should familiarize himself with the study area to be able to train the representative signatures.

Evaluation of the three classified maps was carried out using classification accuracy assessment in terms of mapping accuracy where results are summarized in Table 24 (see Chapter 5). The overall accuracies of DP maps were 86.8%, 88%, and 90.7% for young, medium, and mature DP respectively. The area of each category was calculated and found to be 4,193.86 ha 1,672.14 ha, and 1,722.05 ha for mature, medium, and young DP plantations respectively. It was revealed that the total DP plantations areas represented around 64.62% of the total vegetated areas in Abu Dhabi (mostly located in the east and south parts). This was expected due to the importance given to DP in the farming system of the emirate and the adopted government policies in granting farms to the local population.

Furthermore, comparing the results of DP maps produced using Landsat-8 OLI and WV-2 imagery, showed a big difference between the two methods. Landsat-8 OLI gave an area equal to 20,893.5 ha while; classifying WV-2 images gave an area of only 7,588.05 ha. It is well known that, in general, classifying the Landsat-8 OLI images would overestimate the areas of DP plantations compared to the classified WV-2 ones. A similar remark was noticed also by (Stych et al., 2019) who ran a comparison study between Landsat-8 OLI and WV-2 for the classification of forests in Czech and they found that the area of wetland class was almost doubled on the classified Landsat-8 OLI images compared to the classified WV-2 images. This is explained by the fact that DP class areas estimated by the classified Landsat-8 images include the spacing areas

(empty areas) among DP while the classified WV-2 images completely excluded these empty areas considering them as part of the pure soil class. Hence, only DP crowns were delineated and mapped (especially for non-mature DP where there is no overlapping of DP crowns). This is illustrated in a practical example in Figure 38.

Furthermore, it was observed that mature DP showed better overall classification accuracy followed by medium and young DP respectively. This could be attributed to the less background contribution in the overall reflectance of the pixel because of large crown areas covering mature DP; while medium and younger (smaller canopy cover) result in wider spacing and higher exposure of the soil background resulting in a mixed spectral signature. Finally, a marginal improvement in classification was achieved through manual intervention editing in a GIS. The implemented approach proved very promising, with little cost compared to more complex algorithms and expensive data, especially for researches with limited budget, which is the case in most developing countries.
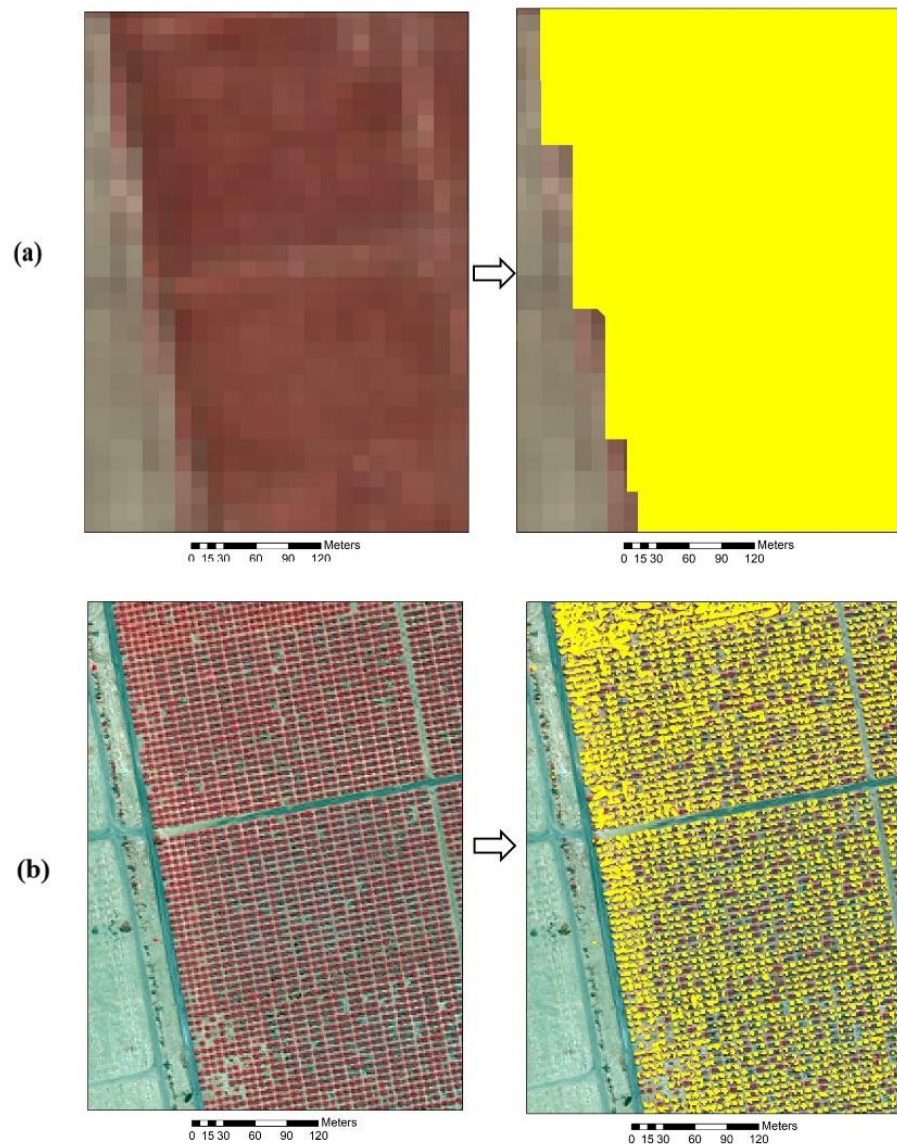
Figure 38: Differences in estimating DP plantations areas at the same farm. The classifying of Landsat-8 OLI image as present in (a) gave 14.02 hectares of DP (yellow color), while (b) classifying of WV-2 image gave 3.77 hectares only (yellow color). This difference is caused by spacing areas among palms that were added to the DP total cover with Landsat-8 images (because of low resolution); while the classified WV-2 images captured and classified these areas as background (non-DP).

The DP plantations structure and plots densities had an effect on the estimation of AGB. It was observed that the palms spacing was different among plots. Moreover, some plots had sparse distribution of DP with no regular spacing system due to human

disturbances. Additionally, other factors than age, such as cultivar and different land management practices, affect the size of CA and Ht of date palms and thus play a role in accumulating biomass and carbon sequestration in DP. For example, DP in some plots were severely suffering from drought stress as they were prepared to be cleared for management purposes (farmers' personal communication). Those plots were excluded latter from the regression analysis thus reducing the size of sample plots from 19 to 16 in the pilot study (Chapter 4) and from 83 to 54 plots in the whole emirate of Abu Dhabi (see Chapter 6 and also Chapter 2, Subsection 2.7.1 Field Data Collection).

For mature DP plots, the study showed that the correlation with single bands was significant only with SWIR bands (see Appendices 6 & 7). Likewise, for mixed age class (see Chapter 4, Table 19) and non-mature DP (see Chapter 6, Table 28), SWIR was found to be the best single bands. These results were consistent with the findings of (Zandler et al., 2015) in their study to model total biomass in extremely low vegetation cover in arid land regions in Tajikistan. They concluded that the SWIR bands of Landsat 8 OLI were useful in detecting shrubs or non-photosynthetic vegetation.

Using a stepwise multiple regression to model AGB in mature DP in the pilot study where 10 field plots were used (see Chapter 4), a combination of SWIR and Red bands yielded best results and improved R^2 value of the model to 0.961 (see Chapter 4, Subsection 4.2.3.1, Equation 16) compared with R^2 values when using the same bands separately (0.398 for R band, 0.445 for SWIR1 band, and 0.553 for SWIR2 band). While the results of the stepwise regression analysis on AGB of the mature DP, after increasing the plot fields to 17 plots (see Chapter 6), showed that a combination of single bands or a combination of VIs does not improve the R^2.

The results of the regression analysis on the AGB of the medium DP and young DP in the pilot study (see Chapter 4) revealed that none of the RS variables of Landsat showed any significant correlation with AGB (except with the single band, SWIR1, and TCB index for medium DP only). This could be attributed to the small sample size of medium and young DP (only three plots for each) which was avoided by increasing the number of sample size to 19 plots for medium DP and 18 plots for young DP (see Chapter 6). For medium DP (19 plots), the correlation was not significant with all single bands and all tested VI's except for DVI and RDVI with R^2 values equal to 0.208 and 0.205, respectively (see Appendix 7). While for young DP (18 plots), the correlation was found to be significant with only NIR with R^2 value equal to 0.283 (see Appendix 7). Although of the significance (P value < 0.05) of the regression analysis for estimating AGB using the RS predictors DVI and RDVI (medium DP) and NIR (young DP), it was found that there was a possibility to improve R^2 by considering medium and young DP as one age class, the non-mature class (non-mature DP) (see Chapter 6, Subsection 6.2.3.2). The regression analysis was run for the 37 non-mature DP plots combining both medium and young DP plot. This has resulted in a stronger relationship between AGB and RS variables in the regression analysis. Except for B, G, and NIR bands and NDGI, all RS variables of Landsat 8 OLI, single bands, and tested VIs, were significantly correlated with AGB of the non-mature DP (see Chapter 6, Table 28).

For both mature DP (> 10 years) and non-mature DP (≤ 10 years), the VIs correlated better with AGB of DP. The findings were consistent with previous studies that used Landsat imageries in estimation forest biomass in different regions. For instance, while examining the relationships between AGB and RS variables including individual band reflectance values and VI's, Günlü et al. (2014) used Landsat TM

reflective bands and found that VI's present better estimation of AGB in Anatolian pine forests with R^2 equal to 0.606 as compared to individual band reflectance with R^2 equal to 0.465. VI's allowed to maximize the sensitivity for recording the green vegetation status (Günlü et al., 2014). The choice of adequately performing VI's depends on type of ecosystem and environmental conditions and spectral information available. As showed in Chapter 4, SR proved to be the best single VI and yielded the strongest correlation among all RS variables of Landsat 8 OLI for AGB of the mixed age DP (using 16 plots). This result agreed with (Clerici et al., 2016b) in their study of forests in Bogotá, Colombia where they found that the best performing AGB estimation model, with an R^2 of 0.582, was based on the ratio vegetation index (RVI), the reciprocal of SR. RVI also appeared in the stepwise multiple regression of VI's combined with DVI and NDGI where they improved the R^2 values for the prediction of AGB for mixed age DP (see Chapter 4, Subsection 4.2.3.3 Equation 20) and therefore giving more accurate estimates of biomass and CS. The R^2 obtained in the multiple regression was 0.952 (see Chapter 4, Subsection 4.2.3.3 Equation 20) compared with R^2 values when using the same VI's separately (0.859 for DVI, 0.731 for NDGI, and 0.833 for RVI).

Generally speaking, the model that used a combination of VI's (DVI, NDGI, and RVI) to predict AGB of the mixed age class DP plantation estimated the AGB with R^2 equal 0.952 and RMSE equal 6.05 ton.ha^{-1} in the pilot study area(see Chapter 4, Table 20). While for the emirate wide study area, the model of the second-order polynomial equation that uses only TCW as RS predictor was the strongest to estimate the biomass of mature DP with R^2 equal 0.7643 and P-value equal to 0.007 (see Chapter 6, Equation 21 and Figure 35), and RMSE of 6.322 ton.ha^{-1}. For non-mature DP, the model of the exponential Equation that uses only RDVI as RS predictor

provided the strongest estimate of biomass with R^2 equal to 0.4987 and P value equal to 0.00002 (see Chapter 6, Equation 24 and Figure 35), while the model validation showed RMSE of 8.040 ton.ha^{-1}. These results are consistent with published literature for other species and study areas such as (Karlson et al., 2015) where Landsat 8 OLI was used for mapping tree canopy cover and predicting AGB in in woodlands landscape of Burkina Faso with R^2 of 0.57 and RMSE of 17.6 ton.ha^{-1}.

The emirate-wide RS-based models to estimate AGB presented in Chapter 6 were applied to Landsat OLI data to estimate AGB. The DP age stage class derived from the high spatial resolution WV-2 data was used to determine the proper model to use when estimating AGB. The resulting map was an emirate wide map of AGB the was subsequently used to calculate CS. This step highlights the strength and uniqueness of the approach adopted in this study where RS-based models, once calibrated, enabled the creation of CS maps from remote sensing data without the need for additional field measurements.

Chapter 8: Conclusion and Recommendations

One of the key objectives of this study was to develop specific allometric biomass equations for assessing carbon sequestration in DP of the UAE and to estimate the potential of DP species to improve soil carbon sequestration in such desert ecosystems (see Chapter 1, Subsection 1.3 Aim and Objectives). Allometric equations using structural variables that could be linked to RS observations were developed for DP at different age stages. Based on field and lab works, CA was found to best estimate CB and SOC, while Ht was the best estimator of TB. The allometric equations developed using these variables allowed the estimation of CB, TB and SOC with coefficients of determination (R^2) of 0.884, 0.835 and 0.952, respectively (see Chapter 3). The allometric equations developed in the early stages of the dissertation were crucial for the development of the RS-based model to predict AGB as they provided the needed input to calibrate the model without further recourse to destructive procedures for measuring AGB in the field. Furthermore, the dissertation showed that the average ratios of the BGB to AGB in DP varied with their maturity stages at values of 0.332 for young, 0.925 for medium (due to the substantial growth of the palm's root system at this stage to support the emergence of the trunk) and 0.496 for mature DP. Additionally, the study showed that the amounts of CS in or contributed by DP were substantial, with significantly higher amounts of SOC compared to other local plants.

AGB and OC values obtained from the allometric equations for a set of pilot sites were used to identify the most significantly correlated RS variables derived from Landsat imagery (see Chapter 4). A combination of Red and Shortwave (SWIR 1 and 2) reflectances yielded the highest correlation for mature DP (> 10 years), whereas a combination of DVI, NDGI and RVI worked better for mixed age palms (see Chapter

4). Expanding the field plots to 54 field plots showed that TCW has the strongest correlation using a second-order polynomial equation to estimate the biomass of mature DP with R^2 equal to 0.7643 and P value equal to 0.007, while the exponential regression equation that uses RDVI as RS predictor was provided the strongest correlation among all RS variables of Landsat 8 OLI for AGB of non-mature DP (≤ 10 years), with an R^2 value of 0.4987 and P value equal to 0.00002.

The development of AGB and OC estimation equations using RS data enabled the calculation of CS over large areas without further need for extensive field work (see Chapter 3), a key tool to accomplish the other objectives of this dissertation (see Chapter 4, 5, and 6).

RS data sets (Landsat-8 OLI and WV-2 imageries) were used for the accurate delineation of DP plantations at different age stages for the whole study area. The dissertation proposes a novel framework based on using multi-source/ multi-sensor data in a hierarchical integrated approach (HIA) to map DP plantations in the Emirate of Abu Dhabi at different age stages (see Chapter 5). First, each pan-sharpened scene of Landsat-8 OLI was classified using an HCM (supervised and unsupervised classification) to create LULC maps. The evaluation of the spectral signatures separations was performed to select the best discriminatory Landsat-8 OLI bands. Interpretation of the seven signatures demonstrated that the shortwave infrared (SWIR1& SWIR2) had the best separability power of all Landsat 8 OLI bands. However, some other combinations were found to be efficient in identifying and mapping the vegetation class such as (RED, SWIRE1, SWIRE2), (RED, GREEN, SWIR1), (RED, GREEN, SWIR2) or (GREEN, SWIR1, SWIR2). Next, the maps were reclassified (recoded) to create a vegetation bitmap encompassing only two classes:

vegetation and non-vegetation. The HCM was applied to the vegetation bitmap to delineate and map DP in the study area. However, at this stage of the classification, mature DP plantations only were depicted due to the limitations of Landsat-8 OLI to separate soil background from the non-mature DP plantations ($\leq$ 10 years, with average crown diameter less than 5 meters). Therefore, the sub-meter WV-2 imagery, covering vegetated areas, were classified using the object-oriented classification (OOC) method, to separate and map the other two DP age stages (medium, and young). At this level, about 829 sub-meter WV-2 images were classified and interpreted to extract and map all categories of DP in the study area. The suitability of the WV-2 satellite data for the identification of tree species was demonstrated. Furthermore, the OOC proved to outperform the pixel-based approach with the near-infrared, red-edge, and green bands being always more important than the other bands to classification.

The areas of DP plantations at the various age stages was calculated and were found to be 4,193.86 ha 1,672.14 ha, and 1,722.05 ha for mature, medium, and young DP, respectively. The total DP plantations areas represented around 65% of the total vegetated areas in Abu Dhabi (mostly located in the eastern and southern parts of the emirate). This was expected due to the importance given to DP in the farming system of the emirate and the adopted government policies in granting farms to the local population. Furthermore, comparing the results of DP maps produced using Landsat-8 OLI and WV-2 imagery, showed a big difference between the two methods. This is because DP class areas estimated by the classified Landsat-8 images include the spacing areas (empty areas) among DP while the classified WV-2 images completely excluded these empty areas considering them as part of the pure soil class. Note that the difference between Landsat and WV-2 results can be reduced if the OOC is tuned to segment the whole farm rather than patches of DP.

The results of the classified maps accuracy assessment indicated a good overall performance of the classification process with an overall accuracy value of about 81.7% for the LULC map and 87% for the vegetation bit-map using Landsat-8 OLI as source data. For DP age stages maps using WV-2 data, the overall accuracies were 86.8%, 88% to 90.7% for young, medium, and mature DP, respectively. Besides, the accuracy of the DP map considering all DP ages had an overall accuracy of 94.5% and a kappa coefficient of 88%.

Furthermore, it was observed that mature DP showed better overall classification accuracy followed by medium DP and young DP respectively. This could be attributed to the less background contribution in the overall reflectance of the pixel because of large crown area coverage of mature DP; while medium and younger (smaller canopy cover) result in wider spacing and higher exposure of the soil background resulting in a mixed spectral signature. Finally, a marginal improvement in classification was achieved through manual editing in a GIS. A final and accurate DP map at three age stages in the emirate of Abu Dhabi (mature, medium, and young) was created. Most of the DP plantations in Abu Dhabi were found to be in Al Ain (east of the emirate) and Liwa (south of the emirate) with more than half of those at the mature stage (> 10 years). The produced DP map was converted to a GIS layer and used as an input to a RS-based biomass model to assess CS in DP plantations in the study area (see Chapter 6).

The implemented approach proved very promising, with minimal cost compared to more complex algorithms and data, especially for limited-budget researches, which is the case in most developing countries. The approach was successful in identifying and mapping mature, medium, and young DP in the study

area with high accuracies. The accurate mapping of three age stages permitted for a better estimation of their CS. The created maps opened the road toward applying a non-destructive approach and to build a RS-based biomass estimation model for assessing AGB and CS in DP in the arid environment of UAE (see Chapter 6). Moreover, the approach can easily be extended to larger areas in the region.

RS-based biomass assessment models for DP were built for quick and reliable estimation of the amounts of AGB and CS which allow for the establishment of a benchmark DP CS map for the Emirate of Abu Dhabi. The methodology proposed in this dissertation relied on both fieldwork and analysis of RS data (see Chapter 2, Subsection 2.4 Overall Methods Flowchart). The work procedures included pre-field preparations to identify sample areas of interest, fieldwork that included sample collection and measurement of plant characteristics, and post-field activity that focused on processing RS data and model development and validation.

In conclusion, the field-based measurements and geospatial approach introduced in this study has the potential to help improve carbon estimation in DP plantations to reduce emissions resulting from deforestation and forest degradation (REDD+) and to design incentive programs in the UAE. The findings are promising and can be used to estimate the amount of AGB and CS in DP plantations in the whole country as well as in arid land in general. Therefore, it can be applied to enhance the decision-making process on sustainable monitoring and management of carbon sequestration by DP in other similar ecosystems.

References

Abburu, S., & Golla, S. B. (2015). Satellite image classification methods and techniques: A review. International Journal of Computer Applications, 119(8), 20–25.

Abd Rabou, A. F. N. (2017). The current status of the date palm (Phoenix dactylifera) and its uses in the Gaza Strip, Palestine. Biodiversitas, Journal of Biological Diversity, 18(3). https://doi.org/10.13057/biodiv/d180324

Abdi, A. M., & Nandipati, A. (2010). Abu Dhabi Island: Analysis of Development and Vegetation Change Using Remote Sensing (1972–2000). In Advances in Earth Observation of Global Change (pp. 43–53). Springer.

Abu Dhabi State of Environment Report: From: Https://www.soe.ae/. (2017). Retrieved on 20 April, 2021.

Achard, F., Eva, H. D., Stibig, H.-J., Mayaux, P., Gallego, J., Richards, T., & Malingreau, J.-P. (2002). Determination of deforestation rates of the world's humid tropical forests. Science, 297(5583), 999–1002.

Adam, N. S., & Jusoh, I. (2018). Allometric Model for Predicting Aboveground Biomass and Carbon Stock of Acacia Plantations in Sarawak, Malaysia. BioResources, 13(4), 7381–7394.

Adeyeri, O. E., Akinsanola, A. A., & Ishola, K. A. (2017). Investigating surface urban heat island characteristics over Abuja, Nigeria: Relationship between land surface temperature and multiple vegetation indices. Remote Sensing Applications: Society and Environment, 7, 57–68.

Ahlström, A., Raupach, M. R., Schurgers, G., Smith, B., Arneth, A., Jung, M., Reichstein, M., Canadell, J. G., Friedlingstein, P., & Jain, A. K. (2015). The dominant role of semi-arid ecosystems in the trend and variability of the land CO2 sink. Science, 348(6237), 895–899.

Aholoukpè, H. N. S., Dubos, B., Deleporte, P., Flori, A., Amadji, L. G., Chotte, J.-L., & Blavet, D. (2018). Allometric equations for estimating oil palm stem biomass in the ecological context of Benin, West Africa. Trees, 32(6), 1669–1680.

Al Ahbabi, A. (2013). LULC change analysis of Abu Dhabi region between 1986 and 2010: Extracted from a mosaic of Landsat imageries of Abu Dhabi Emirate between 1973 and 2010. Master thesis, UAE University, UAE.

Al-Ahmadi, F. S., & Hames, A. S. (2009). Comparison of four classification methods to extract land use and land cover from raw satellite images for some remote arid areas, kingdom of Saudi Arabia. Earth, 20(1), 167–191.

Alhameli, S., & Alshehhi, M. (2004). Images are an outstanding evidence of rapid development "A perfect example from United Arab Emirates (UAE)". Proceedings of the ISPRS XXth Congress, Commission PS IC, Working Group II/4, XXXV, Part B, 4, 505, Istanbul, Turkey.

Alhammadi, M. S., & Kurup, S. S. (2012). Impact of salinity stress on date palm (Phoenix dactylifera L)–A review. In Crop Production Technologies. InTech.

Allen, S. E., Grimshaw, H. M., Parkinson, J. A., & Quarmby, C. (1974). Chemical analysis of ecological materials. Blackwell Scientific Publications.

Al-Rawai, A. A. K. (2004). Impacts of the Alien Invasive Prosopis Juliflora (Swartz) Dc. On The Flora and Soils of the UAE and Feasibility of Using It in the Afforestation of Saline Habitats. Master thesis, UAE University, UAE.

Al-Shuwaihi, A. (2009). Monitoring Al Ain City urban growth dynamics between 1972 and 2000 by integrating remote sensing and GIS techniques. Master thesis, UAE University, UAE.

Aly, A. A., Al-Omran, A. M., Sallam, A. S., Al-Wabel, M. I., & Al-Shayaa, M. S. (2016a). Vegetation cover change detection and assessment in arid environment using multi-temporal remote sensing images and ecosystem management approach. Solid Earth, 7(2), 713–725.

Anderson, G. L., Hanson, J. D., & Haas, R. H. (1993). Evaluating Landsat Thematic Mapper derived vegetation indices for estimating above-ground biomass on semiarid rangelands. Remote Sensing of Environment, 45(2), 165–175.

Anderson, J. R. (1976). A land use and land cover classification system for use with remote sensor data (Vol. 964). US Government Printing Office.

AOAD, Arab Organization for Agricultural Development. (2008). Arab Agricultural Statistics Yearbook, PART III: Plant Production. Statistics Division 28.

Aranha, J. T., Viana, H. F., & Rodrigues, R. (2008). Vegetation classification and quantification by satellite image processing. A case study in North Portugal. International Conference and Exhibition on Bioenergy, 7. April 6th – 9th 2008, Portugal.

Archibald, S., & Bond, W. J. (2003). Growing tall vs growing wide: Tree architecture and allometry of Acacia karroo in forest, savanna, and arid environments. Oikos, 102(1), 3–14.

Ardö, J., & Olsson, L. (2003). Assessment of soil organic carbon in semi-arid Sudan using GIS and the CENTURY model. Journal of Arid Environments, 54(4), 633–651.

Aronson, J., Kigel, J., Shmida, A., & Klein, J. (1992). Adaptive phenology of desert and Mediterranean populations of annual plants grown with and without water stress. Oecologia, 89(1), 17–26.

Asari, N., Suratman, M. N., Jaafar, J., & Khalid, M. M. (2013). Estimation of above ground biomass for oil palm plantations using allometric equations. 4th International Conference on Biology, Environment and Chemistry. Selangor, Malaysia.

Attarchi, S., & Gloaguen, R. (2014). Improving the estimation of above ground biomass using dual polarimetric PALSAR and ETM+ data in the Hyrcanian mountain forest (Iran). Remote Sensing, 6(5), 3693–3715.

Avery, T. E., & Burkhart, H. E. (2015). Forest measurements. Waveland Press.

Baccini, A., Laporte, N., Goetz, S. J., Sun, M., & Dong, H. (2008). A first map of tropical Africa's above-ground biomass derived from satellite imagery. Environmental Research Letters, 3(4), 045011. https://doi.org/10.1088/1748-9326/3/4/045011

Baig, M. H. A., Zhang, L., Shuai, T., & Tong, Q. (2014). Derivation of a tasselled cap transformation based on Landsat 8 at-satellite reflectance. Remote Sensing Letters, 5(5), 423–431.

Bakr, N., Weindorf, D. C., Bahnassy, M. H., Marei, S. M., & El-Badawi, M. M. (2010). Monitoring land cover changes in a newly reclaimed area of Egypt using multi-temporal Landsat data. Applied Geography, 30(4), 592–605.

Bannari, A., Morin, D., Bonn, F., & Huete, A. R. (1995). A review of vegetation indices. Remote Sensing Reviews, 13(1–2), 95–120.

Baral, A., & Guha, G. S. (2004). Trees for carbon sequestration or fossil fuel substitution: The issue of cost vs. carbon benefit. Biomass and Bioenergy, 27(1), 41–55.

Barbosa, J. M., Broadbent, E. N., & Bitencourt, M. D. (2014). Remote sensing of aboveground biomass in tropical secondary forests: A review. International Journal of Forestry Research, 2014, 10–14.

Baret, F., Guyot, G., & Major, D. J. (1989). TSAVI: A vegetation index which minimizes soil brightness effects on LAI and APAR estimation. Geoscience and Remote Sensing Symposium, 1989. IGARSS'89. 12th Canadian Symposium on Remote Sensing., 1989 International, 3, 1355–1358.

Basuki, T. M., Van Laake, P. E., Skidmore, A. K., & Hussin, Y. A. (2009). Allometric equations for estimating the above-ground biomass in tropical lowland Dipterocarp forests. Forest Ecology and Management, 257(8), 1684–1694.

Baumann, G. (2009). How to assess rangeland condition in semiarid ecosystems? The indicative value of vegetation in the High Atlas Mountains, Morocco. Universität zu Köln.

Baumann, M., Levers, C., Macchi, L., Bluhm, H., Waske, B., Gasparri, N. I., & Kuemmerle, T. (2018). Mapping continuous fields of tree and shrub cover across the Gran Chaco using Landsat 8 and Sentinel-1 data. Remote Sensing of Environment, 216, 201–211.

Benz, U. C., Hofmann, P., Willhauck, G., Lingenfelder, I., & Heynen, M. (2004). Multi-resolution, object-oriented fuzzy analysis of remote sensing data for GIS-ready information. ISPRS Journal of Photogrammetry and Remote Sensing, 58(3–4), 239–258.

Bestelmeyer, B. T., Okin, G. S., Duniway, M. C., Archer, S. R., Sayre, N. F., Williamson, J. C., & Herrick, J. E. (2015). Desertification, land use, and the transformation of global drylands. Frontiers in Ecology and the Environment, 13(1), 28–36.

Biederman, J. A., Scott, R. L., Bell, T. W., Bowling, D. R., Dore, S., Garatuza-Payan, J., Kolb, T. E., Krishnan, P., Krofcheck, D. J., & Litvak, M. E. (2017). CO 2 exchange and evapotranspiration across dryland ecosystems of southwestern North America. Global Change Biology, 23(10), 4204–4221.

Birth, G. S., & McVey, G. R. (1968). Measuring the color of growing turf with a reflectance spectrophotometer 1. Agronomy Journal, 60(6), 640–643.

Blaschke, T. (2010). Object based image analysis for remote sensing. ISPRS Journal of Photogrammetry and Remote Sensing, 65(1), 2–16.

Bohlman, S., & O'Brien, S. (2006). Allometry, adult stature and regeneration requirement of 65 tree species on Barro Colorado Island, Panama. Journal of Tropical Ecology, 22(2), 123–136.

Bradley, A. V., Haughan, A. E., Al-Dughairi, A., & McLaren, S. J. (2019). Spatial variability in shrub vegetation across dune forms in central Saudi Arabia. Journal of Arid Environments, 161, 72–84.

Brady, N. C., & Weil, R. R. (1999). The nature and properties of soil 12th ed. Prentice-Hall Inc. Upper Saddle River, New Jersey.

Brown, I. F., Martinelli, L. A., Thomas, W. W., Moreira, M. Z., Ferreira, C. C., & Victoria, R. A. (1995). Uncertainty in the biomass of Amazonian forests: An example from Rondonia, Brazil. Forest Ecology and Management, 75(1), 175–189.

Brown, S. (1997). Estimating biomass and biomass change of tropical forests: A primer (Vol. 134). Food & Agriculture Org.

Brown, S., Gillespie, A. J., & Lugo, A. E. (1989). Biomass estimation methods for tropical forests with applications to forest inventory data. Forest Science, 35(4), 881–902.

Bryceson, K. P. (1991). Likely locust infestation areas in western New South Wales, Australia, located by satellite. Geocarto International, 6(4), 21–37.

Cairns, M. A., Brown, S., Helmer, E. H., & Baumgardner, G. A. (1997). Root biomass allocation in the world's upland forests. Oecologia, 111(1), 1–11.

Campbell, J. B., & Wynne, R. H. (2011). Introduction to remote sensing. Guilford Press.

Carlos, R. S., Sylvio, P. eacute llicoNetto, Ana, P. D. C., Aur eacute lio, L. ccedil o R., Alexandre, B., & Mateus, N. I. S. (2015). Quantifying biomass and carbon stocks in oil palm (Elaeis guineensis Jacq.) in Northeastern Brazil. African Journal of Agricultural Research, 10(43), 4067–4075. https://doi.org/10.5897/AJAR2015.9582

Castel, T., Guerra, F., Ruiz, A., Albarran, V., Caraglio, Y., & Houllier, F. (2000). Retrieval biomass of a large Venezuelan pine plantation using JERS-1 SAR data. Geoscience and Remote Sensing Symposium, 2000. Proceedings. IGARSS 2000. IEEE 2000 International, 1, 396–398.

Chave, J., Andalo, C., Brown, S., Cairns, M. A., Chambers, J. Q., Eamus, D., Fölster, H., Fromard, F., Higuchi, N., & Kira, T. (2005). Tree allometry and improved estimation of carbon stocks and balance in tropical forests. Oecologia, 145(1), 87–99.

Cheng, T., Song, R., Li, D., Zhou, K., Zheng, H., Yao, X., Tian, Y., Cao, W., & Zhu, Y. (2017). Spectroscopic Estimation of Biomass in Canopy Components of Paddy Rice Using Dry Matter and Chlorophyll Indices. Remote Sensing, 9(4), 319. https://doi.org/10.3390/rs9040319

Cheng, Z., Gamarra, J. G. P., & Birigazzi, L. (2014). Inventory of allometric equations for estimation tree biomass-a database for China. Rome, Italy: UNREDD Programme.

Chepkochei, L. C. (2011). Object-oriented image classification of individual trees using Erdas Imagine objective: Case study of Wanjohi area, Lake Naivasha Basin, Kenya. Proceedings of the Kenya Geothermal Conference, Nairobi, Kenya, 2123.

Cho, M. A., Mathieu, R., Asner, G. P., Naidoo, L., van Aardt, J., Ramoelo, A., Debba, P., Wessels, K., Main, R., & Smit, I. P. (2012). Mapping tree species composition in South African savannas using an integrated airborne spectral and LiDAR system. Remote Sensing of Environment, 125, 214–226.

Chong, K. L., Kanniah, K. D., Pohl, C., & Tan, K. P. (2017). A review of remote sensing applications for oil palm studies. Geo-Spatial Information Science, 20(2), 184–200.

Cihlar, J., Denning, S., Ahem, F., Arino, O., Belward, A., Bretherton, F., Cramer, W., Dedieu, G., Field, C., & Francey, R. (2002). Initiative to quantify terrestrial carbon sources and sinks. Eos, Transactions American Geophysical Union, 83(1), 1–7. https://doi.org/10.1029/2002EO000002

Clark, M. L., Roberts, D. A., & Clark, D. B. (2005). Hyperspectral discrimination of tropical rain forest tree species at leaf to crown scales. Remote Sensing of Environment, 96(3), 375–398.

Clerici, N., Rubiano, K., Abd-Elrahman, A., Posada Hoestettler, J. M., & Escobedo, F. J. (2016b). Estimating aboveground biomass and carbon stocks in periurban Andean secondary forests using very high resolution imagery. Forests, 7(7), 138. https://doi.org/10.3390/f7070138

Clewley, D., Lucas, R., Accad, A., Armston, J., Bowen, M., Dwyer, J., Pollock, S., Bunting, P., McAlpine, C., & Eyre, T. (2012). An approach to mapping forest growth stages in Queensland, Australia through integration of ALOS PALSAR and Landsat sensor data. Remote Sensing, 4(8), 2236–2255.

Cole, T. G., & Ewel, J. J. (2006). Allometric equations for four valuable tropical tree species. Forest Ecology and Management, 229(1), 351–360.

Congalton, R. G. (1991). A review of assessing the accuracy of classifications of remotely sensed data. Remote Sensing of Environment, 37(1), 35–46.

Corley, R. H. V., Hardon, J. J., & Tan, G. Y. (1971). Analysis of growth of the oil palm (Elaeis guineensisJacq.) I. Estimation of growth parameters and application in breeding. Euphytica, 20(2), 307–315.

Corley, R. Hereward V., & Tinker, P. B. (2008). The oil palm. John Wiley & Sons.

Corona-Núñez, R. O., Campo, J., & Williams, M. (2018). Aboveground carbon storage in tropical dry forest plots in Oaxaca, Mexico. Forest Ecology and Management, 409, 202–214.

Da Silva, F., Suwa, R., Kajimoto, T., Ishizuka, M., Higuchi, N., & Kunert, N. (2015). Allometric equations for estimating biomass of Euterpe precatoria, the most abundant palm species in the Amazon. Forests, 6(2), 450–463.

Dahy, B., Issa, S., Ksiksi, T., & Saleous, N. (2019). Non-Conventional Methods as a New Alternative for the Estimation of Terrestrial Biomass and Carbon Sequestered: Mini Review. World Journal of Agriculture and Soil Science. https://doi.org/10.33552/WJASS.2019.04.000579

Dahy, B., Issa, S., Ksiksi, T., & Saleous, N. (2020). Geospatial Technology Methods for Carbon Stock Assessment: A Comprehensive Review. IOP Conference Series: Earth and Environmental Science, 540, 012036. https://doi.org/10.1088/1755-1315/540/1/012036

Das, S., & Singh, T. P. (2012). Correlation analysis between biomass and spectral vegetation indices of forest ecosystem. International Journal of Engineering Research and Technology, 1(5), 1-13.

De Sy, V., Herold, M., Achard, F., Asner, G. P., Held, A., Kellndorfer, J., & Verbesselt, J. (2012). Synergies of multiple remote sensing data sources for REDD+ monitoring. Current Opinion in Environmental Sustainability, 4(6), 696–706.

Deans, J. D., Moran, J., & Grace, J. (1996). Biomass relationships for tree species in regenerating semi-deciduous tropical moist forest in Cameroon. Forest Ecology and Management, 88(3), 215–225.

Deng, S., Shi, Y., Jin, Y., & Wang, L. (2011). A GIS-based approach for quantifying and mapping carbon sink and stock values of forest ecosystem: A case study. Energy Procedia, 5, 1535–1545.

Dewi, S., Khasanah, N., Rahayu, S., Ekadinata, A., & Van Noordwijk, M. (2009). Carbon footprint of Indonesian palm oil production: A pilot study. Bogor, Indonesia. World Agroforestry Centre-ICRAF, SEA Regional Office, 8.

Dick OB, W. N. (2015). Estimating above Ground Biomass and Carbon Stock in the Lake Hawassa Watershed, Ethiopia by Integrating Remote Sensing and Allometric Equations. Forest Research: Open Access, 04(03). https://doi.org/10.4172/2168-9776.1000151

Diédhiou, I., Diallo, D., Mbengue, A. A., Hernandez, R. R., Bayala, R., Diémé, R., Diédhiou, P. M., & Sène, A. (2017). Allometric equations and carbon stocks in tree biomass of Jatropha curcas L. in Senegal's Peanut Basin. Global Ecology and Conservation, 9, 61–69.

Dietze, M. C., Wolosin, M. S., & Clark, J. S. (2008). Capturing diversity and interspecific variability in allometries: A hierarchical approach. Forest Ecology and Management, 256(11), 1939–1948.

Diouf, A., & Lambin, E. F. (2001). Monitoring land-cover changes in semi-arid regions: Remote sensing data and field observations in the Ferlo, Senegal. Journal of Arid Environments, 48(2), 129–148.

Dohai, B. S. (2007). Modeling Of Invasive Exotic Plants Dynamics in Arid Region Using Remote Sensing and GIS: A Case Study of Prosopis Juliflora in the UAE. Theses. https://scholarworks.uaeu.ac.ae/all_theses/512

Duncanson, L., Rourke, O., & Dubayah, R. (2015). Small sample sizes yield biased allometric equations in temperate forests. Scientific Reports, 5, 1–13.

Ebuy, J., Lokombe, J. P., Ponette, Q., Sonwa, D., & Picard, N. (2011). Allometric Equation for Predicting Aboveground Biomass of Three Tree Species. Journal of Tropical Forest Science, 23(2), 125–132.

Eggleston, H. S., Buendia, L., Miwa, K., Ngara, T., & Tanabe, K. (2006). IPCC guidelines for national greenhouse gas inventories. Institute for Global Environmental Strategies, Hayama, Japan, 2, 48–56.

Eisfelder, C., Kim, H. O., & Kuenzer, C. (2018). Multi-layer Land Cover Data for Remote-Sensing based Vege- tation Modelling for South Korea. 12. https://elib.dlr.de/119318/ .

Eisfelder, C., Kuenzer, C., & Dech, S. (2012). Derivation of biomass information for semi-arid areas using remote-sensing data. International Journal of Remote Sensing, 33(9), 2937–2984.

Ekoungoulou, R., Liu, X., Loumeto, J. J., Ifo, S. A., Bocko, Y. E., Fleury, E. K., & Niu, S. (2014). Tree Allometry in Tropical Forest of Congo for Carbon Stocks Estimation in Above-Ground Biomass. Open Journal of Forestry, 4(5), 481.http://www.scirp.org/journal/PaperInformation.aspx?PaperID=50690&#abstract

El Tahir, B. A., Ahmed, D. M., Ardö, J., Gaafar, A. M., & Salih, A. A. (2009). Changes in soil properties following conversion of Acacia senegal plantation to other land management systems in North Kordofan State, Sudan. Journal of Arid Environments, 73(4–5), 499–505.

Elhag, M. (2016). Evaluation of different soil salinity mapping using remote sensing techniques in arid ecosystems, Saudi Arabia. Journal of Sensors, 2016. https://doi.org/10.1155/2016/7596175

El-Juhany, L. I. (2010). Degradation of date palm trees and date production in Arab countries: Causes and potential rehabilitation. Australian Journal of Basic and Applied Sciences, 4(8), 3998–4010.

Elzinga, C. L., Salzer, D. W., & Willoughby, J. W. (1998). Measuring & Monitering Plant Populations. US Bureau of Land Management Papers.

EU EDGAR. (2017). Emissions Database for Global Atmospheric Research. http://edgar.jrc.ec.europa.eu/overview.php?v=CO2andGHG1970-2016&dst=CO2pc&sort=des9 (Date accessed on 20th Feb. 2021 at 7:45 PM Abu Dhab)

FAO. (1982). Plant Production and Protection. Date Production and Protection Paper No. 35. p. 294. http://www.fao.org/3/w5897e/w5897e6c.htm

FAOSTAT. (2013). Crop Production, Statistics Division. Food and Agriculture Organization of the United Nations.

Felker, P. (2009). Unusual physiological properties of the arid adapted tree legume Prosopis and their applications in developing countries. Perspectives in Biophysical Plant Ecophysiology: A Tribute to Park S Nobel. Mexico City: Universidad Nacional Autónoma de México, 221–55.

Figueiredo, M. V. B., Vilar, J. J., & Burity, H. A. (1999). Alleviation of water stress effects in cowpea by Bradyrhizobium spp. Inoculation. Plant and Soil, 207(1), 67–75.

Fonton, N. H., Medjibé, V., Djomo, A., Kondaoulé, J., Rossi, V., Ngomanda, A., & Maïdou, H. (2017). Analyzing accuracy of the power functions for modeling aboveground biomass rediction in Congo basin tropical forests. Open Journal of Forestry, 7(4), 388–402.

Foody, G. M. (2002). Status of land cover classification accuracy assessment. Remote Sensing of Environment, 80(1), 185–201.

Gernhardt, S., Adam, N., Eineder, M., & Bamler, R. (2010). Potential of very high resolution SAR for persistent scatterer interferometry in urban areas. Annals of GIS, 16(2), 103–111.

Gevana, D., & Im, S. (2016). Allometric models for Rhizophora stylosa Griff. In dense monoculture plantation in the Philippines. Malaysian Forester, 79, 39–53.

Ghasemi, N., Sahebi, M. R., & Mohammadzadeh, A. (2011). A review on biomass estimation methods using synthetic aperture radar data. International Journal of Geomatics and Geosciences, 1(4), 776–788.

Gibbs, H. K., Brown, S., Niles, J. O., & Foley, J. A. (2007). Monitoring and estimating tropical forest carbon stocks: Making REDD a reality. Environmental Research Letters, 2(4), 045023. https://iopscience.iop.org/article/10.1088/1748-9326/2/4/045023.

Gilbertson, J. K., Kemp, J., & Van Niekerk, A. (2017). Effect of pan-sharpening multi-temporal Landsat 8 imagery for crop type differentiation using different classification techniques. Computers and Electronics in Agriculture, 134, 151–159.

Gitelson, A. A., Kaufman, Y. J., & Merzlyak, M. N. (1996). Use of a green channel in remote sensing of global vegetation from EOS-MODIS. Remote Sensing of Environment, 58(3), 289–298.

Gizachew, B., Solberg, S., N\a esset, E., Gobakken, T., Bollands\a as, O. M., Breidenbach, J., Zahabu, E., & Mauya, E. W. (2016). Mapping and estimating the total living biomass and carbon in low-biomass woodlands using Landsat 8 CDR data. Carbon Balance and Management, 11(1), 1–14.

Goodman, R. C., Phillips, O. L., del Castillo Torres, D., Freitas, L., Cortese, S. T., Monteagudo, A., & Baker, T. R. (2013). Amazon palm biomass and allometry. Forest Ecology and Management, 310, 994–1004. https://doi.org/10.1016/j.foreco.2013.09.045

Goudie, A. S., Parker, A. G., & Al-Farraj, A. (2000). Coastal change in Ras al Khaimah (United Arab Emirates): A cartographic analysis. Geographical Journal, 166(1), 14–25.

Greenberg, J. A., Dobrowski, S. Z., & Ustin, S. L. (2005). Shadow allometry: Estimating tree structural parameters using hyperspatial image analysis. Remote Sensing of Environment, 97(1), 15–25.

Günlü, A., Ercanli, I., Başkent, E. Z., & Çakır, G. (2014). Estimating aboveground biomass using Landsat TM imagery: A case study of Anatolian Crimean pine forests in Turkey. Annals of Forest Research, 57(2), 289–298.

Guo, L. B., & Gifford, R. M. (2002). Soil carbon stocks and land use change: A meta analysis. Global Change Biology, 8(4), 345–360.

Haughton, N., Abramowitz, G., De Kauwe, M. G., & Pitman, A. J. (2018). Does predictability of fluxes vary between FLUXNET sites? Biogeosciences, 15(14). https://doi.org/10.5194/bg-15-4495-2018.

Hebbar, R., Ravishankar, H. M., Subramoniam, S. R., Uday, R., & Dadhwal, V. K. (2014). Object oriented classification of high resolution data for inventory of horticultural crops. The International Archives of Photogrammetry, Remote Sensing and Spatial Information Sciences, 40(8), 745. doi:10.5194/isprsarchives-XL-8-745-2014

Henry, M., Picard, N., Trotta, C., Manlay, R., Valentini, R., Bernoux, M., & Saint André, L. (2011). Estimating tree biomass of sub-Saharan African forests: A review of available allometric equations. Silva Fennica, 45(3B), 477–569.

Henson, I. E., & Chang, K. C. (2003). Oil palm plantations and forest loss an objective appraisal. Proceedings of the PIPOC 2003 International Palm Oil Congress, Malaysian Palm Oil Board, 960–974.

Holm, A. M., Cridland, S. W., & Roderick, M. L. (2003). The use of time-integrated NOAA NDVI data and rainfall to assess landscape degradation in the arid shrubland of Western Australia. Remote Sensing of Environment, 85(2), 145–158.

Holmgren, P., Masakha, E. J., & Sjöholm, H. akan. (1994). Not all African land is being degraded: A recent survey of trees on farms in Kenya reveals rapidly increasing forest resources. Ambio, 23(7), 390–395.

Houghton, R. A., Hall, F., & Goetz, S. J. (2009). Importance of biomass in the global carbon cycle. Journal of Geophysical Research: Biogeosciences, 114(G2). https://doi.org/10.1029/2009JG000935

Huete, A. R. (1988). A soil-adjusted vegetation index (SAVI). Remote Sensing of Environment, 25(3), 295–309.

Hughes, R. F., Kauffman, J. B., & Jaramillo, V. J. (1999). Biomass, carbon, and nutrient dynamics of secondary forests in a humid tropical region of Mexico. Ecology, 80(6), 1892–1907.

Humphrey, V., Zscheischler, J., Ciais, P., Gudmundsson, L., Sitch, S., & Seneviratne, S. I. (2018). Sensitivity of atmospheric CO_2 growth rate to observed changes in terrestrial water storage. Nature, 560(7720), 628–631.

Husch, B., Miller, C. I., & Beers, T. W. (1982). Forest measurements. John Wiley & Sons, Inc., New York.

Husin, M., Zakaria, Z. Z., & Hassan, A. H. (1987). Potentials of oil palm by-products as raw materials for agro-based industries. IPMKSM.

Iizuka, K., & Tateishi, R. (2015). Estimation of CO_2 sequestration by the forests in Japan by discriminating precise tree age category using remote sensing techniques. Remote Sensing, 7(11), 15082–15113.

Im, J., & Jensen, J. R. (2008). Hyperspectral remote sensing of vegetation. Geography Compass, 2(6), 1943–1961.

Imagine Objective tools. (ERDAS Imagine User Guide, 2020). Imagine Objective tools.

Immitzer, M., Atzberger, C., & Koukal, T. (2012). Tree species classification with random forest using very high spatial resolution 8-band WorldView-2 satellite data. Remote Sensing, 4(9), 2661–2693.

Jara, M. C., Henry, M., Réjou-Méchain, M., Wayson, C., Zapata-Cuartas, M., Piotto, D., Guier, F. A., Lombis, H. C., López, E. C., & Lara, R. C. (2015). Guidelines for documenting and reporting tree allometric equations. Annals of Forest Science, 72(6), 763–768.

Jawak, S. D., Devliyal, P., & Luis, A. J. (2015). A comprehensive review on pixel oriented and object oriented methods for information extraction from remotely sensed satellite images with a special emphasis on cryospheric applications. Advances in Remote Sensing, 4(03), 177. doi: 10.4236/ars.2015.43015

Jawak, S. D., Luis, A. J., Panditrao, S. N., Khopkar, P. S., & Jadhav, P. S. (2013). Advancement in landcover classification using very high resolution remotely sensed 8-band WorldView-2 satellite data. International Journal of Earth Sciences and Engineering, 6(02), 1742–1749.

Jiang, Z., Huete, A. R., Didan, K., & Miura, T. (2008). Development of a two-band enhanced vegetation index without a blue band. Remote Sensing of Environment, 112(10), 3833–3845.

Jongbloed, M. (2003). The comprehensive guide to the wild flowers of the United Arab Emirates. Environmental Research and Wildlife Development Agency.

Joshi, H. G., & Ghose, M. (2014). Community structure, species diversity, and aboveground biomass of the Sundarbans mangrove swamps. Tropical Ecology, 55(3), 283–303.

Jucker, T., Caspersen, J., Chave, J., Antin, C., Barbier, N., Bongers, F., Dalponte, M., van Ewijk, K. Y., Forrester, D. I., & Haeni, M. (2017). Allometric equations for integrating remote sensing imagery into forest monitoring programmes. Global Change Biology, 23(1), 177–190.

Kader, A. A., & Hussein, A. M. (2009). Harvesting and postharvest handling of dates. ICARDA, Aleppo, Syria, 4, 15. https://doi.org/10.1002/9781118292419.ch5

Kamarudzaman, A., Mohd Hashim, T., Mohd, A., & Teah, C. H. (1995). Zero burning-An environmentally friendly replanting technique. PORIM International Palm Oil Congress: Update and Vision (Agriculture) September 22-25 Kuala Lumpur, Malaysia.

Kamusoko, C., & Aniya, M. (2009). Hybrid classification of Landsat data and GIS for land use/cover change analysis of the Bindura district, Zimbabwe. International Journal of Remote Sensing, 30(1), 97–115.

Kankare, V., Vastaranta, M., Holopainen, M., Räty, M., Yu, X., Hyyppä, J., Hyyppä, H., Alho, P., & Viitala, R. (2013). Retrieval of forest aboveground biomass and stem volume with airborne scanning LiDAR. Remote Sensing, 5(5), 2257–2274.

Kappen, L., Lange, O. L., Schulze, E.-D., Evenari, M., & Buschbom, U. (1972). Extreme water stress and photosynthetic activity of the desert plant Artemisia herba-alba Asso. Oecologia, 10(2), 177–182.

Karlson, M., Ostwald, M., Reese, H., Sanou, J., Tankoano, B., & Mattsson, E. (2015). Mapping tree canopy cover and aboveground biomass in Sudano-Sahelian woodlands using Landsat 8 and random forest. Remote Sensing, 7(8), 10017–10041.

Kelsey, K. C., & Neff, J. C. (2014). Estimates of aboveground biomass from texture analysis of Landsat imagery. Remote Sensing, 6(7), 6407–6422.

Ketterings, Q. M., Coe, R., van Noordwijk, M., & Palm, C. A. (2001). Reducing uncertainty in the use of allometric biomass equations for predicting above-ground tree biomass in mixed secondary forests. Forest Ecology and Management, 146(1–3), 199–209.

Khalid, H., Zin, Z. Z., & Anderson, J. M. (1999a). Quantification of oil palm biomass and nutrient value in a mature plantation. I. Above-ground biomass. Journal of Oil Palm Research, 11(1), 23–32.

Khalid, H., Zin, Z. Z., & Anderson, J. M. (1999b). Quantification of oil palm biomass and nutrient value in a mature plantation. II. Below-ground biomass. Journal of Oil Palm Research, 11(2), 63–71.

Khalid, N., & Hamid, J. R. A. (2017). Development of Allometric Equation for Estimating Aboveground Biomass in Ampang Forest Reserve, Malaysia. J Biodivers Manage Forestry 6: 1. Of, 4, 2. doi:10.4172/2327-4417.1000173

King, D. A. (1990). Allometry of saplings and understorey trees of a Panamanian forest. Functional Ecology, 27–32.

Koala, J., Sawadogo, L., Savadogo, P., Aynekulu, E., Heiskanen, J., & Saïd, M. (2017). Allometric equations for below-ground biomass of four key woody species in West African savanna-woodlands. Silva Fennica.

Korom, A., & Matsuura, T. (2016). Relationships between crown size and aboveground biomass of oil palms: An evaluation of allometric models. Sains Malaysiana, 45(4), 523–533.

Ksiksi, T. S. (2012). Acacia trotilis and Calotropis procera: Do They Substantially Promote Soil Carbon Sequestration? Open Journal of Soil Science, 2(02), 116. doi.org/10.4236/ojss.2012.22017

Kuemmerle, T., Radeloff, V. C., Perzanowski, K., & Hostert, P. (2006). Cross-border comparison of land cover and landscape pattern in Eastern Europe using a hybrid classification technique. Remote Sensing of Environment, 103(4), 449–464.

Kumar, L., & Mutanga, O. (2017). Remote Sensing of Above-Ground Biomass. Remote Sensing, 9(9), 935. https://doi.org/10.3390/rs9090935

Kumar, L., Sinha, P., Taylor, S., & Alqurashi, A. F. (2015). Review of the use of remote sensing for biomass estimation to support renewable energy generation. Journal of Applied Remote Sensing, 9(1), 097696–097696.

Kux, H. J., & Souza, U. D. (2012). Object-based image analysis of WORLDVIEW-2 satellite data for the classification of mangrove areas in the city of São Luís, Maranhão State, Brazil. ISPRS Ann. Photogramm. Remote Sens. Spat. Inf. Sci, 4, 95–100.

Labrecque, S., Fournier, R. A., Luther, J. E., & Piercey, D. (2006). A comparison of four methods to map biomass from Landsat-TM and inventory data in western Newfoundland. Forest Ecology and Management, 226(1), 129–144.

Lack, N., & Bleisch, S. (2010). Object-based change detection for a cultureal-historical survey of the landscape-from cow trails to walking paths. The International Archives of the Photogrammetry, Remote Sensing and Spatial Information Sciences, 38. 38 Proceedings of the Geographic object-based image analysis (GEOBIA) Ghent, Belgium.

Lackner, K. S. (2003). A guide to CO2 sequestration. Science, 300(5626), 1677–1678.

Lal, R. (2004). Soil carbon sequestration to mitigate climate change. Geoderma, 123(1), 1–22. https://doi.org/10.1016/j.geoderma.2004.01.032

Lal, Rattan. (2001). Potential of desertification control to sequester carbon and mitigate the greenhouse effect. Climatic Change, 51(1), 35–72.

Lal, Rattan. (2002). Soil carbon dynamics in cropland and rangeland. Environmental Pollution, 116(3), 353–362.

Le Maire, G., François, C., Soudani, K., Berveiller, D., Pontailler, J.-Y., Bréda, N., Genet, H., Davi, H., & Dufrêne, E. (2008). Calibration and validation of hyperspectral indices for the estimation of broadleaved forest leaf chlorophyll content, leaf mass per area, leaf area index and leaf canopy biomass. Remote Sensing of Environment, 112(10), 3846–3864.

Lemenih, M., & Itanna, F. (2004). Soil carbon stocks and turnovers in various vegetation types and arable lands along an elevation gradient in southern Ethiopia. Geoderma, 123(1–2), 177–188.

Li, D., Ke, Y., Gong, H., & Li, X. (2015). Object-based urban tree species classification using bi-temporal WorldView-2 and WorldView-3 images. Remote Sensing, 7(12), 16917–16937.

Li, M., Tan, Y., Pan, J., & Peng, S. (2008). Modeling forest aboveground biomass by combining spectrum, textures and topographic features. Frontiers of Forestry in China, 3(1), 10–15.

Lillesand, T., Kiefer, R. W., & Chipman, J. (2014). Remote sensing and image interpretation. John Wiley & Sons.

Litton, C. M., & Boone Kauffman, J. (2008). Allometric models for predicting aboveground biomass in two widespread woody plants in Hawaii. Biotropica, 40(3), 313–320.

Liu, D., & Xia, F. (2010). Assessing object-based classification: Advantages and limitations. Remote Sensing Letters, 1(4), 187–194.

Lo, C. P., & Choi, J. (2004). A hybrid approach to urban land use/cover mapping using Landsat 7 Enhanced Thematic Mapper Plus (ETM+) images. International Journal of Remote Sensing, 25(14), 2687–2700.

Lu, D., Mausel, P., Brondizio, E., & Moran, E. (2002). Assessment of atmospheric correction methods for Landsat TM data applicable to Amazon basin LBA research. International Journal of Remote Sensing, 23(13), 2651–2671.

Lu, Dengsheng. (2006). The potential and challenge of remote sensing-based biomass estimation. International Journal of Remote Sensing, 27(7), 1297–1328.

Lu, Dengsheng, & Weng, Q. (2004). Spectral mixture analysis of the urban landscape in Indianapolis with Landsat ETM+ imagery. Photogrammetric Engineering & Remote Sensing, 70(9), 1053–1062.

Lugo, A. E., & Brown, S. (1992). Tropical forests as sinks of atmospheric carbon. Forest Ecology and Management, 54(1), 239–255. https://doi.org/10.1016/0378-1127(92)90016-3

Mahmood, H., Siddique, M. R., Costello, L., Birigazzi, L., Abdullah, S. R., Henry, M., Siddiqui, B. N., Aziz, T., Ali, S., & Al Mamun, A. (2019). Allometric models for estimating biomass, carbon and nutrient stock in the Sal zone of Bangladesh. IForest-Biogeosciences and Forestry, 12(1), 69. doi: https://doi.org/10.3832/ifor2758-011

Main-Knorn, M., Moisen, G. G., Healey, S. P., Keeton, W. S., Freeman, E. A., & Hostert, P. (2011). Evaluating the remote sensing and inventory-based estimation of biomass in the western Carpathians. Remote Sensing, 3(7), 1427–1446.

Makinde, E. O., Womiloju, A. A., & Ogundeko, M. O. (2017). The geospatial modelling of carbon sequestration in Oluwa Forest, Ondo State, Nigeria. European Journal of Remote Sensing, 50(1), 397–413.

Mangiarotti, S., Mazzega, P., Jarlan, L., Mougin, E., Baup, F., & Demarty, J. (2008). Evolutionary bi-objective optimization of a semi-arid vegetation dynamics model with NDVI and $\sigma 0$ satellite data. Remote Sensing of Environment, 112(4), 1365–1380.

Maulana, S. I., Wibisono, Y., & Utomo, S. (2016). Development of local allometric equation to estimate total aboveground biomass in Papua tropical forest. Indonesian Journal of Forestry Research, 3(2), 107–118.

Maynard, C. L., Lawrence, R. L., Nielsen, G. A., & Decker, G. (2007). Modeling vegetation amount using bandwise regression and ecological site descriptions as an alternative to vegetation indices. GIScience & Remote Sensing, 44(1), 68–81.

McGwire, K., Minor, T., & Fenstermaker, L. (2000). Hyperspectral mixture modeling for quantifying sparse vegetation cover in arid environments. Remote Sensing of Environment, 72(3), 360–374.

McMorrow, J. (2001). Linear regression modelling for the estimation of oil palm age from Landsat TM. International Journal of Remote Sensing, 22(12), 2243–2264.

Mokany, K., Raison, R., & Prokushkin, A. S. (2006). Critical analysis of root: Shoot ratios in terrestrial biomes. Global Change Biology, 12(1), 84–96.

Montaghi, A., Corona, P., Dalponte, M., Gianelle, D., Chirici, G., & Olsson, H. akan. (2013). Airborne laser scanning of forest resources: An overview of research in Italy as a commentary case study. International Journal of Applied Earth Observation and Geoinformation, 23, 288–300.

Monteith, J. L. (1972). Solar radiation and productivity in tropical ecosystems. Journal of Applied Ecology, 9(3), 747–766.

Morel, A. C., Fisher, J. B., & Malhi, Y. (2012). Evaluating the potential to monitor aboveground biomass in forest and oil palm in Sabah, Malaysia, for 2000–2008 with Landsat ETM+ and ALOS-PALSAR. International Journal of Remote Sensing, 33(11), 3614–3639. https://doi.org/10.1080/01431161.2011.631949

Mróz, M., & Sobieraj, A. (2004). Comparison of several vegetation indices calculated on the basis of a seasonal SPOT XS time series, and their suitability for land cover and agricultural crop identification. Technical Sciences, 7(7), 39–66.

Mugiraneza, T., Nascetti, A., & Ban, Y. (2019). WorldView-2 Data for Hierarchical Object-Based Urban Land Cover Classification in Kigali: Integrating Rule-Based Approach with Urban Density and Greenness Indices. Remote Sensing, 11(18), 2128. https://doi.org/10.3390/rs11182128

Mundia, C. N., & Aniya, M. (2005). Analysis of land use/cover changes and urban expansion of Nairobi city using remote sensing and GIS. International Journal of Remote Sensing, 26(13), 2831–2849.

Mutanga, O., & Rugege, D. (2006). Integrating remote sensing and spatial statistics to model herbaceous biomass distribution in a tropical savanna. International Journal of Remote Sensing, 27(16), 3499–3514.

Mutanga, Onisimo, & Skidmore, A. K. (2004). Narrow band vegetation indices overcome the saturation problem in biomass estimation. International Journal of Remote Sensing, 25(19), 3999–4014.

Mwanamwenge, J., Loss, S. P., Siddique, K. H. M., & Cocks, P. S. (1999). Effect of water stress during floral initiation, flowering and podding on the growth and yield of faba bean (Vicia faba L.). European Journal of Agronomy, 11(1), 1–11.

Myint, S. W., Gober, P., Brazel, A., Grossman-Clarke, S., & Weng, Q. (2011b). Per-pixel vs. Object-based classification of urban land cover extraction using high spatial resolution imagery. Remote Sensing of Environment, 115(5), 1145–1161.

N\a esset, E., & Økland, T. (2002). Estimating tree height and tree crown properties using airborne scanning laser in a boreal nature reserve. Remote Sensing of Environment, 79(1), 105–115.

Nagaraja, A. (2009). Predicting susceptible areas of mango malformation through remote sensing and GIS [PhD Dissertation]. Indian Agricultural Research Institute, New Delhi, India.

National Center of Meterology (1995 -2018). website: https://www.ncm.ae/en/climate-reports yearly.html?id=8802. Reterived on 18 September 2020.

Nyssen, J., Temesgen, H., Lemenih, M., Zenebe, A., Haregeweyn, N., & Haile, M. (2008). Spatial and temporal variation of soil organic carbon stocks in a lake retreat area of the Ethiopian Rift Valley. Geoderma, 146(1–2), 261–268.

Ohmann, J. L., & Gregory, M. J. (2002). Predictive mapping of forest composition and structure with direct gradient analysis and nearest-neighbor imputation in coastal Oregon, USA. Canadian Journal of Forest Research, 32(4), 725–741.

Oldeland, J., Dorigo, W., Wesuls, D., & Jürgens, N. (2010). Mapping bush encroaching species by seasonal differences in hyperspectral imagery. Remote Sensing, 2(6), 1416–1438.

Olsen, J. L., Miehe, S., Ceccato, P., & Fensholt, R. (2015). Does EO NDVI seasonal metrics capture variations in species composition and biomass due to grazing in semi-arid grassland savannas? Biogeosciences, 12(14), 4407–4419.

Ozdemir, I. (2008). Estimating stem volume by tree crown area and tree shadow area extracted from pan-sharpened Quickbird imagery in open Crimean juniper forests. International Journal of Remote Sensing, 29(19), 5643–5655.

Ozdemir, Ibrahim, & Karnieli, A. (2011). Predicting forest structural parameters using the image texture derived from WorldView-2 multispectral imagery in a dryland forest, Israel. International Journal of Applied Earth Observation and Geoinformation, 13(5), 701–710.

Pandit, S., Tsuyuki, S., & Dube, T. (2018). Estimating above-ground biomass in sub-tropical buffer zone community Forests, Nepal, using Sentinel 2 data. Remote Sensing, 10(4), 601. https://doi.org/10.3390/rs10040601

Patel, N. K., Saxena, R. K., & Shiwalkar, A. (2007). Study of fractional vegetation cover using high spectral resolution data. Journal of the Indian Society of Remote Sensing, 35(1), 73–79.

Pearson, R. L., & Miller, L. D. (1972). Remote mapping of standing crop biomass for estimation of the productivity of the shortgrass prairie. Remote Sensing of Environment, VIII, 1355.

Pflugmacher, D. (2011). Remote sensing of forest biomass dynamics using Landsat-derived disturbance and recovery history and lidar data. Oregon State University.

Phiri, D., & Morgenroth, J. (2017). Developments in Landsat land cover classification methods: A review. Remote Sensing, 9(9), 967. https://doi.org/10.3390/rs9090967

Picard, N., Saint-André, L., & Henry, M. (2012). Manual for building tree volume and biomass allometric equations: From field measurement to prediction, FAO; Food and Agricultural Organization of the United Nations.

Pinty, B., & Verstraete, M. M. (1992). GEMI: A non-linear index to monitor global vegetation from satellites. Vegetatio, 101(1), 15–20.

Ponce-Hernandez, R., Koohafkan, P., & Antoine, J. (2004). Assessing carbon stocks and modelling win-win scenarios of carbon sequestration through land-use changes (Vol. 1). Food & Agriculture Org.

Popescu, S. C., Wynne, R. H., & Nelson, R. F. (2003). Measuring individual tree crown diameter with lidar and assessing its influence on estimating forest volume and biomass. Canadian Journal of Remote Sensing, 29(5), 564–577.

Poulter, B., Frank, D., Ciais, P., Myneni, R. B., Andela, N., Bi, J., Broquet, G., Canadell, J. G., Chevallier, F., & Liu, Y. Y. (2014). Contribution of semi-arid ecosystems to interannual variability of the global carbon cycle. Nature, 509(7502), 600–603.

Pradhan, R., Ghose, M. K., & Jeyaram, A. (2010). Land cover classification of remotely sensed satellite data using bayesian and hybrid classifier. International Journal of Computer Applications, 7(11), 1–4.

Prayogo, C., Sari, R. R., Asmara, D. H., Rahayu, S., & Hairiah, K. (2018). Allometric Equation for Pinang (Areca catechu) Biomass and C Stocks. AGRIVITA, Journal of Agricultural Science, 40(3), 382–389.

Pribyl, D. W. (2010). A critical review of the conventional SOC to SOM conversion factor. Geoderma, 156(3), 75–83.

Qi, J., Chehbouni, A., Huete, A. R., Kerr, Y. H., & Sorooshian, S. (1994). A modified soil adjusted vegetation index. Remote Sensing of Environment, 48(2), 119–126. https://doi.org/10.1016/0034-4257(94)90134-1

Qi, J., Huete, A. R., Cabot, F., & Chehbouni, A. (1994). Bidirectional properties and utilizations of high-resolution spectra from a semiarid watershed. Water Resources Research, 30(5), 1271–1279.

Qureshi, A., Badola, R., & Hussain, S. A. (2012). A review of protocols used for assessment of carbon stock in forested landscapes. Environmental Science & Policy, 16, 81–89.

Ramachandran, A., Jayakumar, S., Haroon, R. M., Bhaskaran, A., & Arockiasamy, D. I. (2007). Carbon sequestration: Estimation of carbon stock in natural forests using geospatial technology in the Eastern Ghats of Tamil Nadu, India. Current Science, 323–331.

Ramankutty, N., Gibbs, H. K., Achard, F., Defries, R., Foley, J. A., & Houghton, R. A. (2007). Challenges to estimating carbon emissions from tropical deforestation. Global Change Biology, 13(1), 51–66.

Ramos, M. L. G., Parsons, R., Sprent, J. I., & James, E. K. (2003). Effect of water stress on nitrogen fixation and nodule structure of common bean. Pesquisa Agropecuária Brasileira, 38(3), 339–347.

Rees, A. R., & Tinker, P. B. H. (1963). Dry-matter production and nutrient content of plantation oil palms in Nigeria. Plant and Soil, 19(1), 19–32.

Reinartz, P., Müller, R., Hoja, D., Lehner, M., & Schroeder, M. (2005). Comparison and fusion of DEM derived from SPOT-5 HRS and SRTM data and estimation of forest heights. Proc. EARSeL Workshop on 3D-Remote Sensing, Porto, Vol. 1, Portugal.

Rembold, F., Carnicelli, S., Nori, M., & Ferrari, G. A. (2000). Use of aerial photographs, Landsat TM imagery and multidisciplinary field survey for land-cover change analysis in the lakes region (Ethiopia). International Journal of Applied Earth Observation and Geoinformation, 2(3–4), 181–189.

Ren, H., Zhou, G., & Zhang, X. (2011). Estimation of green aboveground biomass of desert steppe in Inner Mongolia based on red-edge reflectance curve area method. Biosystems Engineering, 109(4), 385–395.

Richardson, A. J., & Wiegand, C. L. (1977). Distinguishing vegetation from soil background information. Photogrammetric Engineering and Remote Sensing, 43(12), 1541–1552.

Ritchie, J. C., & Rango, A. (1996). Remote sensing applications to hydrology: Introduction. Hydrological Sciences Journal, 41(4), 429–431.

Rizvi, R. H., Newaj, R., Srivastava, S., & Yadav, M. (2019). MApping trees on farmlands using OBIA method and high resolution satellite data: a case study of Koraput district, ODISHA. ISPRS - International Archives of the Photogrammetry, Remote Sensing and Spatial Information Sciences, XLII-3/W6, 617–621. https://doi.org/10.5194/isprs-archives-XLII-3-W6-617-2019

Robinson, C., Saatchi, S., Neumann, M., & Gillespie, T. (2013). Impacts of spatial variability on aboveground biomass estimation from L-band radar in a temperate forest. Remote Sensing, 5(3), 1001–1023.

Rosema, A. (1993). Using METEOSAT for operational evapotranspiration and biomass monitoring in the Sahel region. Remote Sensing of Environment, 46(1), 27–44.

Rosenfield, G. H., & Fitzpatrick-Lins, K. (1986). A coefficient of agreement as a measure of thematic classification accuracy. Photogrammetric Engineering and Remote Sensing, 52(2), 223–227.

Roujean, J.-L., & Breon, F.-M. (1995). Estimating PAR absorbed by vegetation from bidirectional reflectance measurements. Remote Sensing of Environment, 51(3), 375–384.

Rouse, J. (1974). Monitoring the vernal advancement of retrogradation of natural vegetation, NASA/GSFG, Type III. Final Report, greenbelt, MD, 371.

Rozenstein, O., & Karnieli, A. (2011). Comparison of methods for land-use classification incorporating remote sensing and GIS inputs. Applied Geography, 31(2), 533–544.

Russell, C. E. (1983). Nutrient cycling and productivity of native and plantation forests at Jari Florestal, Para, Brazil. University of Georgia.

Sahay, B., Chakraborty, A., Chaudhary, K. K., Laxman, B., Murthy, C., & Rao, P. (2017). Mapping Multiple Horticulture Crops using Object Oriented Classification Techniques. 9. In: 38th Asian Conference on Remote Sensing.

Sajdak, M., Velázquez-Martí, B., & López-Cortés, I. (2014). Quantitative and qualitative characteristics of biomass derived from pruning Phoenix canariensis hort. Ex Chabaud. And Phoenix dactilifera L. Renewable Energy, 71, 545–552.

Saldarriaga, J. G., West, D. C., Tharp, M. L., & Uhl, C. (1988). Long-term chronosequence of forest succession in the upper Rio Negro of Colombia and Venezuela. The Journal of Ecology, 938–958.

Salem Issa, & Al Shuwaihi, A. (2012). Characterization of Al Ain city urban growth using multi-temporal remote sensing data and GIS. Int Geoinformatics Res Dev J, 3, 1–17.

Salem Issa, Dahy, B. S., & Saleous, N. (2020). Accurate mapping of date plams at different age-stages for the purpose of estimating their biomass. ISPRS Annals of Photogrammetry, Remote Sensing and Spatial Information Sciences, V-3–2020, 461–467. https://doi.org/10.5194/isprs-annals-V-3-2020-461-2020

Salem Issa, Dahy, B., Ksiksi, T., & Saleous, N. (2020a). A Review of Terrestrial Carbon Assessment Methods Using Geo-Spatial Technologies with Emphasis on Arid Lands. Remote Sensing, 12(12), 2008. https://doi.org/10.3390/rs12122008

Salem Issa, Dahy, B., Ksiksi, T., & Saleous, N. (2020b). Allometric equations coupled with remotely sensed variables to estimate carbon stocks in date palms. Journal of Arid Environments, 182, 104264. https://doi.org/10.1016/j.jaridenv.2020.104264

Salem Issa, Dahy, B., Saleous, N., & Ksiksi, T. (2019). Carbon stock assessment of date palm using remote sensing coupled with field-based measurements in Abu Dhabi (United Arab Emirates). International Journal of Remote Sensing, 0(0), 1–20. https://doi.org/10.1080/01431161.2019.1602795

Salem Issa, & Dohai, B. (2008). GIS analyisis of invasive prosopis juliflura dyanamics in two selected sites from the united arab emirates. Canadian Journal of Pure and Applied Sciences, 235. pp. 235–242.

Schlerf, M., Atzberger, C., & Hill, J. (2005). Remote sensing of forest biophysical variables using HyMap imaging spectrometer data. Remote Sensing of Environment, 95(2), 177–194.

Schreuder, H. T., Gregoire, T. G., & Wood, G. B. (1993). Sampling methods for multiresource forest inventory. John Wiley & Sons.

Schucknecht, A., Meroni, M., Kayitakire, F., Rembold, F., & Boureima, A. (2015). Biomass estimation to support pasture management in Niger. The International Archives of Photogrammetry, Remote Sensing and Spatial Information Sciences, 40(7), 109. doi: 10.5194/isprsarchives-XL-7-W3-109-2015.

Shafri, H. Z., Hamdan, N., & Saripan, M. I. (2011). Semi-automatic detection and counting of oil palm trees from high spatial resolution airborne imagery. International Journal of Remote Sensing, 32(8), 2095–2115.

Shaharum, N. S. N., Shafri, H. Z. M., Gambo, J., & Abidin, F. A. Z. (2018). Mapping of Krau Wildlife Reserve (KWR) protected area using Landsat 8 and supervised classification algorithms. Remote Sensing Applications: Society and Environment, 10, 24–35.

Shahid, S. A., & Abdelfattah, M. A. (2008). Soils of abu dhabi emirate. Terrestrial Environment of Abu Dhabi Emirate. Environment Agency, Abu Dhabi, 71–91.

Shahin, S. M., and M. Salem. (2014). "Review Future Concerns on Irrigation Requirements of Date Palm Tree in the United Arab Emirates (UAE): Call for Quick Actions". The 5th International Date Palm Conference, Date Palm Improvement Section, Abu Dhabi, March 16–18, 255–262.

Shaker, A., Yan, W. Y., & El-Ashmawy, N. (2012). Panchromatic satellite image classification for flood hazard assessment. Journal of Applied Research and Technology, 10(6), 902–911.

Shila, H. (2010). Comparison of Land Covers Classification Methods in Etm+ Satellite Images (Case Study: Ghamishloo Wildlife Refuge). Journal of Environmental Research and Development, 5(2), 279–293.

Shiver, B. D., & Borders, B. E. (1996). Sampling techniques for forest resource inventory. John Wiley and Sons.

Sileshi, G. W. (2014). A critical review of forest biomass estimation models, common mistakes and corrective measures. Forest Ecology and Management, 329, 237–254.

Singh, M., Malhi, Y., & Bhagwat, S. (2014). Evaluating land use and aboveground biomass dynamics in an oil palm–dominated landscape in Borneo using optical remote sensing. Journal of Applied Remote Sensing, 8(1), 083695. https://doi.org/10.1117/1.JRS.8.083695

Singh, S. L., Sahoo, U. K., Kenye, A., & Gogoi, A. (2018). Assessment of Growth, Carbon Stock and Sequestration Potential of Oil Palm Plantations in Mizoram, Northeast India. Journal of Environmental Protection, 9(09), 912. doi 10.4236/jep.2018.99057

Smith, W. K., Dannenberg, M. P., Yan, D., Herrmann, S., Barnes, M. L., Barron-Gafford, G. A., Biederman, J. A., Ferrenberg, S., Fox, A. M., Hudson, A., Knowles, J. F., MacBean, N., Moore, D. J. P., Nagler, P. L., Reed, S. C., Rutherford, W. A., Scott, R. L., Wang, X., & Yang, J. (2019). Remote sensing of dryland ecosystem structure and function: Progress, challenges, and opportunities. Remote Sensing of Environment, 233, 111401. https://doi.org/10.1016/j.rse.2019.111401

Sohl, T. L. (1999). Change Analysis in the United Arab Emirates: An Investigation of Techniques. 65(nr 4), str. 475–484.

Song, C., Dickinson, M. B., Su, L., Zhang, S., & Yaussey, D. (2010). Estimating average tree crown size using spatial information from Ikonos and QuickBird images: Across-sensor and across-site comparisons. Remote Sensing of Environment, 114(5), 1099–1107.

Sonnenschein, R., Kuemmerle, T., Udelhoven, T., Stellmes, M., & Hostert, P. (2011). Differences in Landsat-based trend analyses in drylands due to the choice of vegetation estimate. Remote Sensing of Environment, 115(6), 1408–1420.

Southworth, J., Nagendra, H., & Tucker, C. (2002). Fragmentation of a landscape: Incorporating landscape metrics into satellite analyses of land-cover change. Landscape Research, 27(3), 253–269.

Srestasathiern, P., & Rakwatin, P. (2014). Oil palm tree detection with high resolution multi-spectral satellite imagery. Remote Sensing, 6(10), 9749–9774.

St-Onge, B., Hu, Y., & Vega, C. (2008). Mapping the height and above-ground biomass of a mixed forest using lidar and stereo Ikonos images. International Journal of Remote Sensing, 29(5), 1277–1294.

Stych, P., Jerabkova, B., Lastovicka, J., Riedl, M., & Paluba, D. (2019). A comparison of worldview-2 and landsat 8 images for the classification of forests affected by bark beetle outbreaks using a support vector machine and a neural network: A case study in the sumava mountains. Geosciences, 9(9), 396. https://doi.org/10.3390/geosciences9090396

Suganuma, H., Abe, Y., Taniguchi, M., Tanouchi, H., Utsugi, H., Kojima, T., & Yamada, K. (2006). Stand biomass estimation method by canopy coverage for application to remote sensing in an arid area of Western Australia. Forest Ecology and Management, 222(1), 75–87. https://doi.org/10.1016/j.foreco.2005.10.014

Sunaryathy, P. I., Kanniah, K. D., & Tan, K. P. (2015). Estimating Aboveground Biomass of Oil Palm Trees by Using the Destructive Method. World Journal of Agricultural Research, 3(1), 17–19.

Svoray, T., Shoshany, M., Curran, P. J., Foody, G. M., & Perevolotsky, A. (2001). Relationship between green leaf biomass volumetric density and ERS-2 SAR backscatter of four vegetation formations in the semi-arid zone of Israel. International Journal of Remote Sensing, 22(8), 1601–1607.

Svoray, Tal, & Shoshany, M. (2003). Herbaceous biomass retrieval in habitats of complex composition: A model merging SAR images with unmixed Landsat TM data. IEEE Transactions on Geoscience and Remote Sensing, 41(7), 1592–1601.

Tan, K. P., Kanniah, K. D., & Cracknell, A. P. (2013). Use of UK-DMC 2 and ALOS PALSAR for studying the age of oil palm trees in southern peninsular Malaysia. International Journal of Remote Sensing, 34(20), 7424–7446.

Terakunpisut, J., Gajaseni, N., & Ruankawe, N. (2007). Carbon sequestration potential in aboveground biomass of Thong Pha Phum national forest, Thailand. Applied Ecology and Environmental Research, 5(2), 93–102.

Thakur, T., & Swamy, S. L. (2012). Analysis of land use, diversity, biomass, C and nutrient storage of a dry tropical forest ecosystem of India using satellite remote sensing and GIS techniques. Proceedings of International Forestry and Environment Symposium, 15. pp. 273–278.

Thenkabail, P. S., Stucky, N., Griscom, B. W., Ashton, M. S., Diels, J., van der Meer, B., & Enclona, E. (2004). Biomass estimations and carbon stock calculations in the oil palm plantations of African derived savannas using IKONOS data. International Journal of Remote Sensing, 25(23), 5447–5472. https://doi.org/10.1080/01431160412331291279

Tian, F., Brandt, M., Liu, Y. Y., Verger, A., Tagesson, T., Diouf, A. A., Rasmussen, K., Mbow, C., Wang, Y., & Fensholt, R. (2016). Remote sensing of vegetation dynamics in drylands: Evaluating vegetation optical depth (VOD) using AVHRR NDVI and in situ green biomass data over West African Sahel. Remote Sensing of Environment, 177(Supplement C), 265–276. https://doi.org/10.1016/j.rse.2016.02.056

Tsitsi, B. (2016). Remote sensing of aboveground forest biomass: A review. Tropical Ecology, 57(2), 125–132.

Tucker, C. J. (1979). Red and photographic infrared linear combinations for monitoring vegetation. Remote Sensing of Environment, 8(2), 127–150.

Tucker, C. J., Vanpraet, C. L., Sharman, M. J., & Van Ittersum, G. (1985). Satellite remote sensing of total herbaceous biomass production in the Senegalese Sahel: 1980–1984. Remote Sensing of Environment, 17(3), 233–249.

Turner, D. P., Cohen, W. B., Kennedy, R. E., Fassnacht, K. S., & Briggs, J. M. (1999). Relationships between leaf area index and Landsat TM spectral vegetation indices across three temperate zone sites. Remote Sensing of Environment, 70(1), 52–68.

Turner, W., Rondinini, C., Pettorelli, N., Mora, B., Leidner, A. K., Szantoi, Z., Buchanan, G., Dech, S., Dwyer, J., & Herold, M. (2015). Free and open-access satellite data are key to biodiversity conservation. Biological Conservation, 182, 173–176.

United Nation. (2019). The Kyoto Protocol—Status of Ratification | UNFCCC [Https://unfccc.int/process/the-kyoto-protocol/status-of-ratification]. Retrivied on 20 April 2021.

Van der Hoek, Y., Solas, S. Á., & Peñuela, M. C. (2019). The palm Mauritia flexuosa, a keystone plant resource on multiple fronts. Biodiversity and Conservation, 1–13.

Vashum, K. T., & Jayakumar, S. (2012). Methods to estimate above-ground biomass and carbon stock in natural forests-A review. J. Ecosyst. Ecogr, 2(4), 1–7.

Vicharnakorn, P., Shrestha, R. P., Nagai, M., Salam, A. P., & Kiratiprayoon, S. (2014). Carbon stock assessment using remote sensing and forest inventory data in Savannakhet, Lao PDR. Remote Sensing, 6(6), 5452–5479.

Walkley, A., & Black, I. A. (1934). An examination of the Degtjareff method for determining soil organic matter, and a proposed modification of the chromic acid titration method. Soil Science, 37(1), 29–38.

Wallerman, J., Fransson, J. E., Bohlin, J., Reese, H., & Olsson, H. (2010). Forest mapping using 3D data from SPOT-5 HRS and Z/I DMC. 2010 IEEE International Geoscience and Remote Sensing Symposium, 64–67.

Wang, J., Chen, J., Ju, W., & Li, M. (2010). IA-SDSS: A GIS-based land use decision support system with consideration of carbon sequestration. Environmental Modelling & Software, 25(4), 539–553. https://doi.org/10.1016/j.envsoft.2009.09.010

Wang, L., Shi, C., Diao, C., Ji, W., & Yin, D. (2016). A survey of methods incorporating spatial information in image classification and spectral unmixing. International Journal of Remote Sensing, 37(16), 3870–3910.

Wani, A. A., Joshi, P. K., & Singh, O. (2015). Estimating biomass and carbon mitigation of temperate coniferous forests using spectral modeling and field inventory data. Ecological Informatics, 25, 63–70.

Wannasiri, W., Nagai, M., Honda, K., Santitamnont, P., & Miphokasap, P. (2013). Extraction of mangrove biophysical parameters using airborne LiDAR. Remote Sensing, 5(4), 1787–1808.

Western, A. R. (1989). The flora of the United Arab Emirates: An introduction. 188p.-Col. Illus., Maps.. En Geog, 2. Al Ain: United Arab Emirates University.

Wijaya, A., & Gloaguen, R. (2009). Fusion of ALOS Palsar and Landsat ETM data for land cover classification and biomass modeling using non-linear methods. Geoscience and Remote Sensing Symposium, 2009 IEEE International, IGARSS 2009, 3, pp. III–581.

Williams, C. A. (2010). Integration of remote sensing and modeling to understand carbon fluxes and climate interactions in Africa. Ecosystem Function in Savannas: Measurement and Modeling at Landscape to Global Scales, Edited by: Hill, MJ and Hanan, N., CRC Press, Boca Raton, FL, 327–346.

Woebbecke, D. M., Meyer, G. E., Von Bargen, K., & Mortensen, D. A. (1993). Plant species identification, size, and enumeration using machine vision techniques on near-binary images. Optics in Agriculture and Forestry, 1836, 208–220.

Wu, C., Shen, H., Wang, K., Shen, A., Deng, J., & Gan, M. (2016). Landsat imagery-based above ground biomass estimation and change investigation related to human activities. Sustainability, 8(2), 159. https://doi.org/10.3390/su8020159

Wu, X. B., & Archer, S. R. (2005). Scale-dependent influence of topography-based hydrologic features on patterns of woody plant encroachment in savanna landscapes. Landscape Ecology, 20(6), 733–742.

Wylie, B., Denda, I., Pieper, R., Harrington, J., Reed, B., & Southward, G. (1995). Satellite-Based Herbaceous Biomass Estimates in the Pastoral Zone of Niger. Journal of Range Management, 48(2), 159–164. https://doi.org/10.2307/4002804

Xiaoming, F., Yingshi, Z., & Yan, L. (2005). Remote sensing linked modeling of the aboveground biomass of semiarid grassland in Inner Mongolia. Geoscience and Remote Sensing Symposium, 2005. IGARSS'05. Proceedings. 2005 IEEE International, 5, 3047–3050.

Xie, Y., Sha, Z., & Yu, M. (2008). Remote sensing imagery in vegetation mapping: A review. Journal of Plant Ecology, 1(1), 9–23.

Yang, X., & Lo, C. P. (2002). Using A time series of satellite imagery to detect land use and cover changes in Atlanta, Georgia. International Journal of Remote Sensing, 23(9), 1775–1798.

Yuen, J. Q., Fung, T., & Ziegler, A. D. (2016). Review of allometric equations for major land covers in SE Asia: Uncertainty and implications for above-and below-ground carbon estimates. Forest Ecology and Management, 360, 323–340.

Zahabu, E., Mugasha, W. A., Malimbwi, R. E., & Katani, J. Z. (2018). Allometric biomass and volume models for coconut trees. E&D Vision Publishing Ltd.

Zandler, H., Brenning, A., & Samimi, C. (2015). Quantifying dwarf shrub biomass in an arid environment: Comparing empirical methods in a high dimensional setting. Remote Sensing of Environment, 158, 140–155.

Zhao, P., Lu, D., Wang, G., Wu, C., Huang, Y., & Yu, S. (2016). Examining spectral reflectance saturation in Landsat imagery and corresponding solutions to improve forest aboveground biomass estimation. Remote Sensing, 8(6), 469. https://doi.org/10.3390/rs8060469

Zohary, D., & Hopf, M. (2000). Domestication of plants in the Old World: The origin and spread of cultivated plants in West Asia. Europe, and the Nile Valley Oxford University Press, New York.

List of Publications

1. Dahy, B., Issa, S., Ksiksi, T., & Saleous, N. (2020). Geospatial Technology Methods for Carbon Stock Assessment: A Comprehensive Review. *IOP Conference Series: Earth and Environmental Science,* Volume 540. Link: https://iopscience.iop.org/article/10.1088/1755-1315/540/1/012036/meta

2. Issa, S., Dahy, B., Ksiksi, T., & Saleous, N. (2020). Allometric equations coupled with remotely sensed variables to estimate carbon stocks in date palms. *Journal of Arid Environments,* 182, 104264. Link: https://doi-org.uaeu.idm.oclc.org/10.1016/j.jaridenv.2020.104264

3. Issa, S. M**.,** Dahy, B., & Saleous, N. (2020). Accurate mapping of date palms at different age-stages for the purpose of estimating their biomass. *ISPRS Annals of Photogrammetry, Remote Sensing and Spatial Information Sciences*, V-3–2020, 461–467.Link: https://pdfs.semanticscholar.org/1965/e4eb18f84c12e3d0427047e7e855866ad912.pdf

4. Issa, S., Dahy, B., Ksiksi, T., & Saleous, N. (2020). A Review of Terrestrial Carbon Assessment Methods Using Geo-Spatial Technologies with Emphasis on Arid Lands. *Remote Sensing,* 12(12), 2008. Link: https://www.mdpi.com/2072-4292/12/12/2008

5. Dahy, B., Issa, S., Ksiksi, T., & Saleous, N. (2019). Non-Conventional Methods as a New Alternative for the Estimation of Terrestrial Biomass and Carbon Sequestered: Mini Review. *World Journal of Agriculture and Soil Science.* Link: https://irispublishers.com/wjass/fulltext/non-conventional-methods-as-a-new-alternative-for-the-estimation-of-terrestrial-biomass.ID.000579.php

6. Issa, S., Dahy, B., Saleous, N., & Ksiksi, T. (2019). Carbon stock assessment of date palm using remote sensing coupled with field-based measurements in Abu Dhabi (United Arab Emirates). *International Journal of Remote Sensing*, 0(0), 1–20. Link: https://www-tandfonline-com.uaeu.idm.oclc.org/doi/full/10.1080/01431161.2019.1602795

7. Issa, S., Dahy, B., Ksiksi, T., & Saleous, N. (2018). Development of a new allometric equation correlated with RS variables for the assessment of date palm biomass. *Proceedings of the 39th Asian Conference on Remote Sensing (ACRS 2018),* Kuala Lumpur, Malaysia, 15–19 October 2018. Link: https://a-a-r-s.org/proceeding/ACRS2018/ACRS%202018%20PROCEEDING.pdf

*See Appendix 8.

Appendices

Appendix 1: Different field variables used in allometric equations to estimate palm biomass, mostly oil palm (*Elaeis guineensis*).

Source	Output	Allometric Equations	Field Variables
(Saldarriaga et al., 1988)	AGB	$= 1.697 \times 10^{-3} \times DBH^{1.754} \times H^{2.151}$	DBH and H
(Brown, 1997)	Biomass	$= 10.0 + 6.4 \times H$ $= 4.5 + 7.7 \times Ht$	H and Ht
(H. Khalid et al., 1999a)	AGB	$= 725 + 197 \times H$	H
(Hughes et al., 1999)	AGB	$= 0.3060 \times DBH^{1.837} \times 1.035$	DBH
(Henson & Chang, 2003)	Biomass	$= -0.00020823 Age^4 + 0.000153744 Age^3 - 0.011636 Age^2 + 7.3219 Age - 6.3934$	Age
(Thenkabail et al., 2004)	AGBfresh AGBdry	$= 1.5729\ Ht - 8.2835$ $= 0.3747\ Ht + 3.6334$	Ht
(R. Hereward V. Corley & Tinker, 2008)	Trunk biomass Frond biomass	$= 0.1\ \pi\ x\ TD\ x\ H\ x\ (DBH/2)^2$ $= 0.02\ x\ W\ x\ D + 0.21$	H, TD, DBH, W, D, and Age
(Dewi et al., 2009)	AGB	$= 0.0976\ x\ H + 0.0706$	H
(Goodman et al., 2013)	AGB	$= 13.59\ x\ H - 108.8$	H
(Goodman et al., 2013)	AGB	$= 0.0950\ x\ (DF\ x\ DBH^2\ x\ H)$	DF, DBH, and H
(Da Silva et al., 2015)	AGB	$= 0.167 \times (DBH^2\ x\ H\ x\ TD)^{0.883}$	DBH, H, and TD
(Prayogo et al., 2018)	AGB	$= 0.03883\ x\ H\ x\ DBH^{1.2}$	DBH and H
(Zahabu et al., 2018)	AGB	$= 3.7964\ x\ H^{1.8130}$	H

Where DBH is diameter breast height, H is palm height, Ht is trunk height, TD is trunk density, W is frond width, D is frond depth, and DF is dry to fresh weight ratio.

Appendix 2: A summary of limitations and benefits of Optical, RADAR, and LiDAR sensors used for estimating the Above Ground Biomass (AGB) of standing forests.

Sensor Types	Approaches/ Resolutions	Limitations	Benefits
Optical Sensors	*Coarse Resolution Spatial (>100 m)* **Examples**: MODIS, AVHRR, NOAA, METEOSAT and SPOT Vegetation	- Average R value of 0.58, with average predictive of 42% - Saturation of spectral data at high biomass density - Mismatch between the size of field plots, field measurements and pixel size (mixed pixels) - Cloud cover - Limited to discriminating vegetation structure	- Availability of data with huge datasets archived - Estimation and mapping of AGB at continental and global scale -Repetitive, with high temporal frequency increasing the probability of acquiring cloud-free data - Provide consistent spatial data
	Medium Spatial Resolution (10-100 m) **Examples**: TM Landsat, ETM+, OLI and SPOT	- Average R value of 0.68 with average predictive error of 32% - Single pixel can encompass many tree crown or non-crown features - No reliable indicators of biomass in closed canopy structure - Not all texture measures can effectively extract biomass information	-Provide consistent global data - Archived datasets back to 1972 for Landsat - Small to large-scale mapping - Cost-effective (Free)
	Fine Spatial Resolution (<5 m) **Examples:** Quickbird, WorldView-2, and IKONOS	- Need large data storage and processing time - High cost, and more costly when it applies on large areas	- Average R value of 0.75 and average predictive error (27%) - Estimate tree crown size -Validation at localized scale
	Hyperspectral Many, very narrow, and contiguous spectral bands **Examples**: AISA Eagle, HYDICE and ALOS	-Cloud cover -High cost -Suffer from band redundancy and saturation in dense canopy -Computationally intensive and technically demanding	-Average R value of 0.83 -Allows discrimination of subtler differences (species level) -Potential for the future of RS-based biomass estimation models -Integration with LiDAR can improve results.

Appendix 2: A summary of limitations and benefits of Optical, RADAR, and LiDAR sensors used for estimating the Above Ground Biomass (AGB) of standing forests. Continued.

Sensor Types	Approaches/ Resolutions	Limitations	Benefits
RADAR Sensors	Approaches involve the use of either backscatter values or interferometry techniques **Examples:** Microwave/radar i.e., ALOS PALSAR, ERS-1, Envisat and JERS-1.	-Not accurate in mountainous region due to spurious relation between AGB and backscatter values. -Signal saturation in mature forests at various wavelengths (C, L and P bands) -Polarization (e.g., HV and VV) problems -Low spatial resolution makes it inaccurate for AGB assessment at the species level. -Cannot be applied on any vegetation type without considering stand characteristics and ground conditions.	-Measure forest vertical structure -Generally free -Can be accurate for young and sparse forests -Repetitive data Can give an average R value of 0.74, with average predictive error of 25%. Integrating RADAR with multi source data (optical, microwave data and GIS modeling techniques) is a promising approach.
LiDAR Sensors	Using laser light Spatial Resolution: (0.5 cm – 5 m) **Examples:** Carbon 3-D	- Repetitive at high cost and logistics deployment -Requires extensive field data calibration -Highly expensive -Technically demanding	-Penetrate cloud cover and canopy -Among all sensors option, LiDAR is the easiest to use for the extraction of tree attributes for estimating AGB with great accuracy -Accurate for estimating forest biomass in all spatial variability (sparse, young or mature forests) - Average R value of 0.89, with average predictive error equal 14% -Potential for satellite-based system to estimate global forest carbon stock

Appendix 3: Specifications of the RS optical sensors most commonly used for AGB estimation.

Sensor	Type	Bands	Spatial Resolution	Temporal Resolution	Swath	Cost
AVHRR	Multispectral	5 bands (Red, IR, and 3 Thermal IR)	1,100 meters	12 hours	2,500 km	Free
MODIS	Multispectral	36 bands (from Blue to Thermal IR)	250, 500 and 1,000 meters	1-2 days	2,330 km	Free
SPOT VEG	Multispectral	4 bands (Blue, red, NIR, and SWIR)	1,000 meters	1 day	2,250 km	Free
TM	Multispectral	7 bands (3 VIS, 3 IR and Thermal IR)	30 and 120 meters	16 days	185 km	Free
ETM+	Multispectral	9 bands (3 VIS, 3 IR and 2 Thermal IR and 1 PAN)	15, 30 and 60 meters	16 days	185 km	Free
SPOT	Multispectral	4 bands (2 VIS, 1 NIR, and 1 PAN)	5, 10 and 20 meters	26 days	60 km	Commercial
Landsat 8 OLI	Multispectral	11 bands (1 Ultra, 3 VIS, 3 IR, 1 Cirrus, 2 Thermal IR, and 1 PAN)	15, 30 and 100 meters	16 days	185 km	Free
LISS-III (IRS)	Multispectral	5 bands (2 VIS, 2 IR, and 1 PAN)	5.3, 23 and 50 meters	5-24 days	142 km	Commercial
Sentinel-2	Multispectral	13 bands (4 VIS, 6 NIR and 3 SWIR)	10, 20, and 60 meters	5-10 days	290 km	Free
IKONOS	Multispectral	5 bands (3 VIS, 1 IR, and 1 PAN)	1 and 4 meters	3 days	11 km	Commercial
World View2	Multispectral	9 bands (6 VIS, 2 IR, 1 PAN)	1.84 and 0.46 meter	1.1 days	16 km	Commercial
Quickbird	Multispectral	5 bands (4 bands and 1 PAN)	0.61 and 2.44 meter	3 days	16 km	Commercial
HyMap	Hyperspectral	126 bands	2-10 meters	Airborne	2.3 km and 4.6 km	Commercial
AVIRIS	Hyperspectral	224 bands (from VIS to MIR)	2.5 to 20 meters	Airborne	1.9 km and 11 km	Not Commercial

Appendix 4: Different cultivars and age stages from three different farms of the study area are selected to run the destructive method and to build the allometric equations.

No. Palm	Cultivar	Destruction Date	Location	Age (year)
1	LuLu	24-Apr-18	Masakin	2.5
2	Khalas	24-Apr-18	Masakin	2.5
3	Fardh	24-Apr-18	Masakin	3
4	Bumaan	24-Apr-18	Masakin	3
5	Khunaizi	24-Apr-18	Masakin	4
6	Khalas	29-Apr-18	Salamat W.	5
7	Fahel (Male)	29-Apr-18	Salamat W.	7
8	Khunaizi	29-Apr-18	Salamat W.	8
9	Fardh	29-Apr-18	Salamat W.	9
10	Bumaan	29-Apr-18	Salamat W.	10
11	Baghel	25-Apr-18	Qattara	11
12	Jabri	25-Apr-18	Qattara	14
13	Shahem	25-Apr-18	Qattara	16
14	Jash Ramli	25-Apr-18	Qattara	18
15	Neghal	25-Apr-18	Qattara	20

Appendix 5: Linear correlation between RS variables and AGB of date palm (mature, medium, and young). Here, only limited no. of field plots used as a pilot study (see Chapter 4).

Age Class	RS Variable		Constant	Coefficient	R^2	*P* value
Mature	Single Bands	B1	82.854	-0.006	0.368	0.083
		B	61.208	-0.005	0.402	0.067
		G	39360.136	-2.968	0.338	0.100
		R	28059.820	-1.918	0.398	0.068
		NIR	-27103.714	1.687	0.418	0.060
		SWIR1	25730.727	-1.306	0.445	0.049
		SWIR2	22573.920	-1.382	0.553	0.022
	VI's	DVI	-7158.285	1.739	0.792	0.001
		GNDVI	-12773.617	73226.070	0.800	0.001
		NDGI	7264.605	1285.609	0.472	0.041
		NDVI	-7305.021	54391.857	0.760	0.002
		RVI	31001.713	-41113.182	0.772	0.002
		SAVI	-6850.855	35207.940	0.754	0.002
		SR	-20323.290	15959.319	0.762	0.002
		TCB	27435.814	-0.671	0.177	0.259
		TCG	4580.293	2.061	0.797	0.001
		TCW	9663.430	1.743	0.709	0.004
		TVI	-132382.068	124232.050	0.783	0.002
Medium	Single Bands	B1	9929.699	-0.673	0.812	0.286
		B	8090.877	-0.542	0.832	0.269
		G	7105.073	-0.435	0.915	0.189
		R	6000.544	-0.311	0.971	0.108
		NIR	8259.282	-0.354	0.697	0.371
		SWIR1	6023.921	-0.229	1.000	0.010
		SWIR2	5683.790	-0.248	0.942	0.155
	VI's	DVI	72.613	0.246	0.284	0.642
		GNDVI	-58.159	6495.838	0.256	0.662
		NDGI	3016.837	246.754	0.990	0.065
		NDVI	-188.916	11067.297	0.579	0.450
		RVI	6713.056	-7129.192	0.652	0.402
		SAVI	122.490	5545.053	0.436	0.541
		SR	-3647.018	3729.177	0.488	0.508
		TCB	7327.815	-0.152	1.000	0.006
		TCG	1846.698	0.281	0.433	0.543
		TCW	3842.979	0.389	0.973	0.105
		TVI	-19545.673	19487.514	0.256	0.662

Appendix 5: Linear correlation between RS variables and AGB of date palm (mature, medium, and young). Here, only limited no. of field plots used as a pilot study. Continued.

Age Class	RS Variable		Constant	Coefficient	R²	P value
Young	Single Bands	B1	3754.984	-0.244	0.450	0.532
		B	3102.912	-0.198	0.488	0.507
		G	2443.837	-0.135	0.428	0.546
		R	1989.402	-0.089	0.396	0.567
		NIR	2071.747	-0.070	0.128	0.767
		SWIR1	1543.352	-0.043	0.157	0.741
		SWIR2	1372.940	-0.041	0.162	0.736
	VI's	DVI	-1145.877	0.353	0.926	0.175
		GNDVI	-247.854	4399.789	0.233	0.680
		NDGI	1106.782	65.046	0.329	0.611
		NDVI	16.133	4399.789	0.233	0.233
		RVI	3996.000	-4506.168	0.732	0.346
		SAVI	-329.921	4506.168	0.732	0.346
		SR	-3682.755	3233.889	0.880	0.225
		TCB	1955.148	-0.033	0.242	0.673
		TCG	1053.884	0.226	0.675	0.386
		TCW	916.026	0.040	0.053	0.852
		TVI	661.436	0.000	0.480	0.513

Appendix 6: The average amounts of date palm biomass, organic matter, organic carbon, and soil organic carbon at different age stages.

| Item	Average amount (Kg palm^{-1})		
	Young (< 5 year)	Medium (5 – 10 years)	Mature (>10 years)
Crown Biomass (CB)	22.51	65.17	148.5
Trunk Biomass (TB)	0	29.53	135.91
AGB	22.51	94.69	284.41
BGB	7.46	87.61	141.23
Total Biomass	29.97	182.3	425.63
Organic Matter (OM)	27.39	166.56	388.94
Organic Carbon (OC)	15.88	96.62	225.58
SOC	18.09	62.59	92.91
Total Carbon Stock (CS)	33.97	159.21	318.49

Appendix 7: Linear correlation between RS variables and AGB of date palm (mature, medium, and young). Here, 54 field plots were used covering the whole study area of Abu Dhabi (see Chapter 6).

Age Class	RS Variable		Constant	Coefficient	R^2	*P* value
Mature	Single Bands	B1	85.270	-0.047	0.113	0.187
		B	93.557	-0.043	0.143	0.135
		G	107.820	-0.036	0.187	0.083
		R	103.466	-0.029	0.230	0.052
		NIR	149.462	-0.026	0.086	0.255
		SWIR1	115.464	-0.021	0.302	0.022
		SWIR2	102.826	-0.023	0.290	0.026
	VI's	SR	-32.033	37.696	0.545	0.0007
		RVI	131.267	-164.234	0.315	0.019
		DVI	-98.847	0.084	0.412	0.006
		NDGI	100.560	636.247	0.609	0.0002
		NDVI	-17.970	194.545	0.398	0.007
		TVI	-476.939	454.517	0.379	0.009
		GNDVI	-53.452	249.782	0.311	0.020
		RDVI	-47.289	3.911	0.418	0.005
		SAVI	-18.985	131.919	0.413	0.005
		MSAVI	-38.643	175.245	0.337	0.013
		TCB	123.051	-0.013	0.227	0.053
		TCG	0.146	0.060	0.313	0.20
		TCW	84.780	0.037	0.396	0.007

Appendix 7: Linear correlation between RS variables and AGB. Continued.

Age Class	RS Variable		Constant	Coefficient	R²	*P* value
Medium	Single Bands	B1	28.817	-0.007	0.027	0.504
		B	29.653	-0.006	0.026	0.507
		G	31.553	-0.004	0.030	0.479
		R	33.809	-0.005	0.057	0.327
		NIR	24.178	-0.0002	0.0001	0.966
		SWIR1	37.538	-0.004	0.075	0.256
		SWIR2	35.052	-0.004	0.074	0.260
	VI's	SR	-7.827	17.892	0.195	0.058
		RVI	53.020	-50.018	0.159	0.091
		DVI	-3.322	0.018	0.208	0.049
		NDGI	36.484	108.230	0.128	0.132
		NDVI	6.605	64.310	0.164	0.085
		TVI	-125.108	132.281	0.131	0.128
		GNDVI	1.429	59.096	0.081	0.239
		RDVI	0.224	1.191	0.205	0.052
		SAVI	6.695	42.842	0.159	0.091
		MSAVI	3.003	50.018	0.159	0.091
		TCB	34.810	-0.002	0.041	0.407
		TCG	15.280	0.015	0.164	0.085
		TCW	34.943	0.008	0.125	0.137
Young	Single Bands	B1	1.126	0.005	0.172	0.087
		B	1.137	0.004	0.159	0.101
		G	0.260	0.003	0.157	0.103
		R	-0.217	0.002	0.154	0.107
		NIR	-7.186	0.003	0.283	0.023
		SWIR1	-1.031	0.002	0.105	0.190
		SWIR2	0.620	0.002	0.079	0.258
	VI's	SR	8.420	-1.581	0.006	0.753
		RVI	3.403	3.907	0.008	0.723
		DVI	3.091	0.003	0.044	0.404
		NDGI	9.509	23.810	0.036	0.451
		NDVI	7.367	-6.913	0.012	0.661
		TVI	18.283	-11.195	0.007	0.738
		GNDVI	9.674	-11.393	0.031	0.485
		RDVI	5.550	0.042	0.002	0.855
		SAVI	6.978	-3.095	0.006	0.767
		MSAVI	7.310	-3.907	0.008	0.723
		TCB	-2.488	0.001	0.174	0.085
		TCG	6.290	-0.001	0.004	0.802
		TCW	5.885	-0.0001	0.0002	0.951

197

Appendix 8: Parts from first pages of papers that have been published in refereed International Conference proceeding as well as in a peer-reviewed journal while working on this dissertation.
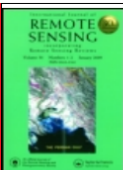
International Journal of Remote Sensing

ISSN: 0143-1161 (Print) 1366-5901 (Online) Journal homepage: https://www.tandfonline.com/loi/tres20

Carbon stock assessment of date palm using remote sensing coupled with field-based measurements in Abu Dhabi (United Arab Emirates)

Salem Issa[a], Basam Dahy[a], Nazmi Saleous[b] and Taoufik Ksiksi[c]

[a]Geology Department, United Arab Emirates University, Al Ain, UAE; [b]Geography Department, United Arab Emirates University, Al Ain, UAE; [c]Biology Department, United Arab Emirates University, Al Ain, UAE

ABSTRACT
This study aims at developing a remote sensing based model to estimate carbon stock (CS) in date palm plantations in the United Arab Emirates (UAE). Data from Landsat 8 OLI were used to assess the

ARTICLE HISTORY
Received 30 September 2018
Accepted 8 February 2019

Journal of Arid Environments 182 (2020) 104264

Contents lists available at ScienceDirect

Journal of Arid Environments

journal homepage: www.elsevier.com/locate/jaridenv

Allometric equations coupled with remotely sensed variables to estimate carbon stocks in date palms

Salem Issa[a,*], Basam Dahy[a], Taoufik Ksiksi[b], Nazmi Saleous[c]

[a] Geology Department, United Arab Emirates University, Al Ain, United Arab Emirates
[b] Biology Department, United Arab Emirates University, Al Ain, United Arab Emirates
[c] Geography Department, United Arab Emirates University, Al Ain, United Arab Emirates

ARTICLE INFO

Keywords:
Above ground biomass
Below ground biomass
Organic carbon
Organic matter
Regression analysis
Soil organic carbon
Vegetation indices

ABSTRACT

This study aims at developing specific allometric biomass equations that can be integrated into a remote sensing (RS) based model for assessing carbon sequestered in date palms. Assessing the potential of date palms to improve soil carbon sequestration was another objective. In a previous study, the authors demonstrated that combinations of visible and short wave single bands (Red, SWIR1, SWIR2) besides vegetation indices (DVI, NDI and RVI) derived from Landsat imagery correlated significantly with date palms' biomass. Here and based on field and lab work, relevant structural variables were identified and used in the development of allometric equations. Results showed that the crown area (CA) best estimated both crown biomass (CB) and soil organic carbon (SOC). Likewise, the trunk height (H) was the best estimator of trunk biomass (TB). Using three soil

remote sensing MDPI

Review

A Review of Terrestrial Carbon Assessment Methods Using Geo-Spatial Technologies with Emphasis on Arid Lands

Salem Issa[1,*], Basam Dahy[1], Taoufik Ksiksi[2] and Nazmi Saleous[3]

[1] Department of Geosciences, College of Science, UAE University, Al Ain, UAE; basam.d@uaeu.ac.ae
[2] Department of Biology, College of Science, UAE University, Al Ain, UAE; tksiksi@uaeu.ac.ae
[3] Department of Geography, College of Science, UAE University, Al Ain, UAE; nazmi.saleous@uaeu.ac.ae
[*] Correspondence: salem.essa@uaeu.ac.ae

Received: 18 April 2020; Accepted: 18 June 2020; Published: 23 June 2020

Abstract: Geo-spatial technologies (i.e., remote sensing (RS) and Geographic Information Systems (GIS)) offer the means to enable a rapid assessment of terrestrial carbon stock (CS) over large areas. The utilization of an integrated RS-GIS approach for above ground biomass (AGB) estimation and precision carbon management is a timely and cost-effective solution for implementing appropriate

Article Metrics Related articles

03 Aug 2020

ACCURATE MAPPING OF DATE PALMS AT DIFFERENT AGE-STAGES FOR THE PURPOSE OF ESTIMATING THEIR BIOMASS

S. M. Issa[1], B. S. Dahy[1], and N. Saleous[2]
[1]Dept. of Geology, College of Science, UAEU, Al Ain, UAE
[2]Dept. of Geography, College of Humanities and Social Sciences, UAEU, Al Ain, UAE

Abstract. The main objective of the current study was to produce an accurate map of date palm (DP) plantations in the Emirate of Abu Dhabi in

---

IOPscience   Q   Journals ▾   Books   Publishing Support   Login ▾

IOP Conference Series: Earth and Environmental Science

PAPER • OPEN ACCESS

Geospatial Technology Methods for Carbon Stock Assessment: A Comprehensive Review

Basam Dahy[1], Salem Issa[1], Taoufik Ksiksi[2] and Nazmi Saleous[3]
Published under licence by IOP Publishing Ltd

📄 Article PDF

PROCEEDINGS ACRS 2018 THE 39TH ASIAN CONFERENCE ON REMOTE SENSING KUALA LUMPUR

Proceedings Asian Conference on Remote Sensing 2018

DEVELOPMENT OF A NEW ALLOMETRIC EQUATION CORRELATED WITH RS VARIABLES FOR THE ASSESSMENT OF CARBON STOCK IN DATE PALM PLANTATIONS

Salem Issa (1), Basam Dahy (1), Taoufik Ksiksi (1), Nazmi Saleous (1)

[1] UAE University, College of Science, P.O. Box 15551, Al Ain, United Arab Emirates
Email: salem.essa@uaeu.ac.ae; basam.d@uaeu.ac.ae

Abstract: The United Arab Emirates (UAE) has the largest number of date palms for any single country in the world with an estimated number of about 42 million palms. Date palm, *Phoenix dactylifera,* is considered as the most important fruit crop in arid regions. In addition to its ability to tolerate harsh weather, high temperature, drought and high levels of salinity, date palm is a good source for carbon sequestration in such ecosystems. The main